REPORT OF HYDROGRAPHIC RESEARCHES No. 15, March, 1980

NEW DETERMINATION OF A MARINE GEOID AROUND JAPAN

Yasuhiro Ganeko

Received 1979 September 10

Abstract

A marine geoid around Japan is computed on the basis of $30' \times 30'$ and $1^\circ \times 1^\circ$ block mean gravity anomalies. The $30' \times 30'$ block data are prepared by reading out the block-averaged gravity anomalies from the published gravity anomaly maps around Japan. The $1^\circ \times 1^\circ$ block data are prepared by taking averages of DMAAC's $1^\circ \times 1^\circ$ global gravity data and Watts and Leeds' $1^\circ \times 1^\circ$ block means. The geoidal heights are computed from the above terrestrial gravity data in combination with the GEM-10 satellite-derived global anomaly field. The GEM-10 model comprises a geopotential coefficient set which is complete up to degree and order 22. The radius of the circular cap area of the numerical Stokes' integration is taken to be 20°. The marked features of the computed geoid are the dents over trench areas. The dents amount occasionally to more than 20 meters relative to the GEM-10 global geoid. The general geoidal high along island arcs is another marked feature of the calculated geoid. Geoid undulations on the land areas of Japan are compared with an astro-geodetic geoid of Japan (Ganeko, 1976). The standard deviation of the undulation differences is 1.4 m, while the standard deviation decreases to 0.8 m if the Hokkaido area is excluded. The astrogeodetic geoid in the Hokkaido area seems to have a tilt downward to the north relative to the gravimetric geoid.

The gravimetric geoid is compared with the Geos-3 altimetric sea surface heights. Altimeter data taken along 12 revolutions of the satellite passing over the region of the gravimetric geoid are used, and the comparison figures for each revolution are presented. The r.m.s. values of differences between altimetric sea surface heights and the gravimetric geoidal heights for each revolution vary within the range from 0.6 to 1.9m except for tilts and constant biases. The total r.m.s. difference is around 1.3m. Differences seem to be large in the region where terrestrial gravity data are sparse and consequently gravimetric geoidal heights are poorly determined.

Detailed investigations are carried out concerning the error sources involved in the procedure of computation of a gravimetric geoid by means of numerical integration of Stokes' formula. The results of the investigations estimate the accuracy of the calculated gravimetric geoid to be around 1.3m in the area near Japan and to be around 1.8m in the gravity data-sparse areas. Terrestrial gravity data errors form the biggest error source under the present availability of the surface gravity data around Japan. The estimated accuracy of the gravimetric geoid is compatible with the comparison results between Geos-3 altimeter data and the gravimetric geoid. The accuracy of the geoidal height difference is also investigated. This kind of error estimation is meaningful because some of the error sources have long correlation distances, so that such error sources

* Astronomical Division

hardly affect the accuracy of the geoidal height difference. As for the calculated geoid, the accuracy of relative geoid undulations over 100km distance is estimated to be around one meter.

Detailed investigations concerning various error sources enable us to get a perspective of the geoid computation of the future. After an investigation of the statistical characteristics of the gravity anomaly field around Japan, we derive requirements for marine gravity surveys to achieve a 10cm geoid. $10'$ block mean gravity anomalies with an accuracy better than 5 mGals must be prepared in the inner area of Stokes' integration, i. e. inside and outside to $2°$ around the area where a 10cm geoid is computed. These block data can be derived from profile gravity observations carried out along parallel ship tracks located every 10 nautical miles. Moreover, we need additional gravity surveys by profile observations made every 15 or 30 nautical miles depending on the roughness of the gravity anomaly field in the outer area extending to a distance of 20 to 30 degrees from the boundary of the inner area. Systematic errors larger than 0.1 mGals in gravity observations must be avoided though a few mGals random errors of point gravity observations are acceptable. Stokes' integration should be carried out in combination with a satellite-derived global gravitational field because long wavelength components of the geopotential field are well determined by the satellite trackings. The flattening of the earth and the sea surface topography must be taken into consideration in the computation of a 10cm marine geoid.

Contents

1. Introduction

The determination of the figure of the earth has been one of the most important problems of the geodetical sciences, and not a few people have made great efforts in this subject. The figure of the earth is formed by the topographic reliefs at land areas and by the quasi-stationary sea surface (mean sea surface). Under the assumption that the mean sea surface realizes a equipotential surface in the earth's gravitational field, and then the mean sea surface is equivalent to the geoid, which is elemental in the expression of the figure of the earth as a reference surface of the topographical heights at land and as a realization of the figure of the earth itself at sea.

The three dimensional rectangular coordinates (X, Y, Z) of the earth's surface in the geocentric coordinate system are obtained from the geographic coordinates (φ, λ), the geometric parameters of the earth ellipsoid a (semimajor axis) and b (semiminor axis), and the ellipsoidal height h of the earth's surface which is the sum of the topographical height H and the geoidal height N (see Figure 1):

$$h=H+N=H^*+\zeta, \tag{1-1}$$

where H^* and ζ are so called normal height and height anomaly whose further explanation will be found in the next chapter. The explicit expressions of X, Y and Z are given by (2-7). It should be noted that equation (2-7) is based on the assumptions that the center of the reference ellipsoid coincides with the center of the earth's gravity and the potential of the geoid is equal to the normal geopotential at the surface of the reference ellipsoid.

The three dimensional geometrical relations of points located on the earth's surface can be determined by the geometrical satellite geodesy (e. g. Yamazaki, 1971), but the positions in the geocentric coordinate system cannot be given by such a geometrical method. The world-wide networks of the satellite tracking stations determined by the geometrical method are translated to the geocentric coordinate expressions by knowing ellipsoidal heights, i. e. geoidal heights, at each satellite tracking station. The least-squares adjustment provides us with the translation parameters and the geometrical parameters of the best-fitting earth ellipsoid (e. g. Schmid, 1974; Mueller, 1974; Gaposchkin, 1974). The long wave-length components of the geoid undulations can be determined by the observations of orbit changes of artificial satellites (e. g. Caputo, 1967), and this method can provide us with geopotential coefficients up to degree 20 (Lerch et al., 1977). A geopotential coefficient set comprising coeffi-cients up to degree 20 can express geoid undulations with an accuracy of ± 4 m on the world-wide average basis (see Figure 30). In other words, on the world-wide average basis, geoid undulations of shorter wave-length components than degree 20 amount to ± 4 m and the satellite-derived global geoid undulations commit errors of ± 4 m even if the low degree harmonics are determined without errors. As we will see in Chapter 3, the differences between detailed geoid and the satellite-derived global geoid sometimes reach 20 meters at a specific area such as trench area. Therefore, the satellite-derived global geoid is insufficient for the use of deriving three dimensional positions of the earth's surface by using equation (2-7). The determination of accurate three demensional positions are necessary for satellite tracking stations whose positions affect the determination of satellite positions directly and for observation sites of the position astronomy, and also the map projections require accurate geoid undulations.

The detailed structures of the geoid undulations can be computed by applying Stokes' formula to terrestrial gravity data. The recent accumulation of sea gravity observations by surface ship gravity meters has made it possible to compute detailed gravimetric geoid not only at land areas but also at ocean areas by the combination of terrestrial gravity data with the satellite-derived gravity anomaly field. The recent works concerning the world-wide detailed gravimetric geoid were made by Marsh and Vincent (1974) and Marsh and Chang (1976a). The Northwest Atlantic area, off east coasts of the United States, is the area where various satellite tracking stations are located and geodetical and geophysical surveys have been carried out with high density. This area has also been selected as the calibration area of the satellite altimetry experiments (Leitao et al., 1975), and much efforts have been concentrated there to obtain an accurate geoid (e. g. Talwani et al., 1972; Marsh and Chang, 1976b).

Detailed geoid undulations at land areas can also be computed by Helmert's formula:

$$N_Q-N_P=-\int_P^Q(\xi\cos A+\eta\sin A)\,ds \tag{1-2}$$

from deflections of the vertical, where ξ and η are the deflection components in the meridian and prime vertical, respectively, and A is the azimuth of the direction of the tangential at a point on the integral path from point P to point Q. We call a geoid computed from deflection observations an "astrogeodetic geoid". The numerical values of deflections of the vertical depend on the adopted deflection of the vertical at the geodetic datum station and the geometric parameters of the reference ellipsoid of the geodetic system, so that the astrogeodetic geoid depends on the geodetic system. Since it is impossible to determine the deflection at the geodetic datum station and the geometric parameters of the best-fitting earth ellipsoid from the geodetic observations made in a restricted land area, astrogeodetic geoids suffer some amount of systematic tilting and distortion against the geocentric coordinate system. On the contrary, the gravimetric geoid computed by Stokes' formula is automatically expressed in the geocentric coordinate system, so that the gravimetric geoid can be of use as a calibration field of astrogeodetic geoids.

Various geodetic systems can be interrelated with each other on the basis of satellite geodesy, and we know the positions of each geodetic datum in a global geodetic coordinate system. In other words, we know translation values of each geodetic datum relative to the global geodetic coordinate system or the deflection values at each geodetic detum station. SAO-SE3 solution (Gaposchkin et al., 1973) estimated the shift of the Tokyo datum station to the global coordinate system as $\Delta\varphi=11.7''$ and $\Delta\lambda=-12.3''$. After applying these shifts to the Tokyo datum, the Japanese astrogeodetic geoid is expressed in the same coordinate system as gravimetric geoid. There have been made several investigations to determine the Japanese astrogeodetic geoid, i. e. Atumi (1933); Kawabata (1939); Okuda (1951); Fischer (1960); Ono (1974); Ganeko (1976). Hagiwara (1967) computed a gravimetric geoid on the land of Japan for the first time from restricted gravity data around

Japan available at that time. Watts and Leeds (1977) drew a gravimetric geoid in the Northwest Pacific area including the adjacent seas of Japan based on $1^\circ \times 1^\circ$ block mean gravity anomalies of their own surface gravity data. Ganeko (in press) made a test calculation of a detailed gravimetric geoid around Japan based on $30' \times 30'$ block mean gravity anomalies, the present paper is a further extension of his preliminary investigations.

Japan is located in a geophysically specific area such as trench and islands-arc system, and moreover the Kuroshio Current, which is one of the strongest ocean currents of the world, is passing by along the south coasts of Japan. So the area around Japan is one of the quite interesting areas in the field not only of geophysics but also of oceanography. It may be surely expected that much more satellite techniques will be applied in these scientific fields, and that the Japan area will necessarily become one of the calibration areas of satellite trackings. In this sense, it may be quite useful to obtain an accurate geoid in this area.

The satellite altimetry has opened a new page of the physical geodesy, for the satellite altimetry provides us with a direct solution concerning the determination of the figure of the earth at ocean areas. This situation may give a new physical meaning to the determination of the marine geoid, an equipotential surface at sea. The sea surface topography ascribes to real existences of various oceanographic phenomena accompanied with motions of sea water, and inversely the observed topography is taken to be a constraint condition for the ocean dynamics.

The test observations of the satellite altimetry by Skylab and Geos-3 have been successfully carried out (e. g. Mourad et al., 1975; Kearsley, 1977). Leitao et al. (1978) succeeded for the first time in relating the differences between altimetric sea surface heights and gravimetric geoidal heights with the sea surface topography due to a strong ocean current of the Gulf Stream. To use both the altimeter data and gravimetric geoid for the oceanographic purpose, 10 cm accuracy may be required for the determination of the satellite positions and for the geoid undulations. The achievement of such accuracy may be one of the main objects of the geometrical and physical geodesy at present.

The present paper attempts to compute a gravimetric geoid around Japan based on the current availability of the terrestrial gravity data in the area and to make detailed investigations to realize the reliability of the computed geoid. The detailed investigations of various error sources involved in the geoidal height computation procedures will tell us what kind of effort should be made to achieve a 10 cm geoid.

2. Procedure of Gravimetric Geoidal Height Comutation

(1) Stokes' Integral

The geoid undulation are computed from terrestrial gravity data by using the conventional Stokes' integral on a unit sphere (Heiskanen and Moritz, 1967, p. 94), which is

$$N = \frac{R}{4\pi G} \iint_{\sigma} \Delta g \, S(\psi) \, d\sigma, \tag{2-1}$$

where R is the mean radius of the earth, G the mean gravity on the whole surface of the earth, Δg so-called free-air gravity anomaly defined on the geoid, and $S(\psi)$ well-known Stokes' function written by

$$S(\psi)=\sum_{l=2}^{\infty}\frac{2l+1}{l-1}P_l(\cos\psi)$$

$$=\operatorname{cosec}\frac{\psi}{2}-6\sin\frac{\psi}{2}+1-5\cos\psi-3\cos\psi l_n\left(\sin\frac{\psi}{2}+\sin^2\frac{\psi}{2}\right) \tag{2-2}$$

(ibid., p. 94). ψ is a parameter of the spherical distance. Equation (2-1) is varid if the reference ellipsoid has the same potential as the geoid and the same mass as the earth (ibid., p. 101). On the other hand, (2-1) is based on approximations such as neglection of the flattening of the earth and approximate treatings of the topographic mass between the geoid and the physical surface of the earth. The spherical approximation causes errors of the order fN, where f is the geometrical flattening of the earth ellipsoid (see 4-(6)).

The geoidal height is computed more accurately by

$$N=\frac{R}{4\pi\gamma}\iint_{\sigma}\Delta g\, S(\psi)d\sigma+\frac{R}{4\pi\gamma}\iint_{\sigma}G_1\, S(\psi)d\sigma+\frac{\bar{g}-\bar{\gamma}}{\gamma}H \tag{2-3a}$$

or

$$N=\zeta+\frac{\bar{g}-\bar{\gamma}}{\gamma}H \tag{2-3b}$$

(ibid., p. 326) on the basis of Molodenskii's theory for the determination of the figure of the earth (Molodenskii et al., 1962). In the equations (2-3a, b), γ is the normal gravity on the telluroid which is defined as a surface where the normal gravitational potential of the reference ellipsoid is the same as the actual potential on the ground (see Figure 1), G_1 the first order correction term of the Molodenskii series solution of the geodetic boundary value problem (ibid., p. 122), $\bar{g}$ the mean gravity along the plumb line between the geoid and the ground, $\bar{\gamma}$ the mean normal gravity along the normal plumb line between the ellipsoid and the telluroid, H the topographic height from the geoid, and ζ the height anomaly which is the distance between the ground and the telluroid (see Figure 1). Then Δg is the ground level gravity anomaly which is defined by

$$\Delta g=g_P-\gamma=g_P-\left(\gamma_0+\frac{\partial\gamma}{\partial h}H^*\right), \tag{2-4}$$

where g_P is the gravity at a point P on the ground, γ the normal gravity on the telluroid, γ_0 the normal gravity at P_0 where P is projected onto the reference ellipsoid, $\partial\gamma/\partial h$ the vertical gradient of the normal gravity, and H^* the normalheight (see Figure 1). Then the potentinl difference between the ground and the geoid is defined by using H^* as follows:

$$\Delta W=-\int_0^{H^*}\gamma\, dh.$$

It is clear that (2-4) differs from the definition of the conventionally and widely-used free-air gravity anomaly:

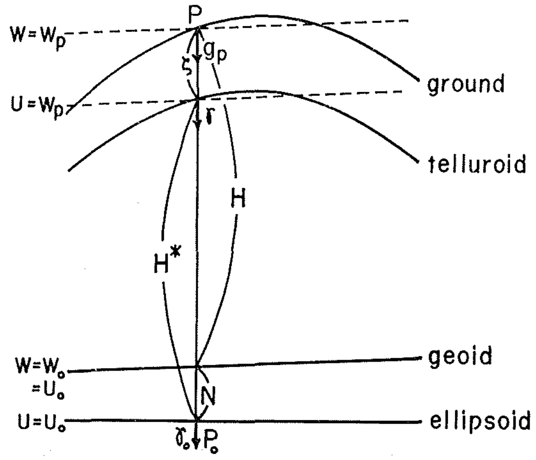

Figure 1 Normal height H^* and height anomaly ζ.

$$\Delta g = g_P - \frac{\partial \gamma}{\partial h} H - \gamma_0,$$

only by the amount

$$\Delta = \frac{\partial \gamma}{\partial h}(H^* - H). \tag{2-5}$$

The difference $H^* - H$ is equivalent to the difference between geoidal height and height anomaly (see Figure 1), that is,

$$H^* - H = N - \zeta = \frac{\bar{g} - \bar{\gamma}}{\bar{\gamma}} H. \tag{2-6}$$

The difference is approximated to Bouguer anomaly Δg_B (in Gals) $\times H$ (in km) meters (Heiskanen and Moritz, 1967, p. 328). The difference is estimated to be 1.1 m in a specific case as at the top of Mt. Fuji ($H = 3776$ m), Japan, and may in general be much less than the case. Therefore, (2-5) is as small as the order of 0.1 mGals, and it is negligible in ocean areas because the sea surface topography is estimated to be the order of 1 m (e.g. Lisitzin, 1974).

The second term in the right-hand side of (2-3a) is as small as or less than one meter (Heiskanen and Moritz, 1967, p. 329). Hagiwara (1972a) obtained the term as about 6 cm at the mountanous area of Tanzawa, Japan, and Hagiwara (1973) ascertained by using a model topographic relief that the term is small even in areas of rugged terrain.

We thus can consider that Stokes' integral (2-1) is a good approximation to height anomaly as far as Δg is understood as the ground level gravity anomaly (2-4), and that (2-1) is also a good approximation to geoidal height especially in ocean areas.

It should be noted that zero-th and first degree terms of the spherical harmonic expansion of geoidal heights automatically vanish in the performance of Stokes' integral over the whole surface of the earth, even if such terms are included in the gravity anomaly data, because of the characteristics of Stokes' function (see (2-2)), so that the computed geoidal heights are free from the ambiguity of the actual size of the earth ellipsoid. Consider the computation formulas of three dimensional coordinates of the earth's surface by using parameters a (semimajor axis) and f (geometrical flattening) of the reference ellipsoid, geoidal height N by Stokes' integral and topographic height H. Then we can write the three dimensional coordinates by the formulas:

$$\left.\begin{aligned} X &= (\bar{N}+N+H)\cos\varphi\cos\lambda, \\ Y &= (\bar{N}+N+H)\cos\varphi\sin\lambda, \\ Z &= \left(\frac{b^2}{a^2}\bar{N}+N+H\right)\sin\varphi, \end{aligned}\right\} \tag{2-7}$$

where the origin of the rectangular coordinate (x, y, z) is located at the center of gravity of the earth, x-axis is in the meridian plane of Greenwich, z-axis coincides with the earth's mean axis of rotation, and y-axis is so chosen as to obtain a right-handed coordinate system. b is the semiminor axis of the ellipsoid calculated by $b=(1-f)$ a, φ and λ are geographic latitude and longitude, and $\bar{N}$ is defined by

$$\bar{N}=\frac{a^2}{(a^2\cos^2\varphi+b^2\sin^2\varphi)^{\frac{1}{2}}}. \tag{2-8}$$

Equation (2-7) may not give an actual position of the earth's surface, because zero degree term of geoidal heights N_0 cannot be determined by Stokes' integral. N_0 is evaluated by

$$N_0=-\frac{R}{2G}\Delta g_0+\frac{k\delta M}{2GR}, \tag{2-9a}$$

or

$$N_0=-\frac{R}{G}\Delta g_0+\frac{\delta W}{G}, \tag{2-9b}$$

where Δg_0 is the mean gravity anomaly over the whole surface of the earth, k the gravitational constant, δM the difference between the masses of the actual earth and the reference ellipsoid, and δW the difference between the potential of the geoid and the normal potential on the surface of the reference ellipsoid (Heiskanen and Moritz, 1967, p. 102). Therefore, in (2-7) N should be replaced by $N+N_0$ to obtain accurate coordinates of the earth's surface. We cannot evaluate N_0 term here because we do not have gravity data of world-wide coverage, so that we assume the term to be zero. Then the geoidal heights evaluated in the present paper are understood to be ones referred to an ellipsoid which has the same potential as the geoid on its surface and the same mass as the earth.

(2) Satellite-Derived Gravity Anomaly and Geoid Undulations

The geopotential outside the earth, except for the potential of centrifugal force by the rotation of the earth, is expressed in a series of Laplace harmonics as follows:

$$V=\frac{kM}{r}\left\{1+\sum_{l=2}^{\infty}\sum_{m=0}^{l}\left(\frac{a}{r}\right)^l[\bar{C}_{lm}\bar{R}_{lm}(\bar{\varphi},\lambda)+\bar{D}_{lm}\bar{S}_{lm}(\bar{\varphi},\lambda)]\right\}, \tag{2-10}$$

where r is the distance from the center of gravity of the earth, kM the product of the gravitational constant and the mass of the earth, $\bar{\varphi}$ and λ the geocentric latitude and longitude, and $\bar{R}_{lm}(\bar{\varphi},\lambda)$ and $\bar{S}_{lm}(\bar{\varphi},\lambda)$ are defined by using a fully normalized associated Legendre function $\bar{P}_{lm}$ as follows:

$$\left.\begin{aligned} \bar{R}_{lm}(\bar{\varphi},\lambda) &= \bar{P}_{lm}(\sin\bar{\varphi})\cos m\lambda, \\ \bar{S}_{lm}(\bar{\varphi},\lambda) &= \bar{P}_{lm}(\sin\bar{\varphi})\sin m\lambda. \end{aligned}\right\} \tag{2-11}$$

$\bar{R}_{lm}$ and $\bar{S}_{lm}$ are normalized so that the average squares of them over the unit sphere is unity :

$$\frac{1}{4\pi}\iint_{\sigma} \bar{R}_{lm}^2\, d\sigma = \frac{1}{4\pi}\iint_{\sigma} \bar{S}_{lm}^2\, d\sigma = 1.$$

The geopotential coefficients $\bar{C}_{lm}$, $\bar{D}_{lm}$ can be determined by observing the orbit changes of artificial satellites moving in the gravitational field of the earth. But the contributions of high degree terms in (2-10) to orbit changes are too small to be detected by satellite trackings. Let L be the highest degree of the geopotential coefficients derivable from satellite trackings. We write the satellite-derived geopotential V_s as

$$V_s = \frac{kM}{r}\left\{1 + \sum_{l=2}^{L}\sum_{m=0}^{l}\left(\frac{a}{r}\right)^l [\bar{C}_{lm}\,\bar{R}_{lm}(\bar{\varphi}, \lambda) + \bar{D}_{lm}\,\bar{S}_{lm}(\bar{\varphi}, \lambda)]\right\}. \tag{2-12}$$

The gravitational potential U of the reference ellipsoid is uniquely defined by Stokes' constants, kM, a, f and ω (angular velocity of the earth's rotation). U is written in a series expression of Laplace harmonics of even degrees and order zero :

$$U = \frac{kM}{r}\left\{1 + \sum_{n=1}^{\infty}\left(\frac{a}{r}\right)^{2n} \bar{C}_{2n}^{\circ}\,\bar{R}_{2n\,0}(\bar{\varphi}, \lambda)\right\} \tag{2-13}$$

which does not include the potential of centrifugal force. The coefficients $\bar{C}_{2n}^{\circ}$ are computed from the given Stokes' constants (Heiskanen and Moritz, 1967, p. 73). We define the satellite-derived disturbing potential T_s by

$$T_s = V_s - U = \frac{kM}{r}\sum_{l=2}^{L}\sum_{m=0}^{l}\left(\frac{a}{r}\right)^l [\bar{C}_{lm}^{*}\,\bar{R}_{lm} + \bar{D}_{lm}\,\bar{S}_{lm}], \tag{1-14}$$

where negligibly small high degree terms in (2-13) are omitted, and $\bar{C}_{lm}^{*}$ are differences between coefficients in (2-12) and those of corresponding degree terms in (2-13).

In an approximation of the spherical earth, we write the satellite-derived disturbing potential T_s as

$$T_s = RG\sum_{l=2}^{L}\sum_{m=0}^{l} [\bar{C}_{lm}^{*}\,\bar{R}_{lm} + \bar{D}_{lm}\,\bar{S}_{lm}], \tag{2-15}$$

and the satellite-derived gravity anomaly Δg_s as

$$\Delta g_s = G\sum_{l=2}^{L}(l-1)\sum_{m=0}^{l} [\bar{C}_{lm}^{*}\,\bar{R}_{lm} + \bar{D}_{lm}\,\bar{S}_{lm}]. \tag{2-16}$$

The satellite-derived geoid undulations are computed from (2-15) by Bruns formula :

$$N_s = \frac{T_s}{G} \tag{2-17}$$

which expresses the global feature of the geoid undulations.

(3) Performance of Stokes' Integral in Combination with Satellite-Derived Gravitational Field

Stokes' integral (2-1) requires gravity anomalies distributed over whole surface of the earth. However, it cannot be expected at present to have terrestrial gravity data coverage over the whole surface of the earth. On the other hand, the terrestrial gravity data exist densely in some areas, by using which we can compute geoid undulatios gravimetrically. When we perform Stokes' integral only over a restricted area, say a spherical cap area whose angular radius is ψ_0 centered at the geoidal height computation point (see Figure 2), the error of the computed geoidal height caused by omitting gravities outside the cap is called truncation error.

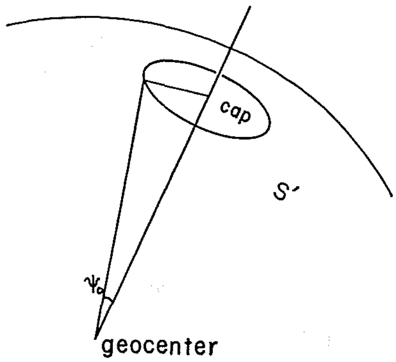

Figure 2 Spherical cap area.

Molodenskii et al. (1962), de Witte (1967) and Hagiwara (1970) evaluated this kind of error. Figure 3 shows the truncation errors evaluated around Japan when cap radius is 10°. To obtain Figure 3, the SAO-SE3 satellite-derived geopotential model (Gaposchkin et al., 1973) is used as the gravitational field outside the cap. Truncation errors are evaluated by the formula:

$$\delta N(\bar{\varphi}, \lambda) = \frac{R}{2G} \sum_{l=2}^{L} Q_l(\psi_0)\, \Delta g_l(\bar{\varphi}, \lambda), \tag{2-18}$$

where $Q_l(\psi_0)$ is Molodenskii truncation function when cap size is ψ_0 (Molodenskii et al., 1962, p. 147) and Δg_l is l-th degree Laplace spherical harmonics of gravity anomaly which is evaluated by

$$\Delta g_l = \Delta g_{sl} = G(l-1) \sum_{m=0}^{l} [\bar{C}^*_{lm} \bar{R}_{lm} + \bar{D}_{lm} \bar{S}_{lm}]. \tag{2-19}$$

The SAO-SE3 geopotential model is composed of a complete geopotential coefficients set up to degree and order 18, then we put $L=18$ in equation (2-18). Hagiwara (1970) obtained the same kind of figure as Figure 3. There exist some numerical differences between two figures since Hagiwara took a different gravity model. Although Figure 3 does not include the effects of more detailed structures of the gravity anomaly field than degree 18, Figure 3 is approximately varid. Because the effects are estimated to be only around one meter (see the curves for $\psi_0=10°$ in Figures 30a, b in Chapter 4). The detailed discussions concerning with truncation error problems will be found in Chapter 4.

As seen in Figure 3, the truncation errors are quite large even in a relative sense, 10 m error difference over Japan area. Therefore, Stokes' integral should be performed by adopting some gravity anomaly informations outside the cap, where terrestrial gravity data do not exist. In this case we adopt satellite-derived gravity anomaly field as the additional gravity data. Though the satellite derived gravity anomaly field includes only low degree terms, a great improvement in diminishing the truncation errors is expected because there will be left the truncation effects only of higher degree terms

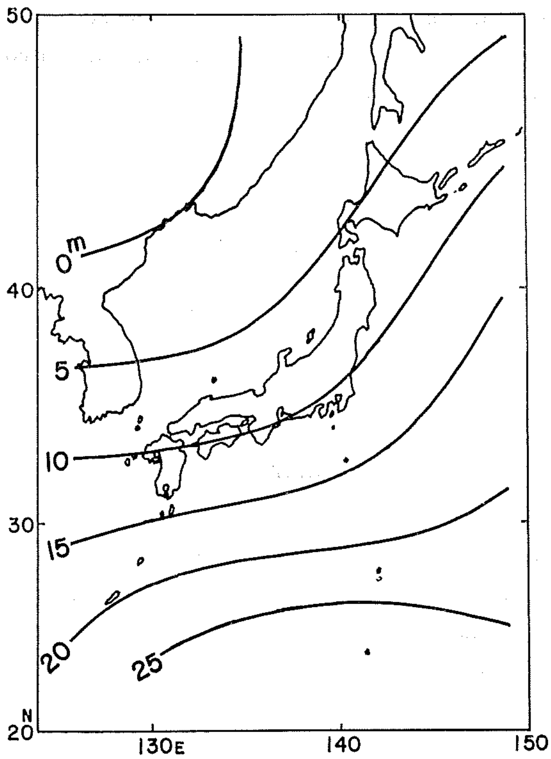

Figure 3 Geoidal height truncation errors for $\psi_0=10°$ evaluated by using SAO-SE3 geopotential coefficient set (18, 18).

than the satellite-derived gravitational field which are the order of one meter as mentioned before.

Let S' be the remaining area of the earth's surface outside the cap (see Figure 2), and we reform Stokes' integral as follows:

$$N=N_{in}+N_{out}, \tag{2-20a}$$

where

$$N_{in}=\frac{R}{4\pi G}\iint_{cap} \Delta g\, S(\psi)\, d\sigma, \tag{2-20b}$$

$$N_{out}=\frac{R}{4\pi G}\iint_{S'} \Delta g_s\, S(\psi)\, d\sigma, \tag{2-20c}$$

and Δg_s is the satellite-derived gravity anomaly given by (2-16). From (2-20a, b, c) we obtain another expression of Stokes' integral:

$$N=N_R+N_S \tag{2-21a}$$

where

$$N_R=\frac{R}{4\pi G}\iint_{cap} (\Delta g-\Delta g_s)\, S(\psi)\, d\sigma, \tag{2-21b}$$

$$N_S=\frac{R}{4\pi G}\iint_{\sigma} \Delta g_s\, S(\psi)\, d\sigma. \tag{2-21c}$$

N_S is equivalent to the satellite derived long wave-length components of geoid undulations which can be evaluated by (2-17), and N_R is the residual short wave-length components of geoid undulations which can be evaluated by integration of residual gravity anomaly $\Delta g - \Delta g_s$ over the cap. Accordingly, numerical integration is necessary only for N_R. We know the undulation of the geoid reaches up to ± 100 m and the average height of the undulation is aroual ± 30 m on the world-wide basis. The total effect of the short wave-length components on the geoid undulation of higher degrees than 20 is estimated to be around ± 4 m on the world-wide average basis (see Chapter 4). Since N_R takes a value much smaller than N_S, some approximation techniques may be applicable to the evaluation of N_R.

3. Computation of a Gravimetric Geoid Around Japan

(1) Numerical Integration of Stokes' Formula

When we perform numerical integration (2-21b), we replace the integral by a summation by using average values of gravity anomalies over certain sized blocks, such as

$$N_R = \frac{R}{4\pi G} \sum_i \overline{\delta g}_i \, q_i, \tag{3-1}$$

where $\overline{\delta g}_i$ is the block mean of the residual gravity anomaly over the i-th block inside the cap area, which is computed from block mean surface gravity anomaly $\overline{\Delta g}_i$ and block mean satellite-derived gravity anomaly $\overline{\Delta g}_{si}$ as follows:

$$\overline{\delta g}_i = \overline{\Delta g}_i - \overline{\Delta g}_{si}. \tag{3-2}$$

In (3-1) q_i is the integration of Stokes' function over the i-th block σ_i, i. e.

$$q_i = \iint_{\sigma_i} S(\psi)\, d\sigma_i\,. \tag{3-3}$$

In the numerical integration of q_i, a block is divided into some subblocks, and the number of subblocks is chosen correspondingly to the size of the block and relative distance between the geoidal height computation point and the block. $\overline{\Delta g}_{si}$ is calculated from (2-16), in the spherical approximation, as

$$\begin{aligned}\overline{\Delta g}_{si} &= \frac{1}{S_i} \iint_{\sigma_i} \Delta g_s\, d\sigma_i \\ &= G \sum_{l=2}^{L} (l-1) \sum_{m=0}^{l} \left[\bar{C}^*_{lm} \frac{1}{S_i} \iint_{\sigma_i} \bar{R}_{lm}\, d\sigma_i + \bar{D}_{lm} \frac{1}{S_i} \iint_{\sigma_i} \bar{S}_{lm}\, d\sigma_i \right]\end{aligned} \tag{3-4}$$

where S_i is the area of block σ_i. Since the satellite-derived gravity anomaly is composed of long wave-length components of the gravity anomaly field, $\overline{\Delta g}_{si}$ is replaceable by a point anomaly Δg_{si} given at the center of block σ_i.

(2) Terrestrial Block Mean Gravity Anomalies

The main problem in the computation of geoidal heights is the preparation of terrestrial gravity anomaly data. The block mean gravity anomalies are read from gravity anomaly maps, or estimated from observed point gravities in and around blocks. The gravity measurements on land and at sea around Japan have been made by various institutions not only in Japan but also in other countries, and gravity anomaly maps have been published. The author prepares block mean gravity anomalies in the land area of Japan and the adjacent seas of Japan on the basis of gravity anomaly maps: GSI (1970), Tomoda and Segawa (1971), Segawa and Bowin (1976), Segawa (1970b, 1976), JHD's gravity anomaly maps (1970—1977), published as a part of series of the Basic Map of the Sea), Stroev (1971), and Ganeko et al. (1978). In reading the block mean gravity anomalies, the basic block size is selected in accordance with the estimated accuracy and the reduced scale of each gravity anomaly map, i. e. equiangular blocks $5' \times 5'$, $10' \times 10'$, $15' \times 15'$ and $30' \times 30'$ are taken. A block bordered by meridians of latitude $S°$ and parallels of longitnde $S°$ is called equiangular "$S° \times S°$ block". On the other hand, we nominate "$S°$ block" for a block formed by partitioning the earth's surface into near-equal areas as an area of $S° \times S°$ block at the equator.

The block gravity anomaly means obtained from the gravity anomaly maps are reduced to $30' \times 30'$ and $1° \times 1°$ block means for the geoidal height computations. The reductions are made by taking averages of smaller blocks included in each $30' \times 30'$ and $1° \times 1°$ blocks. Area A in Figure 4 indicates the area where $30' \times 30'$ block mean gravity anomalies are estimated. The accuracy of the $30' \times 30'$ block means is estimated to be $\pm 10 \sim \pm 18$ mGals from the gravity data density on the assumptions of 10 mGals contouring error of gravity anomaly maps, 10 mGals reading error of $10' \times 10'$ block means

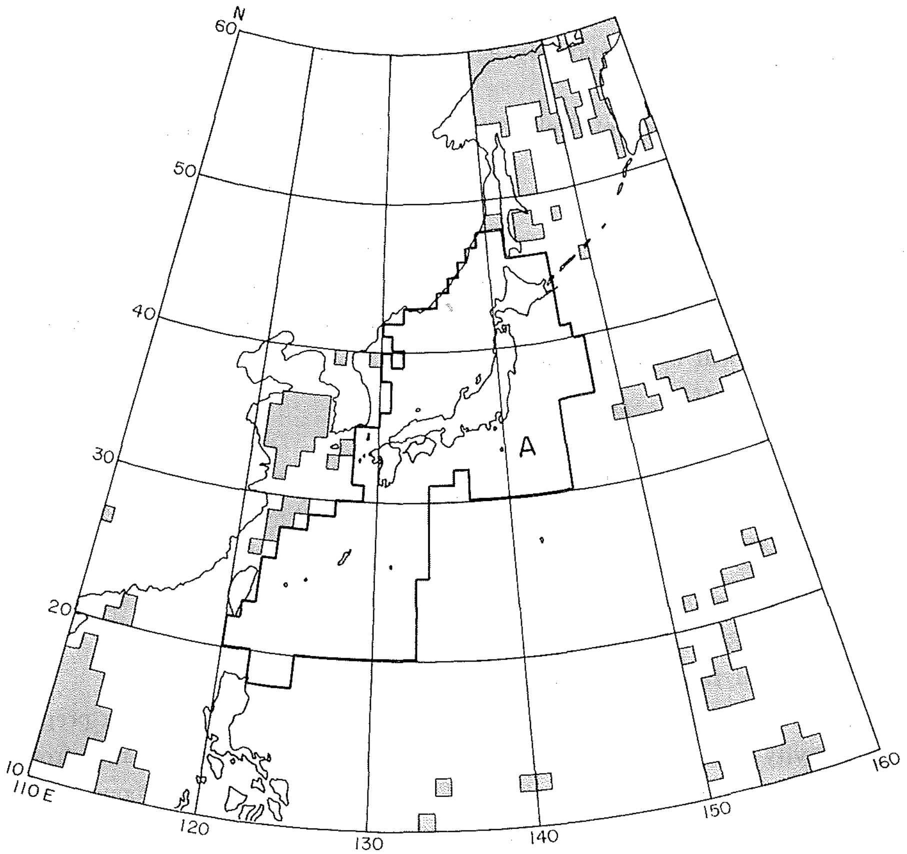

Figure 4 JHDGF-1 gravity anomaly file area: area A. The shaded areas include no gravity data in the world-wide $1° \times 1°$ block mean gravity data files.

and 15 mGals reading error of $15' \times 15'$ and $30 \times 30'$ block means. Although the contouring error may bring about some amount of error correlations among block means located near each other, we neglect the effects because of difficulties in evaluating the effects and consider the contouring errors are random in each block. The reading errors are also considered to be random. Some systematic errors are possibly included in the blocks near and along the coasts of USSR. Fortunately, the possible systematic errors may not cause large geoidal height errors near Japan and in the Pacific area.

The read and reduced block means, i. e. $10' \times 10'$, $15' \times 15'$, $30' \times 30'$ and $1° \times 1°$ block means, are compiled into a machine readable magnetic tape file named as JHDGF-1 (Japan Hydrographic Department Gravity File). The gravity anomalies are based on the JGSN 75 System (Suzuki, 1976) and the Geodetic Reference System 1967 (IAG, 1971). $30' \times 30'$ block mean gravity anomalies compiled into JHDGF-1 are listed in Appendix B.

Since the surface gravity data included in JHDGF-1 file are not sufficient to compute geoid undulations around Japan, other gravity data have to de introduced. We use $1° \times 1°$ block mean anomalies of DMAAC* and Watts and Leeds (1977, referred as LAMONT from now on in this paper) for the area outside the JHDGF-1 region of Figure. 4. The weighted means are taken over the comon $1° \times 1°$ blocks of DMAAC and LAMONT data sets by using the accuracy estimates in DMAAC data and ± 8 mGals equal accuracy assigned to LAMONT data for convenience' sake to produce higher weights than DMAAC data because of high reliability of LAMONT data in the Northwest Pacific area (Watts, private communication). DMAAC data are used on the continental areas where there are no LAMONT data coverage. All the $1° \times 1°$ block means are referred to the Geodetic Reference System 1967. The $1° \times 1°$ blocks which have no gravity anomaly means are indicated by the shaded blocks in Figure 4.

A data file is produced by weighted means of DMAAC and LAMONT. The differences of $1° \times 1°$ block means between JHDGF-1 and this data file is examined over the common blocks, and the histogram of the differences is shown in Figure 5. The total number of common $1° \times 1°$ blocks amounts to 354, the mean difference is -1.1 mGals, and the r. m. s. difference is 13. 6 mGals. We find no large systematic difference between these two data files. From the 13. 6 mGals r. m. s. difference, we may conclude that the average accuracy of $1° \times 1°$ block means in JHDGF-1 is less than 10 mGals. Other statistical characteristics of JHDGF-1 will be investigated in Chapter 5.

(3) Satellite-Derived Gravity Anomalies and Global Geoid Undulations

GEM-9 geopotential model (Lerch et al., 1977) is one of the most recent geopotential coefficient sets derived from satellite tracking data including accurate laser tracking data of high density satellites such as Peole, Starlette and Lageos. GEM-9 model is composed of a complete geopotential coefficient set up to degree and order 20 and some coefficients of resonance terms up to degree 30.

GEM-10 model (Lerch et al., ibid.) was derived by combination of GEM-9 solution and 5° block surface mean gravity anomalies. The model is composed of a complete

* Defence Mapping Agency/Aerospace Center $1° \times 1°$ mean freeair gravity anomaly set (1976)

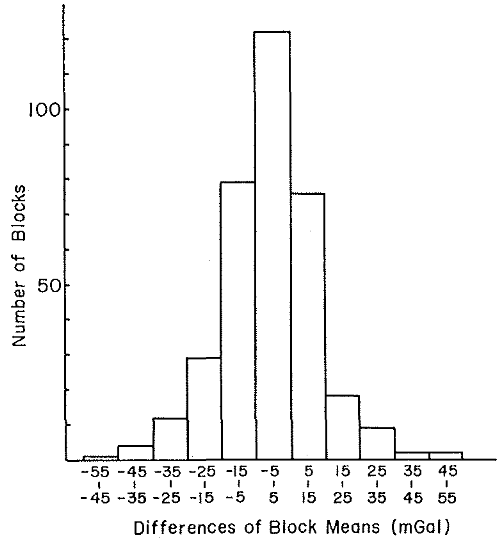

Figure 5 Histogram of the differences of $1°\times1°$ block mean gravity anomalies between JHDGF-1 and the weighted means of DMAAC's and LAMONT's.

geopotential coefficient set up to degree and order 22 and some coefficients of resonance terms up to degree 30. GEM-9 and GEM-10 solutions recomended to use the following physical constants of the earth ellipsoid:

$$\left.\begin{array}{ll} kM=398600.64 & \mathrm{km^3/sec^2}, \\ a=6378140 & \mathrm{m}, \\ f=1/298.255. & \end{array}\right\} \quad (3\text{-}5)$$

The estimated possible errors of the constants are $\pm 0.02\,\mathrm{km^3/sec^2}$ for kM and ± 1 m for a. The accuracies of the geopotential coefficients are estimated to be 1.9 m and 1.5 m respectively for GEM-9 and GEM-10 solutions on the global basis. We adopt the geopotential coefficient set of GEM-10 solution for the satellite-derived gravity anomaly field in the computation of a detailed gravimetric geoid around Japan. Figure 6 is the long wave-length geoid undulations around Japan computed by (2-17) from the geopotential coefficients of GEM-10 solution.

We need one more physical constant ω (angular velocity of the earth's rotation) of the reference ellipsoid to compute the normal gravitational field (2-13), adopting

$$\omega=7.2921151\times10^{-5} \quad 1/\mathrm{sec}. \quad (3\text{-}6)$$

In order to make the surface gravity data compatible with the satellite-derived gravity anomalies, the block mean gravity anomalies based on JGSN 75 and the Geodetic Reference System 1967 must be converted into a new system with adopted Stokes' constants (3-5) and (3-6). The conversions are made by using the equation:

$$\Delta g_{new}=\Delta g_{JGSN75}+\gamma_{1967}-\gamma_{new}, \quad (3\text{-}7)$$

where γ_{1967} and γ_{new} are normal gravities on the reference ellipsoids with Stokes' constants of the Geodetic Reference System 1967, i. e. $kM=398603\,\mathrm{km^3/sec^2}$, $a=6378160$ m, $f=1/298.247167$, $\omega=7.29211515\times10^{-5}$ 1/sec, and newly adopted Stokes' constants (3-5) and

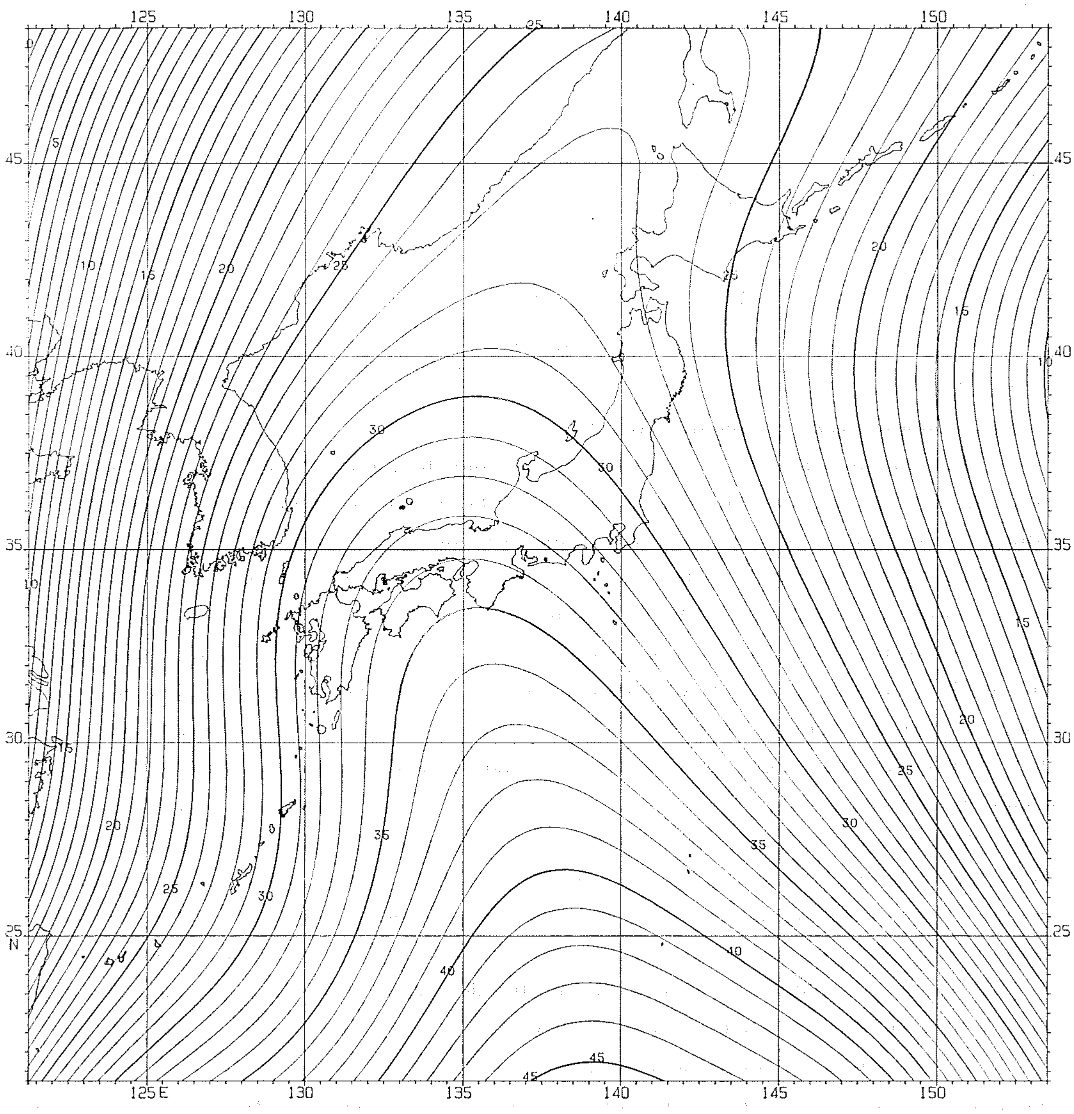

Figure 6 GEM-10 global geoid around Japan. Contour interval: 1 m.

(3-6). Normal gravity on the ellipsoid is given by

$$\gamma = \frac{a\gamma_a \cos^2\varphi + b\gamma_b \sin^2\varphi}{(a^2\cos^2\varphi + b^2\sin^2\varphi)^{\frac{1}{2}}} \tag{3-8}$$

(Heiskanen and Moritz, 1967, p. 70), where φ is geographic latitude and $b = a(1-f)$. γ_a (normal gravity at the equator) and γ_b (normal gravity at the pole) are computed by the formulas (ibid., p. 67):

$$\left.\begin{aligned} \gamma_a &= \frac{kM}{ab}\left(1 - m - \frac{m}{6}\ \frac{e'q'_0}{q_0}\right), \\ \gamma_b &= \frac{kM}{a^2}\left(1 + \frac{m}{3}\ \frac{e'q'_0}{q_0}\right), \end{aligned}\right\} \tag{3-9}$$

where

$$\left.\begin{aligned} m &= \frac{\omega^2 a^2 b}{kM}, \\ e' &= \left(\frac{a^2-b^2}{b^2}\right)^{\frac{1}{2}}, \end{aligned}\right\} \tag{3-10}$$

and

$$\left.\begin{aligned} q_0 &= \frac{1}{2}\left[\left(1+\frac{3}{e'^2}\right)\tan^{-1}e' - \frac{3}{e'}\right], \\ q'_0 &= 3\left(1+\frac{1}{e'^2}\right)\left(1-\frac{1}{e'}\tan^{-1}e'\right)-1. \end{aligned}\right\} \tag{3-11}$$

Ae we see in equations (3-8), (3-9), (3-10) and (3-11), the normal gravity is uniquely defined by Stokes' constants.

(4) Computation of Geoidal Heights

We have finished the preparation for geoidal height computations in the previous sections, and we perform the computation actually in this section. We adopt the cap radius $\psi_0=20°$ and divide the cap area into two parts at $\psi=10°$. $30'\times30'$ block mean gravity anomalies are used in the area of $\psi=0°$ to $10°$ (inner cap), and $1°\times1°$ block mean gravity anomalies are used in the remaining area of the cap from $\psi=10°$ to $20°$ (outer cap). When a $1°\times1°$ block in the inner cap has no $30'\times30'$ block means in it, the $1°\times1°$ block is considered to be composed of four $30'\times30'$ blocks which have the same values of gravity anomaly means as the $1°\times1°$ block. 26 mGals error is assigned to such $30'\times30'$ block means. Zero gravity anomaly and 30 mGals error are assigned to $1°\times1°$ blocks of no gravity data.

At the centers of each $30'\times30'$ block, satellite-derived gravity anomalies are evaluated and they are adopted as the $30'\times30'$ block means of the satellite-derived gravity anomaly instead of evaluating (3-4) strictly. $1°\times1°$ block means of satellite-derived anomaly are given by the average values of four $30'\times30'$ block means. These approximations seem to be plausible because the satellite-derived gravity anomaly changes almost linearly in a small area such as $30'\times30'$ block.

The computations of geoidal heights are carried out at the center of each $30'\times30'$ block, i. e. at every $30'\times30'$ mesh point. q_i in (3-3) is calculated by dividing block σ_i into subblocks. $30'\times30'$ block is divided into 25 subblocks when the distance between the geoidal height computation point and the center of the block is less than $1.5°$, i. e. when $\psi\leqq1.5°$. On the other hand, we take 9 subblocks when $1.5°<\psi\leqq3°$. No subdivisions are made for the $30'\times30'$ blocks when $\psi>3°$ and for $1°\times1°$ blocks in the outer cap area. The residual geoid undulations N_R are computed around Japan using (3-1). Figure 7 shows thus computed residual geoid undulations. We see much detailed features of geoid undulations than satellite-derived ones (cf. Figure 6). It is matter of course that the shorter wave-length undulations than $30'\times30'$ block size, the smallest block size adopted, are not included in this residual geoid. Deep geoidal valleys are found along the trenches and shallow geoidal basins are extending in Japan Sea, Philippine Sea and the Northwest Pacific area. Geoidal highs exist along the island arcs, Korea Peninsula and the continental coast.

We obtain the final results of geoidal height computation by adding the residual geoid Figure 7 to the satellite-derived global geoid Figure 6. The produced final results, i. e. $30' \times 30'$ detailed gravimetric geoid around Japan, are shown in Figure 8. Figure 7 and Figure 8 include a wider area than the JHDGF-1 region (see Figure 4), so that Figures 7 and 8 are for $1° \times 1°$ geoids outside the JHDGF-1 region. Watts and Leeds (1977) computed a gravimetric geoid in the Northwest Pacific Ocean based on their own $1° \times 1°$ block gravity means, and their geoid map includes the area of Figure 8. Comparing these two geoid maps, more detailed geoid undulations can be seen in Figure 8 than Watts and Leeds' because of detailed informations of the gravity anomaly field brought into by smaller block-size.

One of the marked features of the present geoid undulations is over the trench areas characterized by large negative gravity anomalies. Figure 9 shows the geoid section along the parallel at latitude 35° 15′. 22 meters geoidal dent relative to GEM-10 global geoid is seen along the axis of the negative gravity anomalies over the trench. If the geoidal dent is compared with the geoidal high at the mountainous area of the central Japan, the relative undulation of the geoid reaches 26 m within 400 km horizontal distance. The steep geoidal slopes in the land areas accompanied by the geoidal dents over the trench areas are seen at Kanto District and at the southern half of Hokkaido.

Ganeko (1976) obtained an astrogeodetic geoid of Japan by applying a statistical interpolation technique to deflections of the vertical. The relative geoid undulation on the land areas of Japan are compared between the astrogeodetic geoid, converted into SAO-SE3 global geodetic system and shown in Figure 10, and the gravimetric geoid shown in Figure 8. The comparisons are made at every $30' \times 30'$ grid point inside the land areas of Japan, and the standard deviation of 1.4 m is obtained while the standard deviation decreases to 0.8 m when Hokkaido area is excluded. The agreement between two kinds of geoid is fairly good. The geoidal slope to the south in Hokkaido is not so marked in the astrogeodetic geoid as in the gravimetric geoid. On the other hand, we see some amount of geoidal slope to the north in the astrogeodetic geoid at the northern half of Hokkaido, which is not seen in the gravimetric geoid. It is, therefore, considered that there may exist a tilt in the astrogeodetic geoid at Hokkaido probably because of sparse deflection observations at Hokkaido. It may be noted that the geoidal slope at Kanto District seems to have caused a shift of Tokyo Datum to the southeast relative to the global geodetic system.

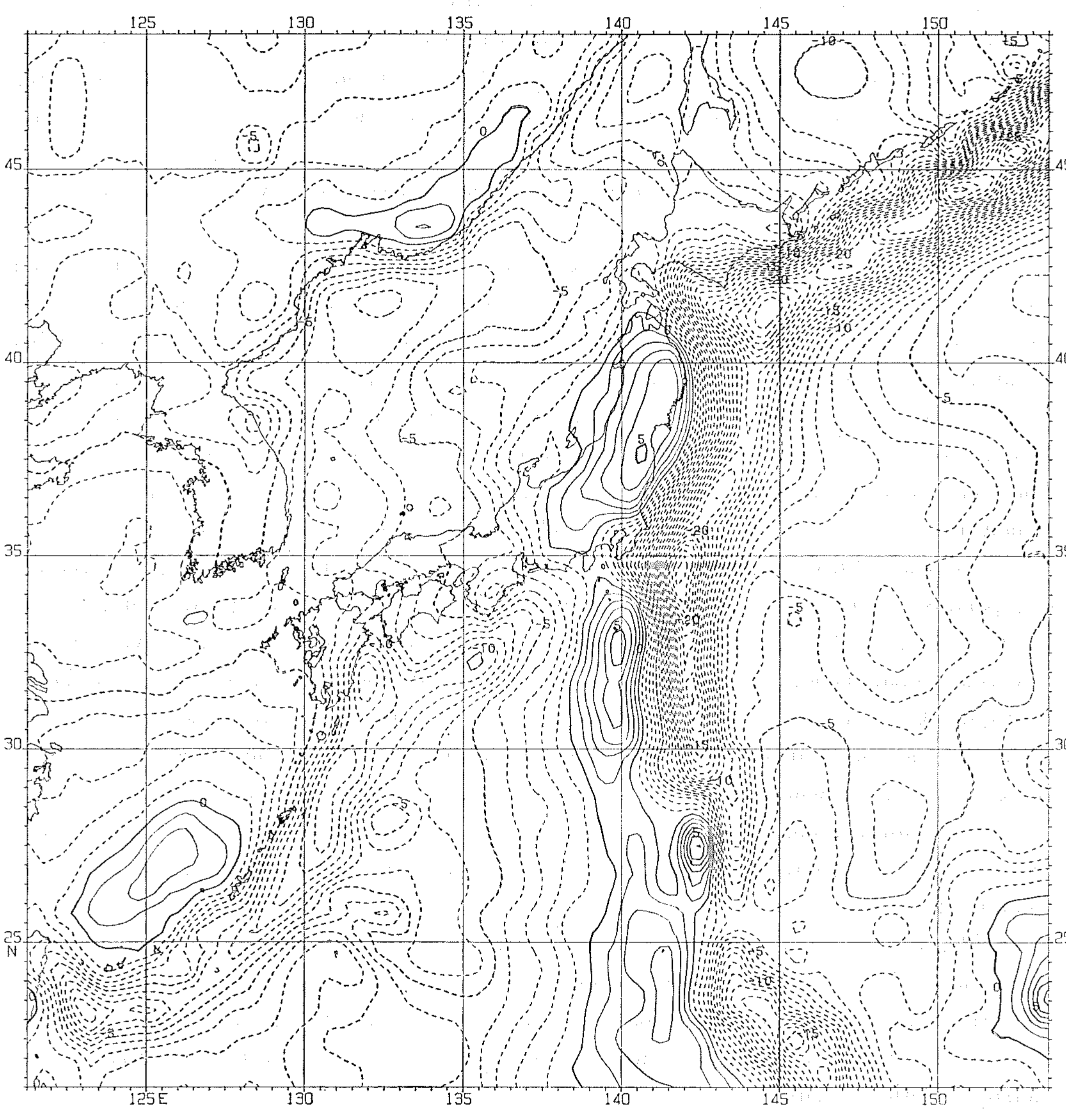

Figure 7 30′×30′ residual geoid on the reference surface: GEM-10 global geoid. Contour interval: 1 m. Broken lines are for negative geoid equiundulation.

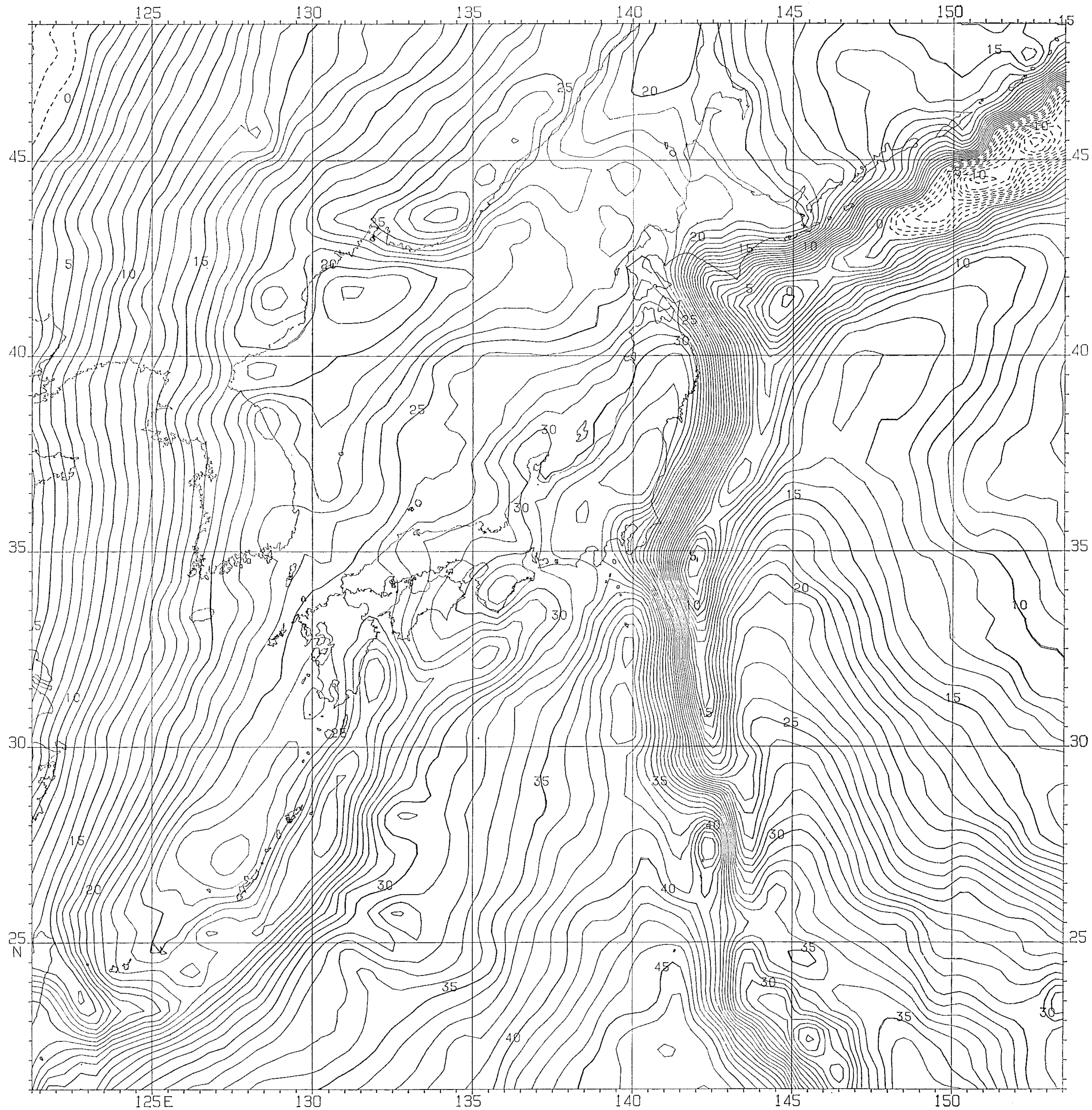

Figure 8 30′×30′ detailed gravimetric geoid computed in combination with GEM-10 geopotential coefficient set and surface gravities of 30′×30′ and 1°×1° block means. Contour interval: 1 m.

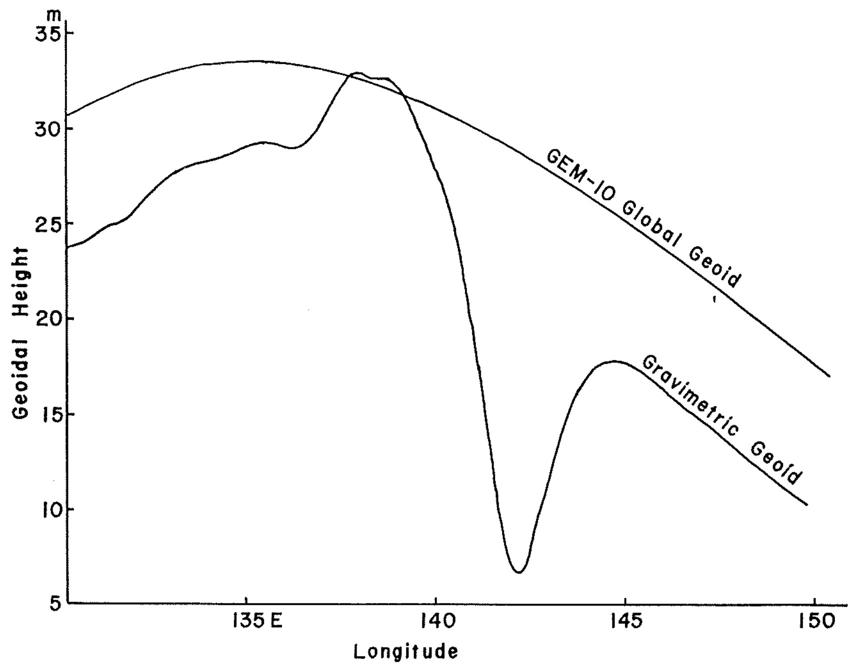

Figure 9 Sections of the GEM-10 global geoid and the 30′×30′ gravimetric geoid along the parallel at latitude 35° 15′ N.

(5) Comparisons Between Computed Gravimetric Geoid and Geos-3 Altimeter Data

Geos-3 satellite launched in April, 1975, has made a great deal of altimeter observations of the sea surface heights (e. g. Kearsley, 1977; Rapp, 1977a; Marsh et al., 1978). In addition, there are some altimeter data in the region of Figure 8. It is quite interesting and valuable to compare the altimeter data and the gravimetric geoid, so that we use altimeter data taken along the subsatellite tracks shown in Figure 11, which have been supplied from NASA (Stanley, 1978, private eommunication). The numbers attached to each track in Figure 11 are the revolution numbers of Geos-3. The tracks with four digits revolution numbers are the data taken at the early stage of the satellite, i. e. from July, 1975 to September, 1975, and those with five digits revolution numbers are the data at later stage, i. e. from August, 1977 to September, 1977. In the former revolutions, large errors exceeding 20 m are occasionally included in the radial component of the satellite positions (Stanley, 1978, private communication). That is seen in revolutions 1411 (see Figure 13) and 2051 (see Figure 17). In the latter revolutions, the accuracy of satellite positions has been improved (ibid.) (see Table 1).

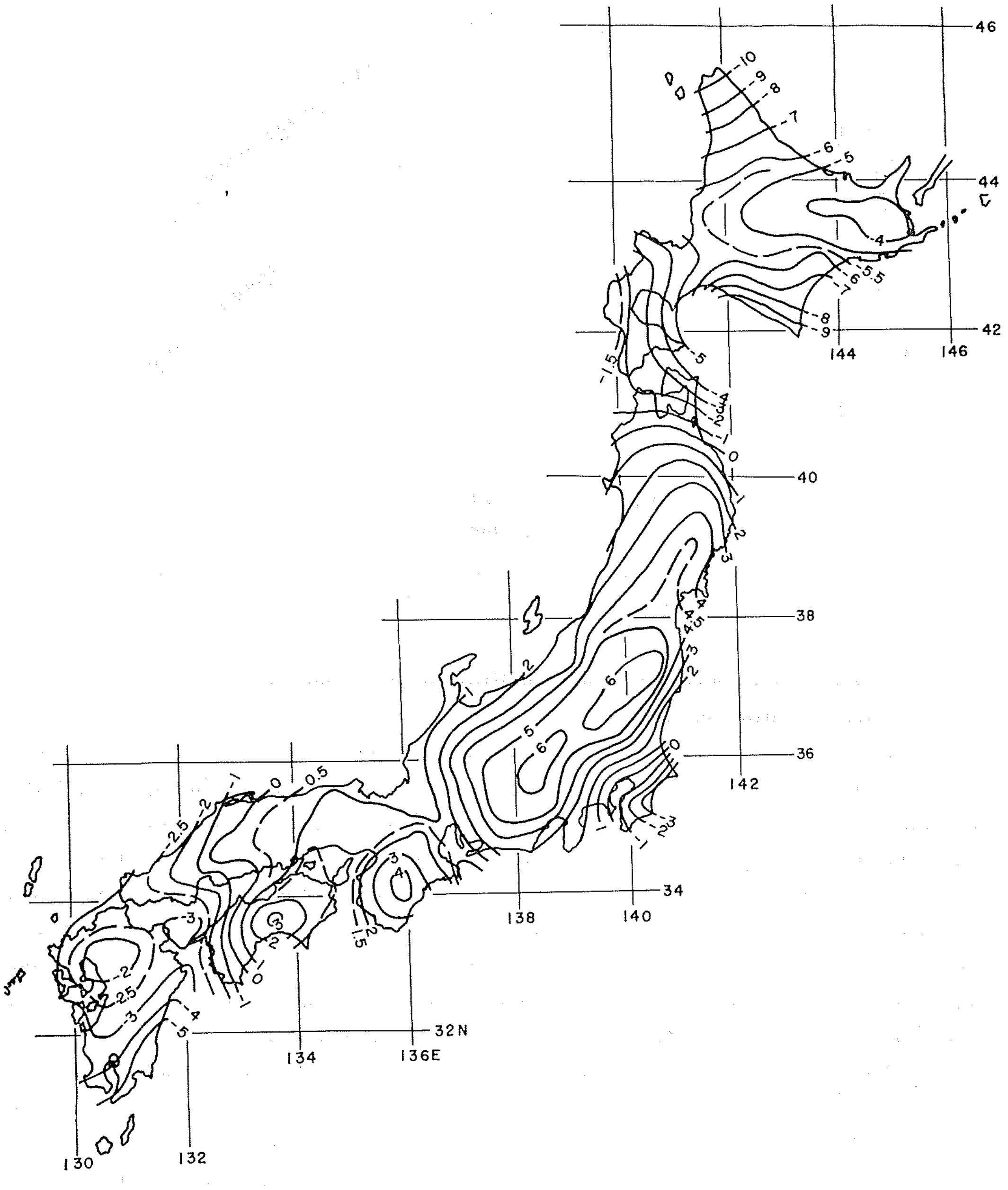

Figure 10 Astrogeodetic geoid of Japan converted into SAO-SE3 global geodetic system (Ganeko, 1976). Contour interval: 1 m.

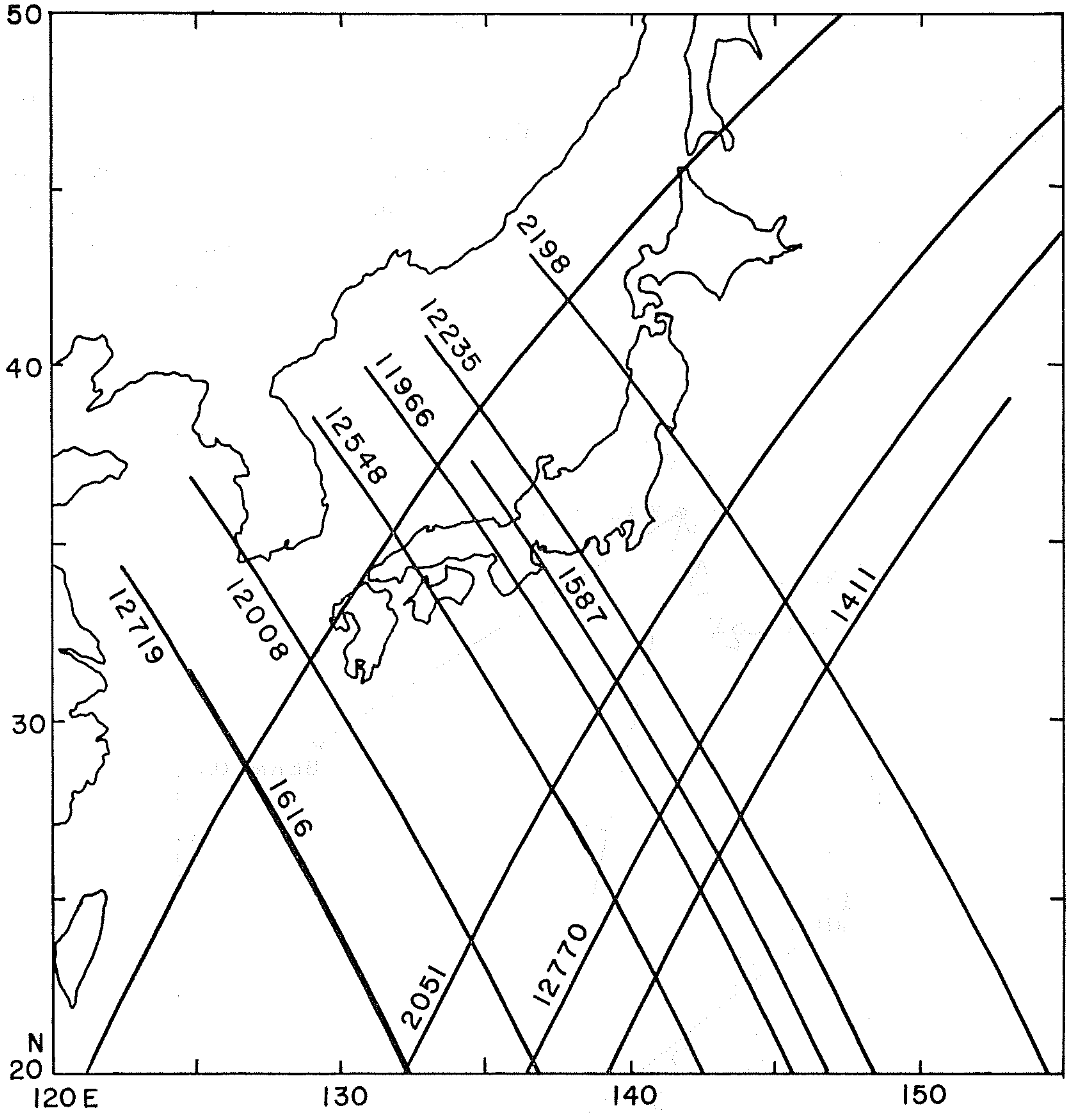

Figure 11 Geos-3 altimetry subsatellite tracks with revolution numbers of the satellite.

The sea surface height determined by the Geos-3 altimeter is the distance between sea surface and the reference ellipsoid whose parameters are $a=6378145$ m and $f=1/298.255$. Altimeter data were calibrated by using laser tracking data obtained at the satellite tracking stations located in the Geos-3 calibration area which is shown in Figure 12 (Leitao et al., 1975).

Figures 13～24 show altimetric sea surface heights, gravimetric geoid profiles along the subsatellite tracks and the differences between altimetric sea surface heights and gravi metric geoidal heights for each revolution in Figure 11. All the altimeter data used here are observations by the short pulse mode (ibid.), and altimeter data rate is 0.1 sec. Altimeter data form a unit data set, called "frame", with 32 or 20 observations corresponding to the adopted telemeter system of high or low data rate. Hence, the period of one frame is 3.276964 sec. or 2.048102 sec., and the period is corresponding to a subsatellite track length of about 22 km or 14 km, respectively. The individual sea surface heights plotted in Figures 13～24 are the average values of altimeter data included in each frame. Distinctions of telemeter systems adopted in each revolution are tabulated in Table 1.

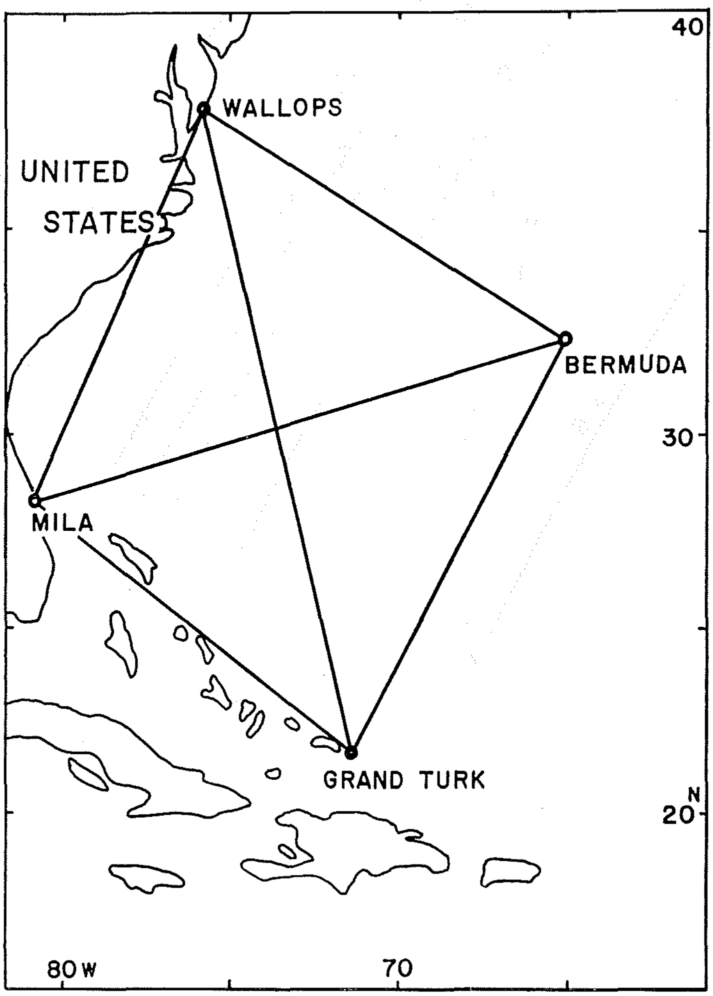

Figure 12 Geos-3 altimeter calibration area (Leitao et al., 1975).

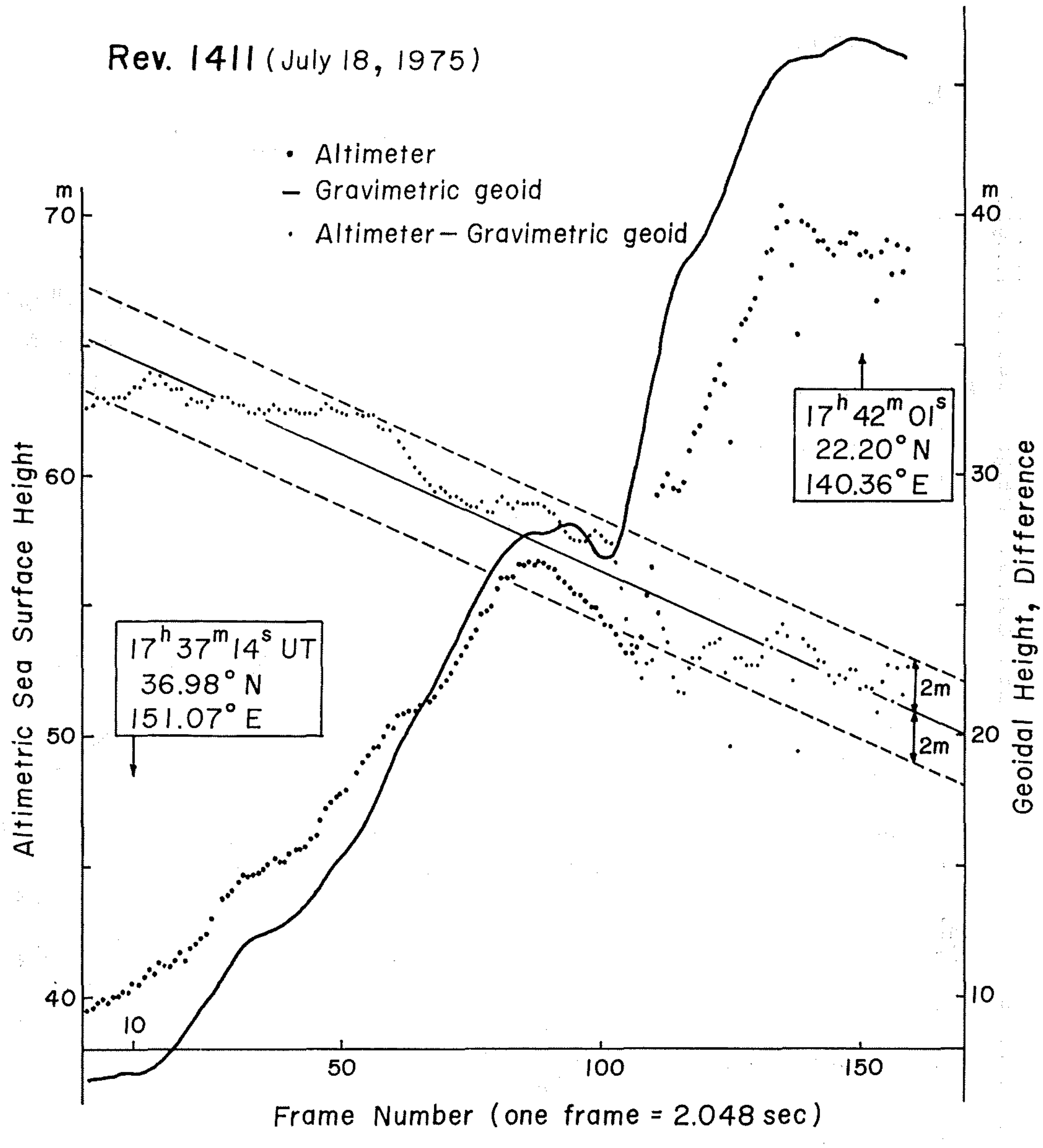

Figure 13 Comparison between Geos-3 altimetric profile (Rev. 1411) and the gravimetric geoid.

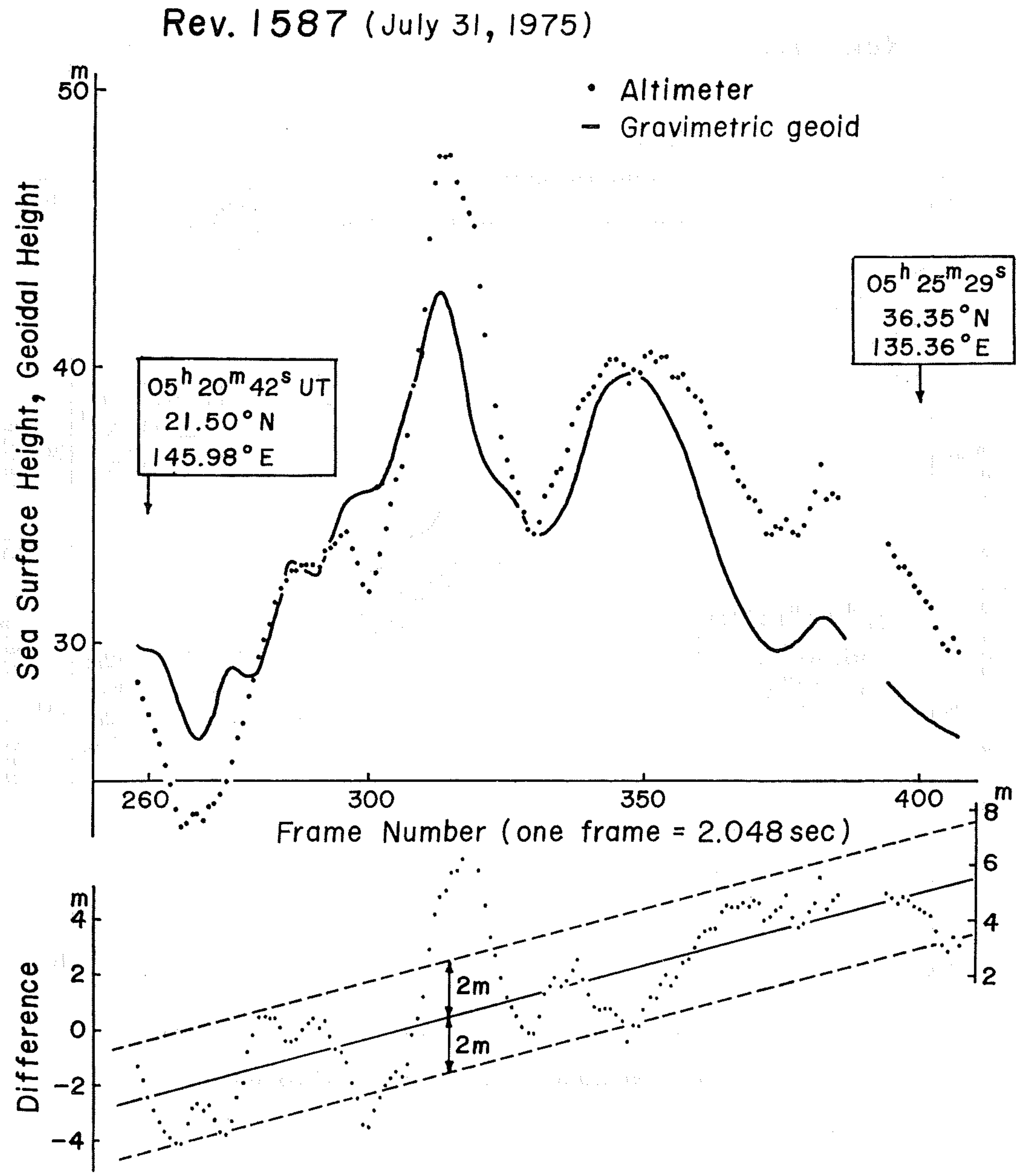

Figure 14 Comparison between Geos-3 altimetric profile (Rev. 1587) and the gravimetric geoid.

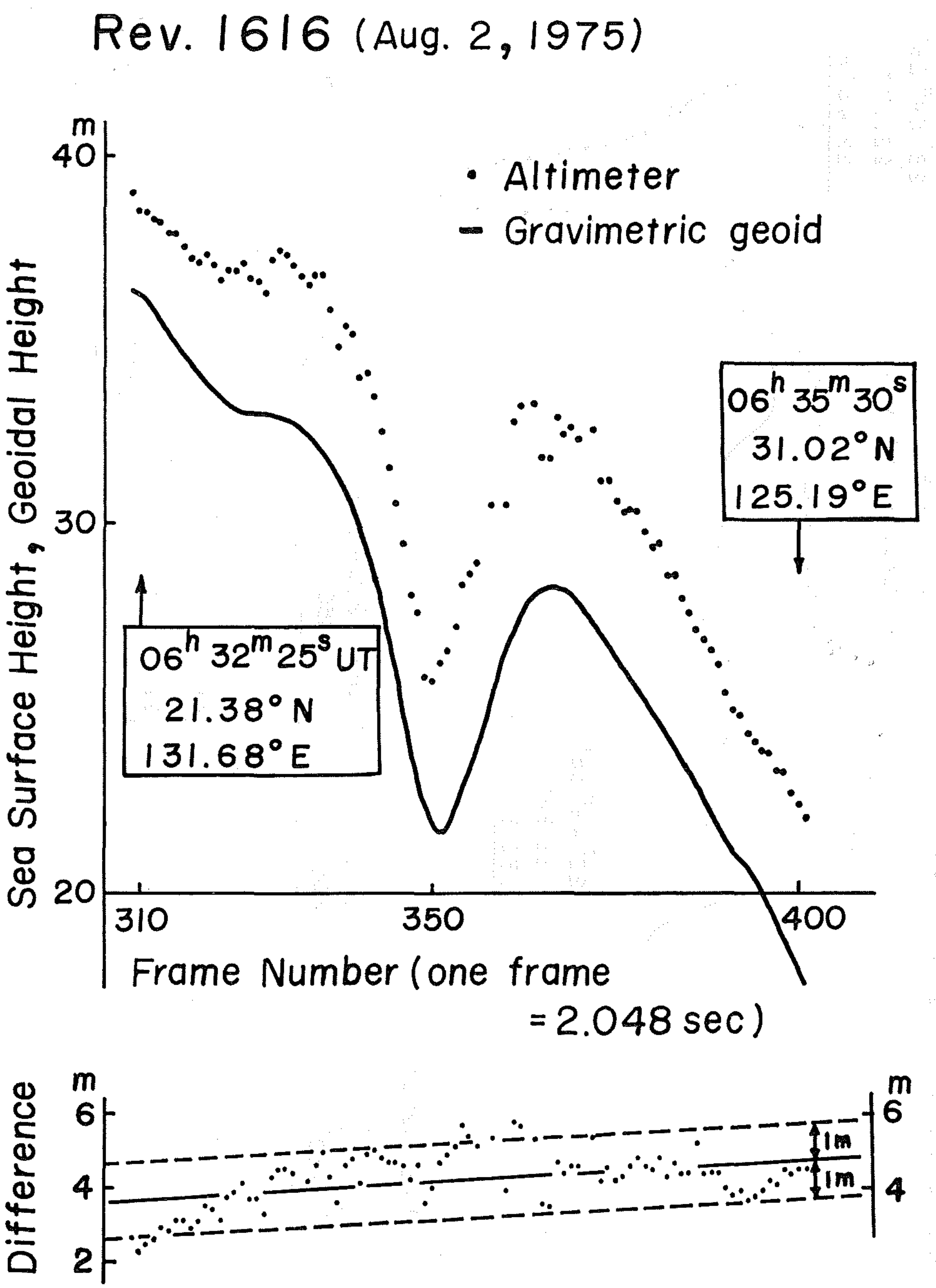

Figure 15 Comparison between Geos-3 altimetric profile (Rev. 1616) and the gravimetric geoid.

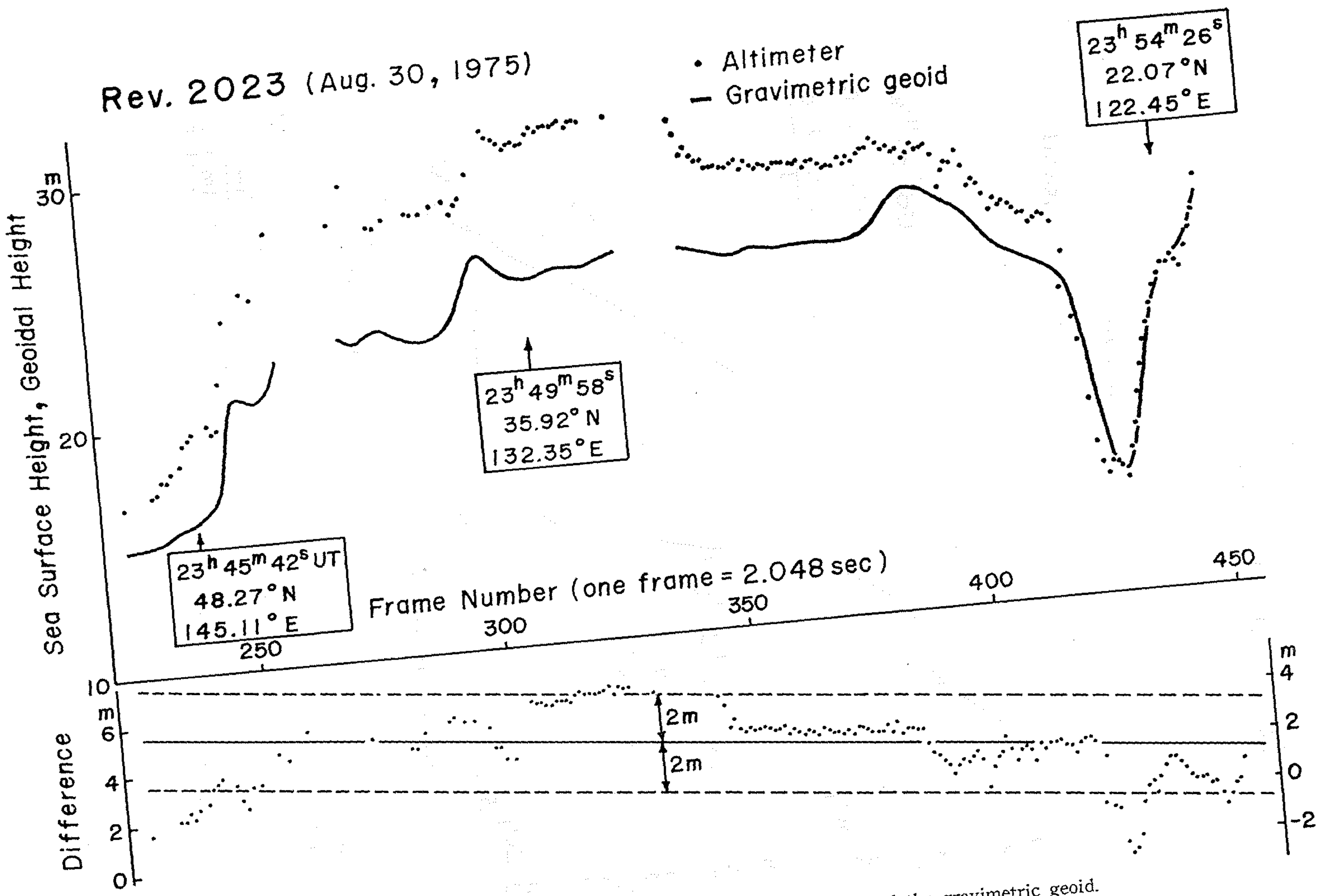

Figure 16 Comparison between Geos-3 altimetric profile (Rev. 2023) and the gravimetric geoid.

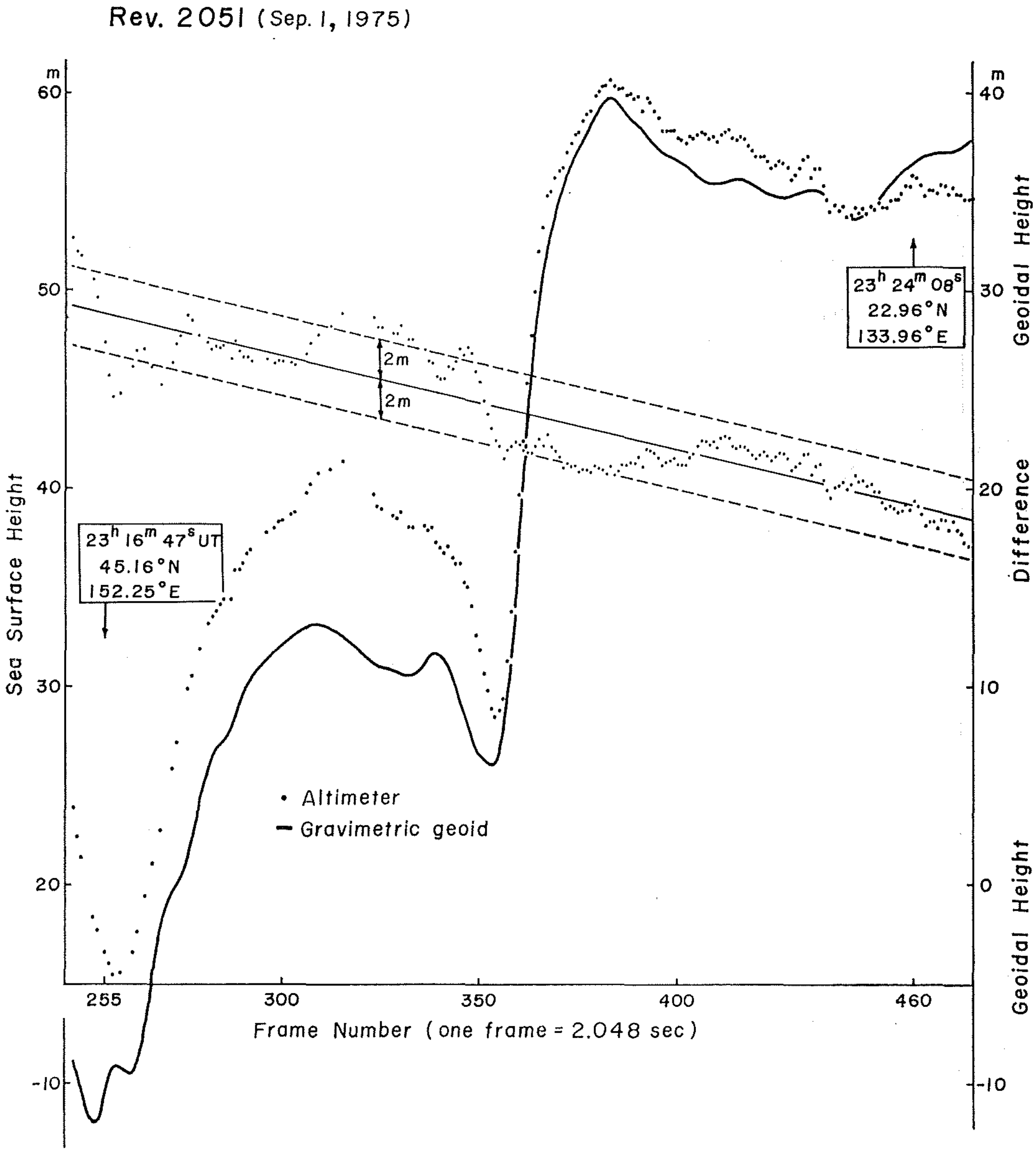

Figure 17 Comparison between Geos-3 altimetric profile (Rev. 2051) and the gravimetric geoid.

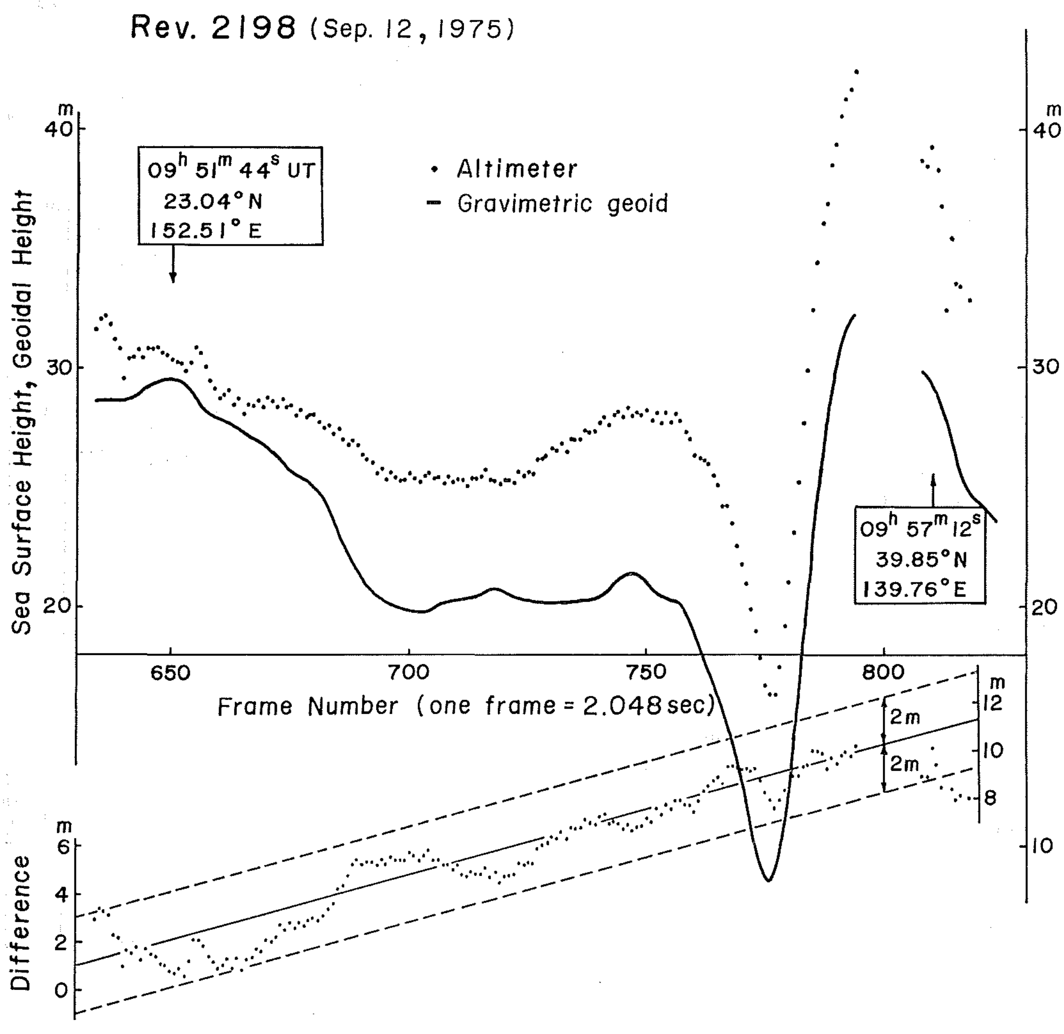

Figure 18 Comparison between Geos-3 altimetric profile (Rev. 2198) and the gravimetric geoid.

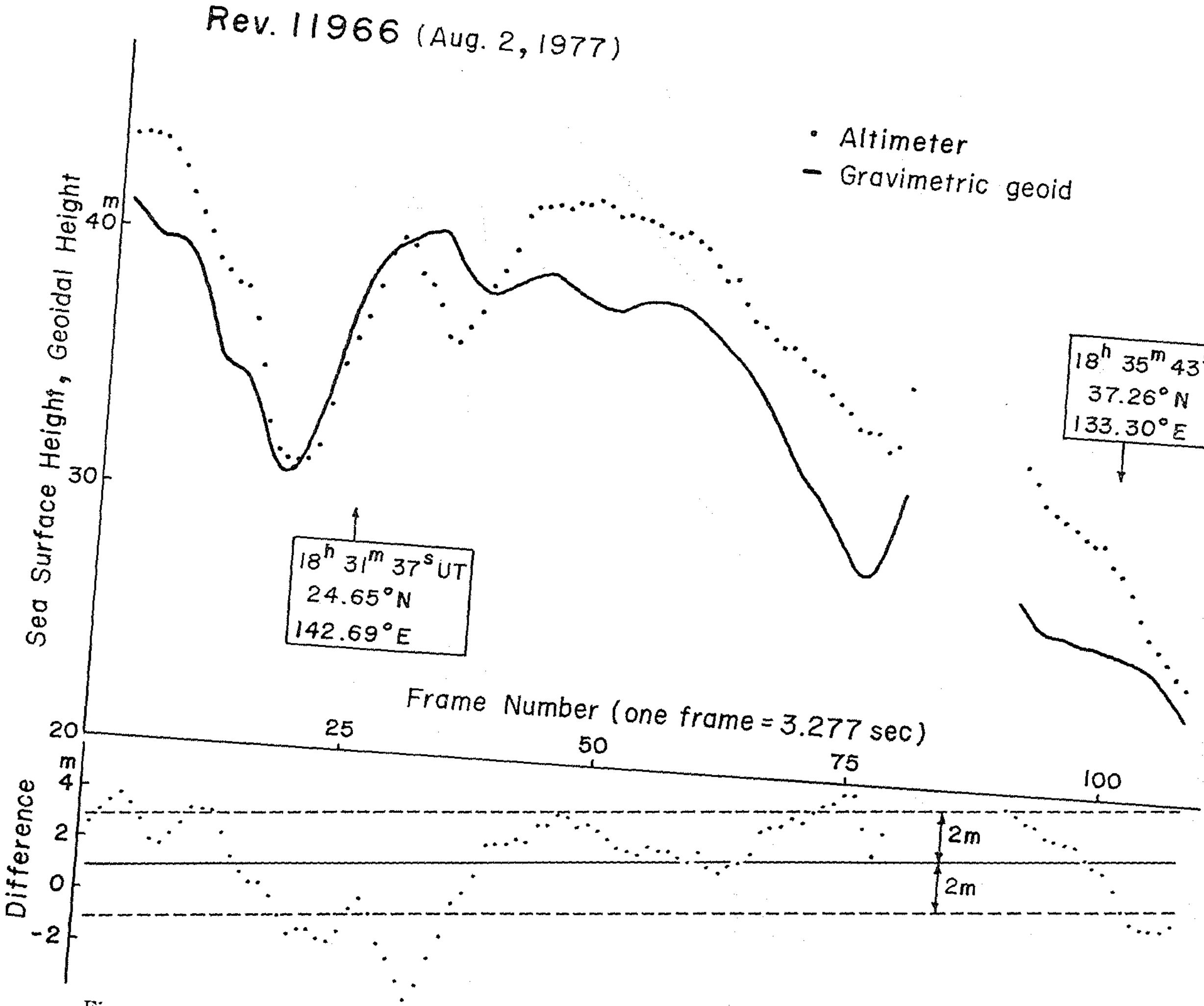

Figure 19 Comparison between Geos-3 altimetric profile (Rev. 11966) and the gravimetric geoid.

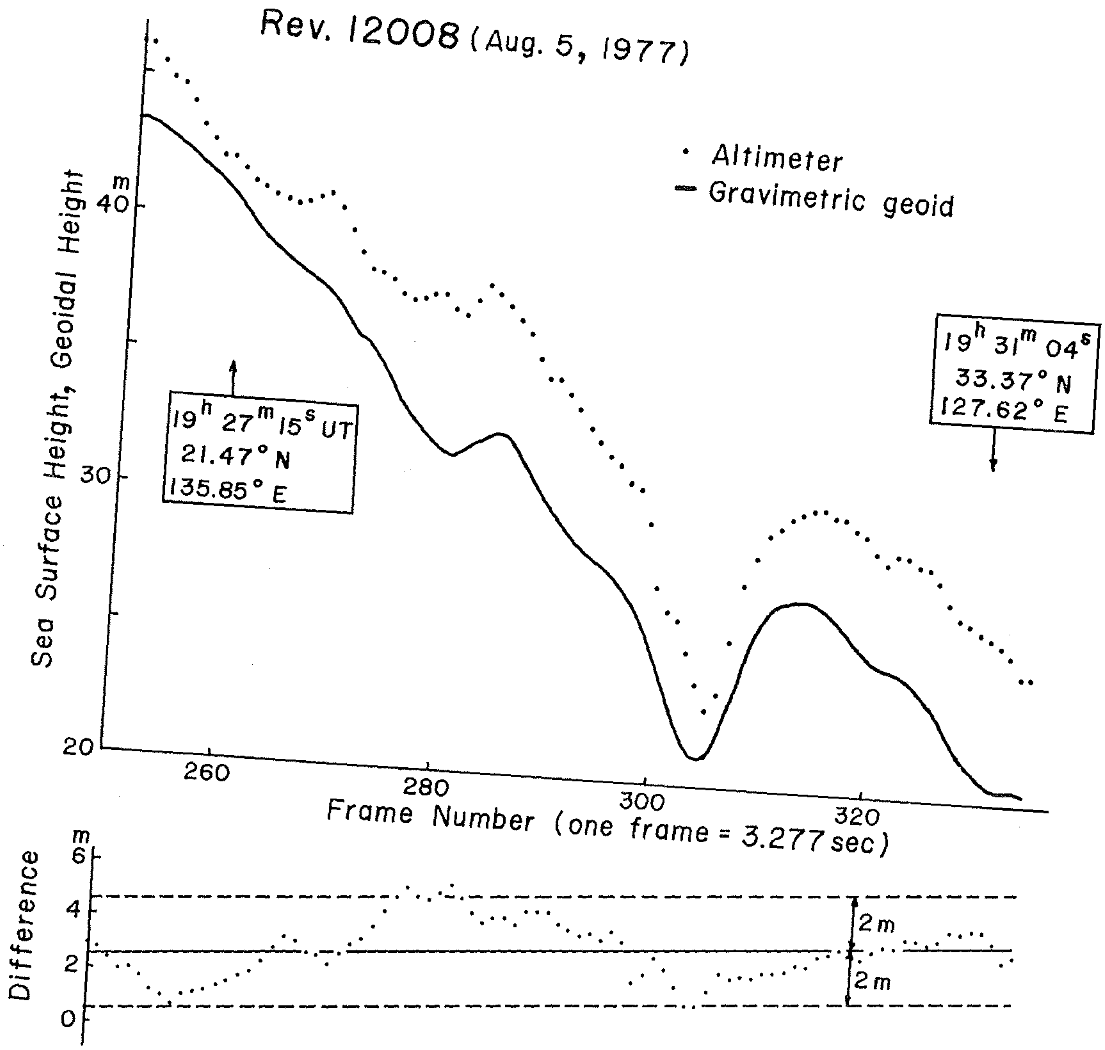

Figure 20 Comparison between Geos-3 altimetric profile (Rev. 12008) and the gravimetric geoid.

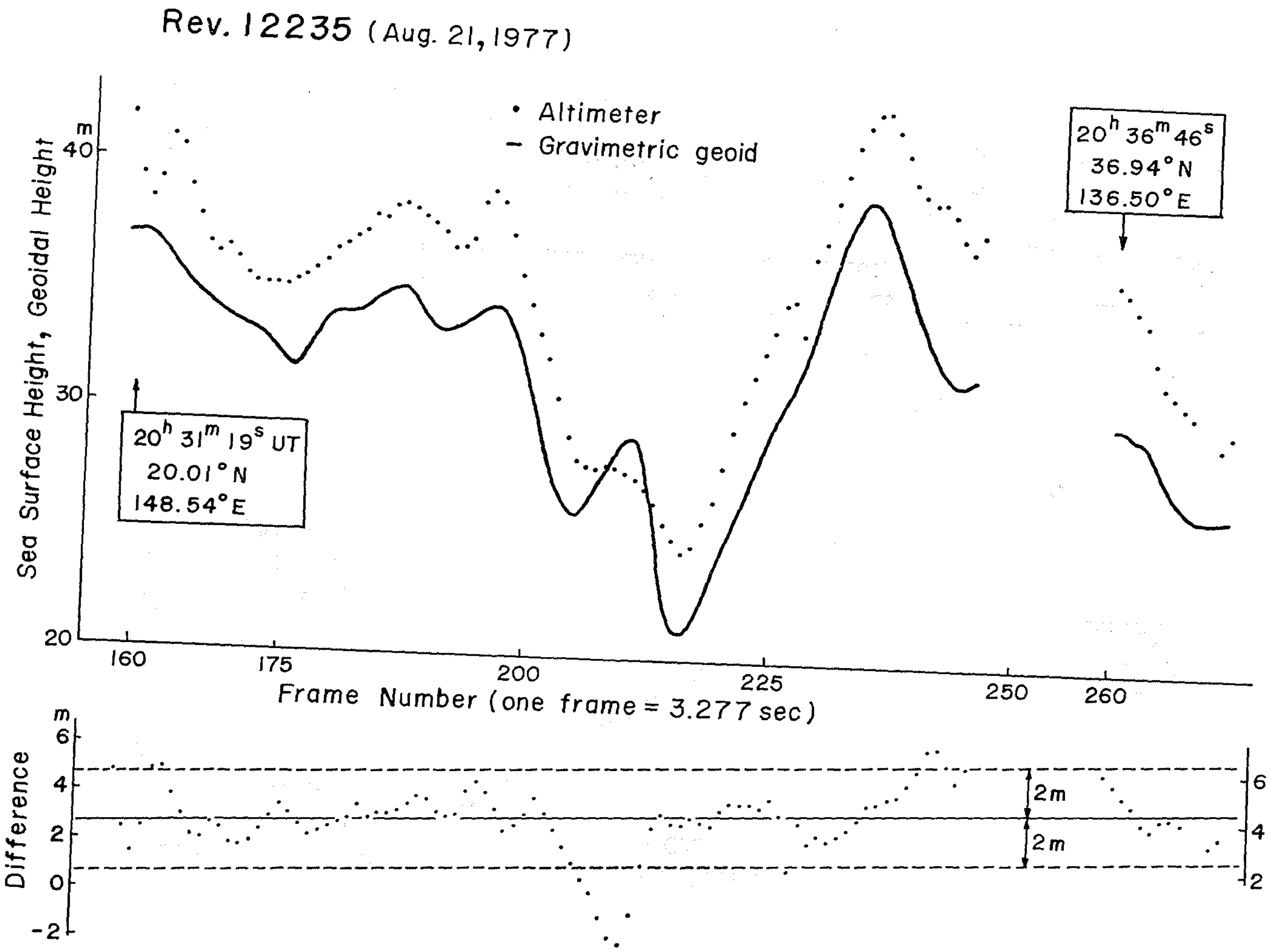

Figure 21 Comparison between Geos-3 altimetric profile (Rev. 12235) and the gravimetric geoid.

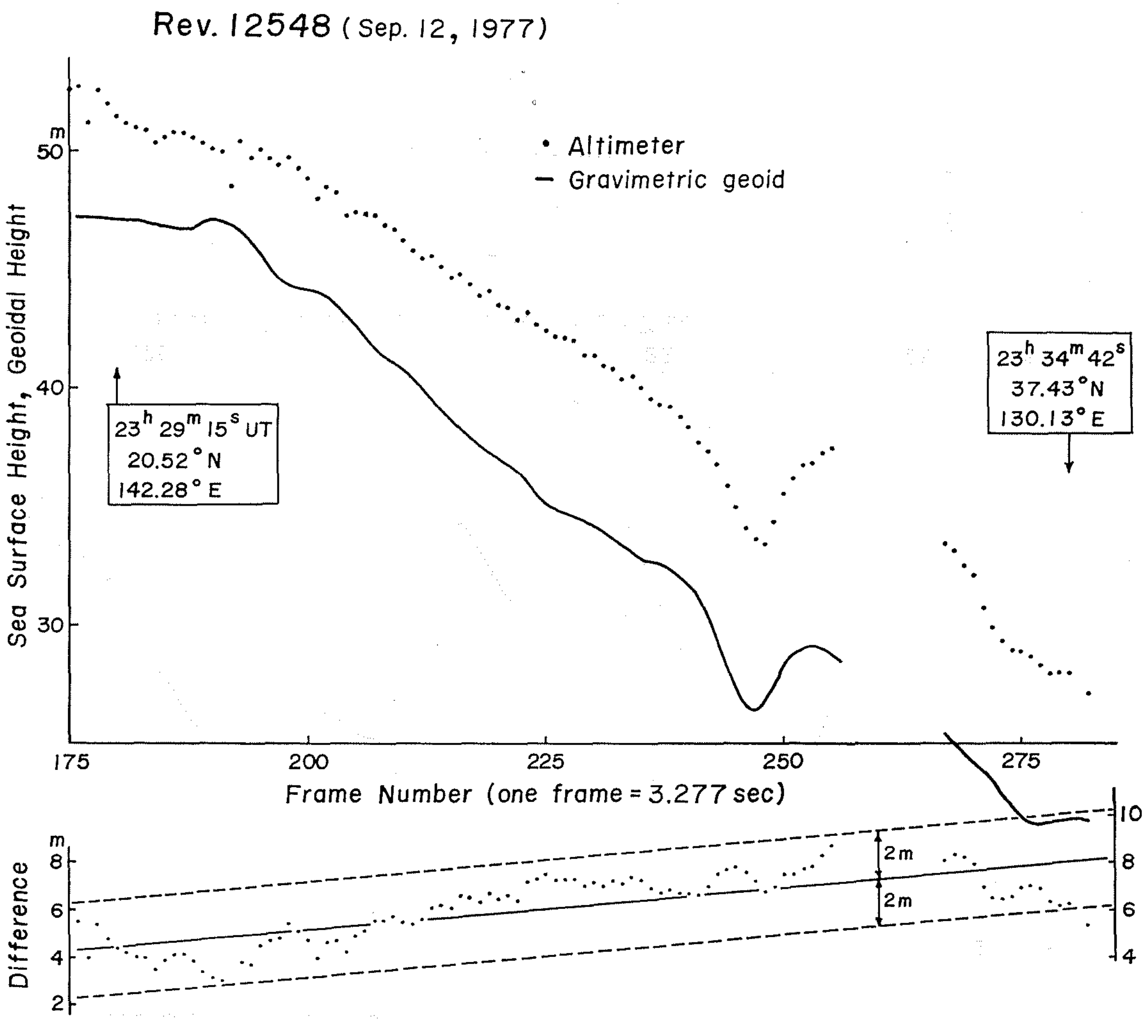

Figure 22 Comparison between Geos-3 altimetric profile (Rev. 12548) and the gravimetric geoid.

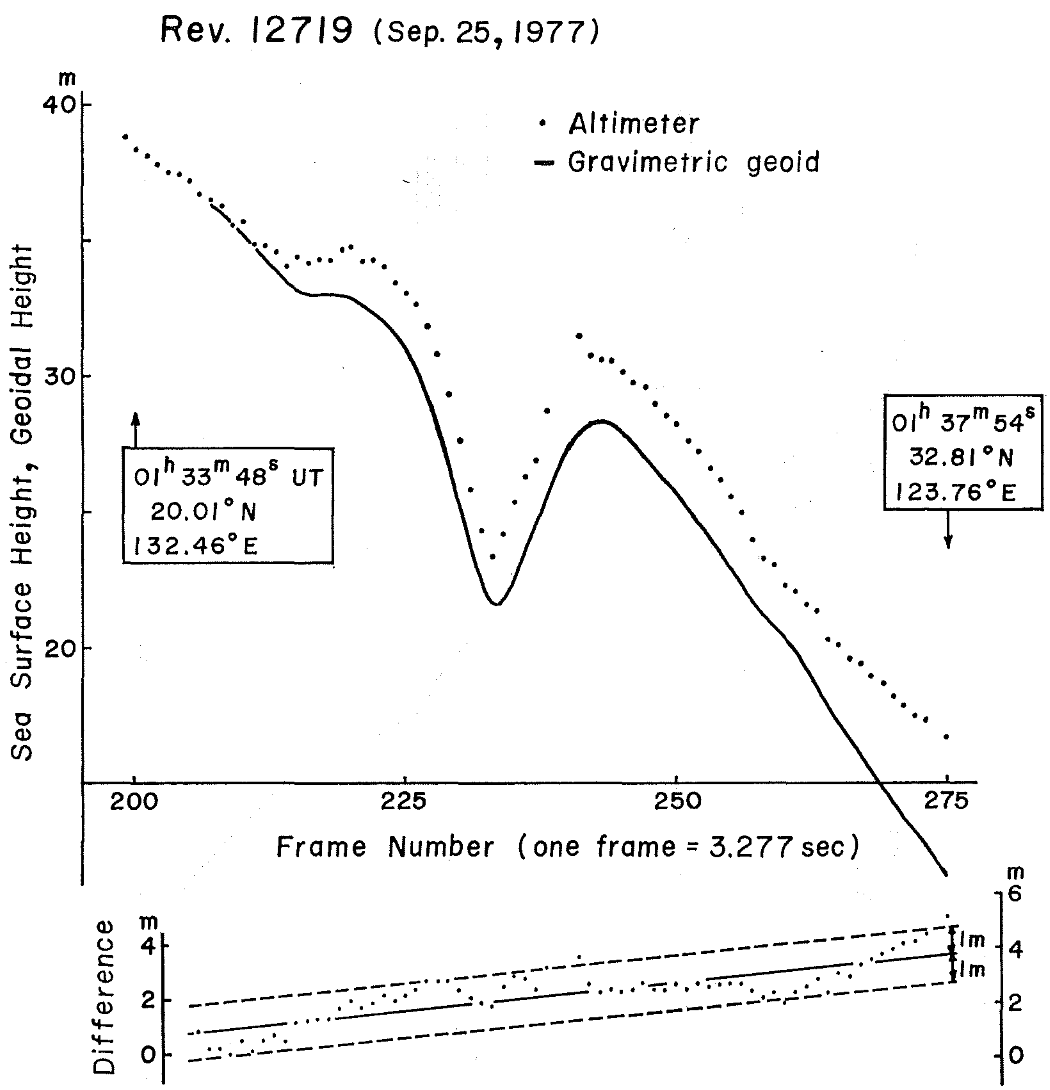

Figure 23 Comparison between Geos-3 altimetric profile (Rev. 12719) and the gravimetric geoid.

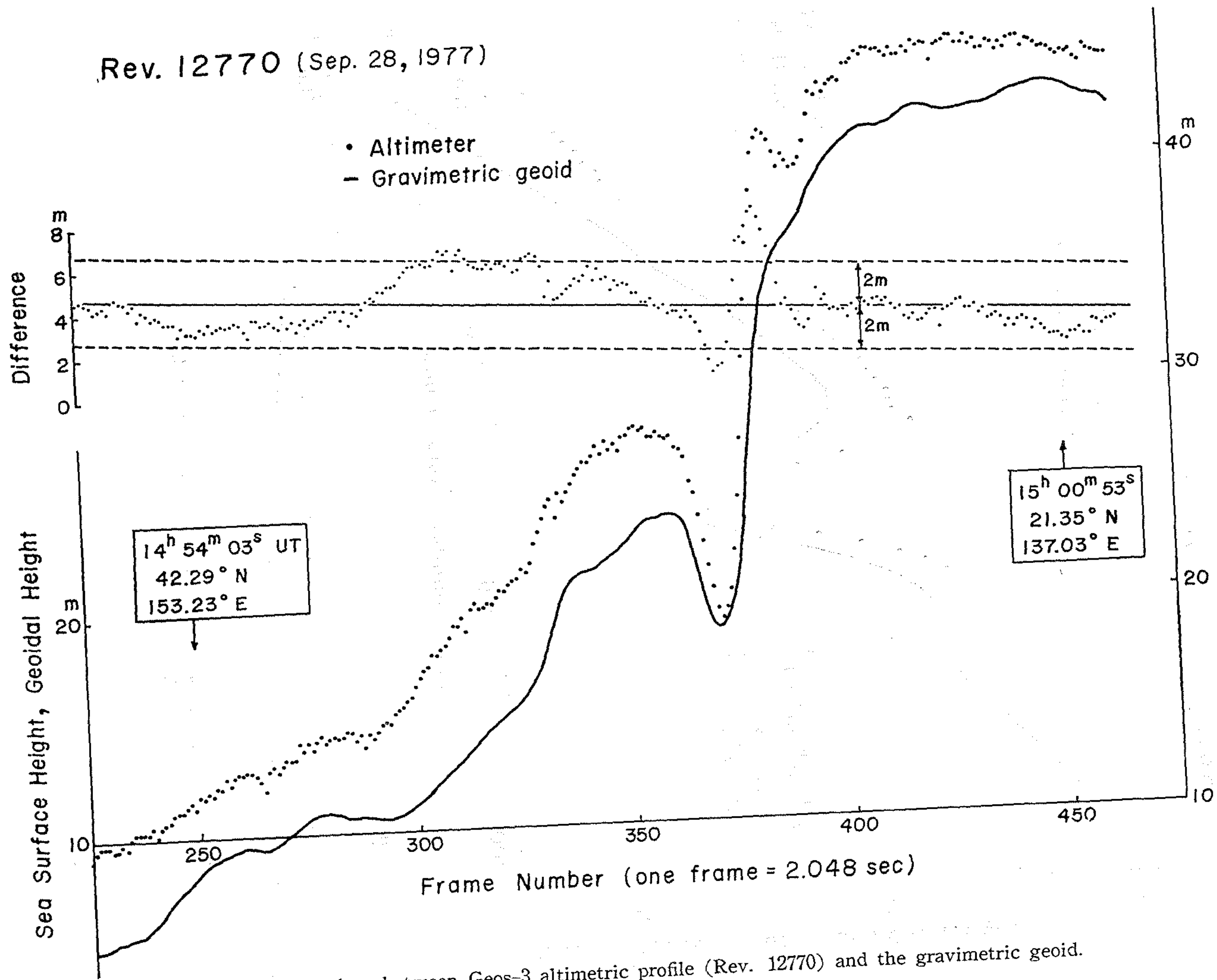

Figure 24 Comparison between Geos-3 altimetric profile (Rev. 12770) and the gravimetric geoid.

Since the altimetric sea surface heights are not corrected by ocean tidal heights and sea surface topographical heights, there may exist differences amounting to about one meter between plotted sea surface heights and geoidal heights. Detailed procedures of the altimeter data processing of Geos-3 are found in Leitao et al. (1975; its revised version, 1976).

As we see in Figures 13~24, the altimetric sea surface heights agree fairly well with the gravimetric geoidal heights except for tiltings and large differences in some parts. To eliminate long wave-length errors included in both profiles, a linear model difference

$$d=bt+a, \tag{3-12}$$

where t is the parameter of time, is fitted to the differences of each revolution by using a least-squares method. The fitted linear model differences are shown along the difference profiles in Figures 13~24. We can see deviations from linear difference amounting to ± 1 to ± 2 m. The parameters of the fitted linear model differences and standard deviations from linear differences are listed in Table 1 for each revolution with some other data of the revolutions. In the least-squares fitting procedures, unreasonable and spikelike sea surface heights, which are apparently wrong data, are omitted, and such data are not protted in the figures.

We find a systematic sign difference among fitted b parameters in Table 1, i.e. b has positive sign for the satellite tracks of south to north direction and vice versa. This implies the facts that geoidal heights become higher than altimetric sea surface heights to the south, and the tilt may be ascribed mainly to the disagreement between the origin of the coordinate system of the satellite altimetry and that of the gravimetric geoid. According to the physical oceanography, the sea surface topographical heights near Japan become higher to the south across the Kuroshio area (e.g. Lisitzin, 1974; Sugimori, 1978). The fact that large bias parts appear in revolutions 1411 and 2051 may be caused by large position errors of Geos-3 satellite as mentioned before, although we have not enough informations to discuss the bias parts further. Standard deviations from the linear model difference of the recent revolutions are generally smaller than those of the early revolutions.

Table 1 Comparisons between altimetric sea surface heights and the gravimetric geoidal heights

Revolution Number	Date	Track Direction	a (m)	b (cm/sec)	S.D. (m)	Frames	Data Rate
1411	1975.7.18	South	35.1	-4.362	1.3	158	Low
1587	7.31	North	-2.5	2.572	1.7	140	L
1616	8.02	N	3.6	0.596	0.7	90	L
2023	8.30	S	5.5	-0.736	1.6	161	L
2051	9.01	S	29.7	-2.176	1.4	192	L
2198	9.12	N	1.2	2.387	1.0	174	L
11966	1977.8.02	N	0.8	0.872	1.9	97	High
12008	8.05	N	2.5	0.822	1.1	86	H
12235	8.21	N	2.6	0.513	1.2	97	H
12548	9.12	N	4.3	1.074	0.9	95	H
12719	9.25	N	0.6	1.275	0.6	67	H
12770	9.28	S	4.8	-0.442	1.2	235	L

That may come from the improvements in the altimeter data processing and the satellite trackings. Revolution 11966 has the biggest standard deviation, which is resulted from large differences around the area of Bonin Islands. Large differences around the area of Bonin Islands are also found in revolutions 1587 and 2051. The gravimetric geoid may be inaccurate around there. We see large differences at the north parts of tracks of revolutions 2023 and 2051, which may indicate that the gravimetric geoid has not correctly determined in the north part of the region of Figure 8 because of sparse gravity data around there. It is noted that revolutions 2198, 11966 and 12548 include large differences in Japan Sea region.

On the basis of the results of comparison between altimetric sea surface heights and gravimetric geoidal heights, we may conclude that the relative undulation of the gravimetric geoid is determined in the accuracy of one to two meters. Other detailed error estimations of geoidal height computation by using Stokes' integral will be made in the next chapter.

4. Error Sources Involved in the Practical Performance of Stokes' Integral and Evaluation of the Computed Gravimetric Geoid

In this chapter we will make detailed investigations concerning with error sources involved in the practical computation of a gravimetric geoid based on Stokes' integral. Such investigation will make a contribution to the evaluation of the gravimetric geoid, which has been presented in the last chapter, and furthermore to the computation of a more accurate gravimetric geoid, i.e. geoid of 10 cm accuracy. A 10 cm geoid will play an important role not only in the geodetical science but also in other earth sciences, e.g. ocean dynamics.

(1) Statistical Characteristics of the Gravity Anomaly Field

The knowledge of the characteristics of the gravity anomaly field is indispensable for the error estimation of geoidal height computation, especially for the estimation of omission errors (see (2) in the present chapter). The characteristics are given mathematically in the statistical expressions. The knowledge of the statistical characteristics of the gravity anomaly field is also useful in the interpolation of gravity anomalies and estimation of block mean gravity anomalies (see Chapter 5). So we study the statistical characteristics of the gravity anomaly field for the conveniences of later sections.

The disturbing potential which is harmonic outside a sphere with a radius R is written in the form:

$$T=\frac{kM}{R}\sum_{l=2}^{\infty}\left(\frac{R}{r}\right)^{l+1}T_l, \tag{4-1}$$

where r is the radial distance and T_l is $l-$th degree Laplace surface harmonics. Let P and Q be points in the space outside the sphere, r_P and r_Q be radial distances of P and Q from the geocenter, and the geocentric angular distance between P and Q be ψ (see Figure 25). The rotationally symmetric spacial covariance function of the disturbing potential is given by

$$K(P,Q)=M\{T_P T_Q\}$$
$$=\left(\frac{kM}{R}\right)^2 \sum_{l=2}^{\infty}\sum_{l'=2}^{\infty}\left(\frac{R}{r_p}\right)^{l+1}\left(\frac{R}{r_Q}\right)^{l'+1} M\{T_l(P)T_{l'}(Q)\}, \tag{4-2}$$

where $M\{\ \}$ indicates the average taken over the possible combinations of points P and Q under the condition: ψ=constant. Then, we get

$$K(P,Q)=\sum_{l=2}^{\infty}\left(\frac{R^2}{r_P r_Q}\right)^{l+1}\sigma_l^2 P_l(\cos\psi) \tag{4-3}$$

(Moritz, 1972, p. 88), where P_l is l-th degree unnormalized Legendre function and σ_l^2 is the degree variance of the disturbing potential. When we use a similar expression for the disturbing potential to (2-15), we can write

$$T_l=\frac{kM}{R}\sum_{m=0}^{l}[\bar{C}_{lm}^{*}\bar{R}_{lm}+\bar{D}_{lm}\bar{S}_{lm}] \tag{4-4}$$

and σ_l^2 is written as follows:

$$\sigma_l^2=\left(\frac{kM}{R}\right)^2\sum_{m=0}^{l}(\bar{C}_{lm}^{*2}+\bar{D}^2_{lm}). \tag{4-5}$$

R is chosen as the radius of a sphere included completely inside the earth (the sphere is called Bjerhammar sphere, (see Figure 25)) so that the disturbing potential T is harmonic on and outside the earth. Consider the case that both of P and Q are located on the surface of the earth. We put approximately $r_P r_Q=R_0^2$, where R_0 is the mean

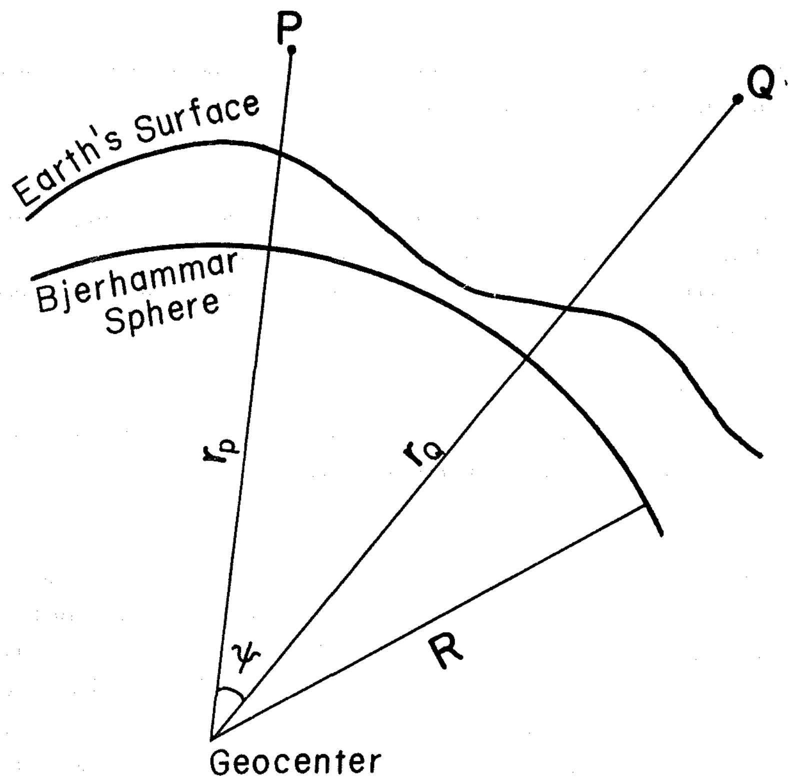

Figure 25 Explanation figure for the derivation of the spacial covariance functions.

radius of the earth, and introduce a parameter $s=(R/R_0)^2$. From (4-3) we get

$$K(\psi)=\sum_{l=2}^{\infty} \sigma_l^2 \, s^{l+1} P_l(\cos\psi) \tag{4-6}$$

as the covariance function of the disturbing potential on the surface of the earth.

By using the relation between gravity anomaly and disturbing potential:

$$\Delta g=-\frac{\partial T}{\partial r}-\frac{2}{r}T$$

(Heiskanen and Moritz, 1967, p. 89), we obtain the covariance function of the gravity anomaly on the earth's surface as follows:

$$C(\psi)=\sum_{l=2}^{\infty} \sigma_l^2(\Delta g) \, s^{l+2} P_l(\cos\psi) \tag{4-7}$$

(Moritz, 1972, p. 89), where $\sigma_l^2(\Delta g)$ is the degree variance of gravity anomaly called "anomaly degree variance". Then σ_l^2 in (4-6) is given by

$$\sigma_l^2=\frac{R^2}{(l-1)^2}\sigma_l^2(\Delta g). \tag{4-8}$$

From (4-5) and (4-8), $\sigma_l^2(\Delta g)$ is expressed by geopotential coefficients as follows:

$$\sigma_l^2(\Delta g)=G^2(l-1)^2\sum_{m=0}^{l}(\bar{C}_{lm}^{*2}+\bar{D}^2_{lm}), \tag{4-9}$$

where

$$G^2=\left(\frac{kM}{R^2}\right)^2.$$

On the other hand, we can compute anomaly degree variances from (4-7) when we know the covariance function of gravity anomaly, i.e.

$$\sigma_l^2(\Delta g)=\frac{2l+1}{2}\, s^{-(l+2)}\int_0^{\pi} C(\psi)P_l(\cos\psi)\sin\psi\, d\psi. \tag{4-10}$$

The statistical characteristics of the gravity anomaly field are thus expressed by the covariance function or degree variances of gravity anomaly.

Kaula (1966) proposed an equation to estimate sizes of the fully normalized geopotential coefficients:

$$\sigma_l(\bar{C}_{lm},\ \bar{D}_{lm})=\frac{10^{-5}}{l^2}, \tag{4-11}$$

and it is called Kaula's rule of thumb. From (4-9) and (4-11), the anomaly degree variance based on Kaula's rule of thumb is written as

$$\sigma_l^2(\Delta g)=G^2(l-1)(2l+1)\frac{10^{-10}}{l^4}, \quad l\geq 3. \tag{4-12}$$

Figure 26a shows the anomaly degree variances expressed by (4-12) and ones based on the satellite-derived geopotential coefficients: GEM-7 (Wagner et al., 1976); GEM-9 (Lerch et al., 1977). As seen in this figure, (4-12) is a fairly good model of the anomaly degree variances at least up to a degree of several tens. Geopotential coefficients are also derived from the combination of satellite tracking data and surface gravity data, or solely from surface gravity data. Figure 26b includes anomaly degree variances based on such geopotential coefficients: GEM-10 (Lerch et al., 1977, combination solution); Rapp's results (Rapp, 1977b, surface gravity data).

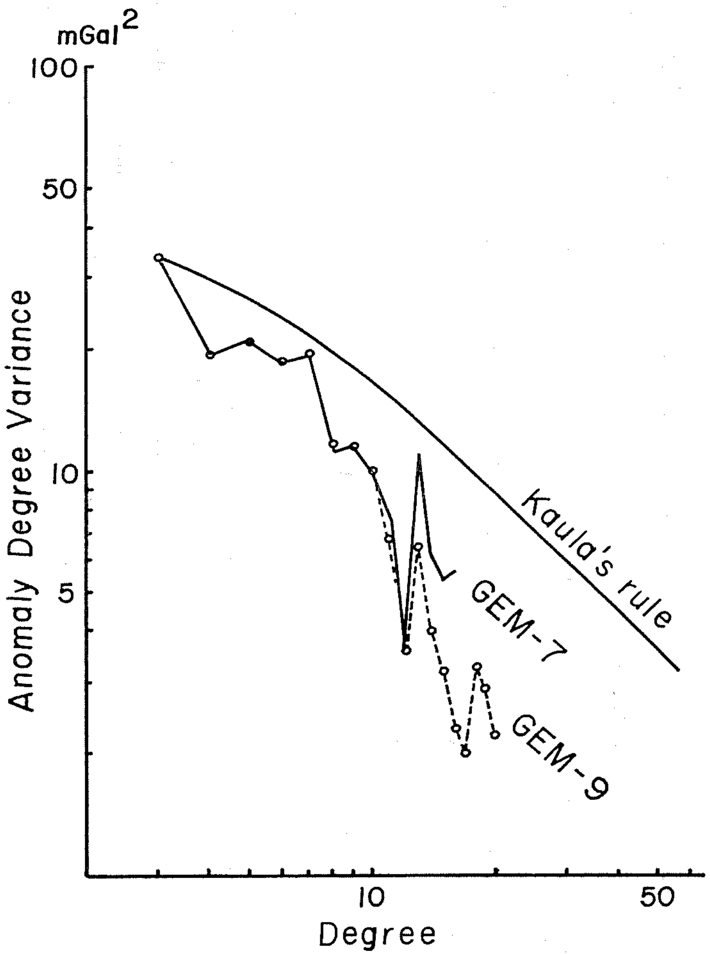

Figure 26a Anomaly degree variances based on Kaula's rule of thumb, GEM-7 and GEM-9 solutions.

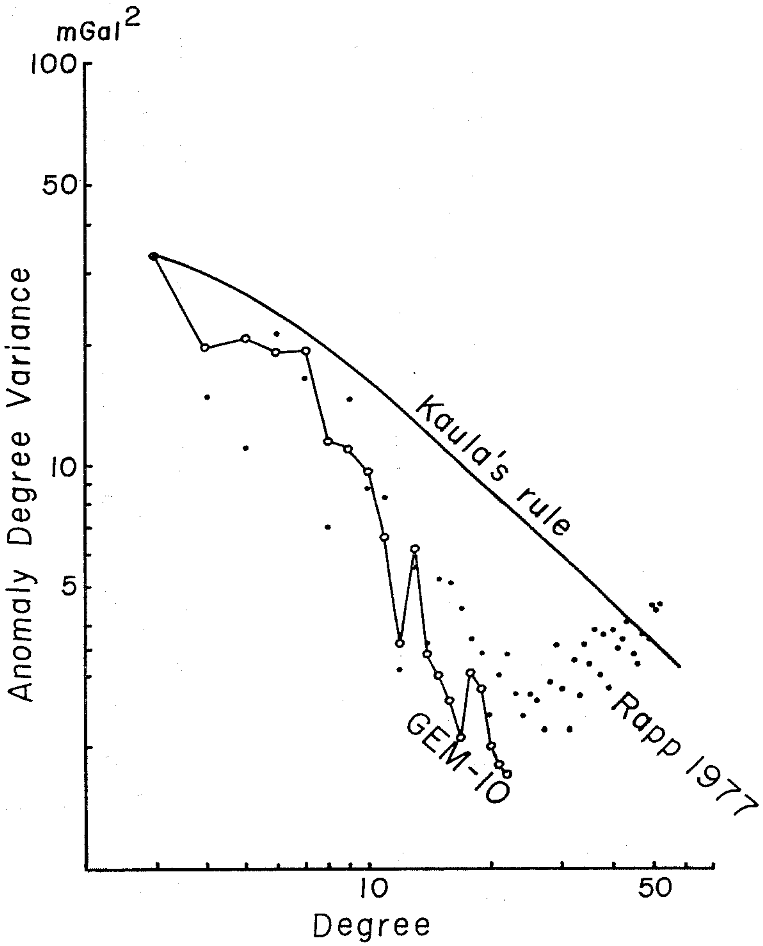

Figure 26b Anomaly degree variances based on Kaula's rule of thumb, GEM-10 and Rapp's solution.

Equation (4-7) is the covariance function of point gravity anomaly, and we can compute covariance functions of block mean gravity anomalies by using the point covariance function. Let σ_P and σ_Q be two blocks whose areas are S_P and S_Q, and ψ be the angular distance between centers of the blocks. The covariance function $\bar{\bar{C}}$ of the block mean gravity anomalies is derived by

$$\bar{\bar{C}}(\psi)=\frac{1}{S_P\,S_Q}\iint\limits_{\sigma_P}\iint\limits_{\sigma_Q} C(\psi')d\sigma_P\,d\sigma_Q, \tag{4-13}$$

where ψ' is the angular distance between $d\sigma_P$ (in σ_P) and $d\sigma_Q$ (in σ_Q). Approximating a square $B°$ block to a circular area with radius $\psi_0=B°/\sqrt{\pi}$ and using (4-7), we obtain the covariance function of mean gravity anomalies of $B°$ block as follows:

$$\bar{\bar{C}}(\psi)=\sum_{l=2}^{\infty}\sigma_l^2(\Delta g)\,s^{l+2}\,\beta_l^2\,P_l(\cos\psi), \tag{4-14}$$

where

$$\beta_l=\cot\frac{\psi_0}{2}\cdot\frac{P_{l1}(\cos\psi_0)}{l(l+1)} \tag{4-15}$$

(see Appendix A). β_l is called smoothing parameter introduced by Pellinen (1966) and Meissl (1971). Rapp (1977b) tabulated the numerical values of β_l up to degree 52 for $B=5°$. Note $\beta_l\to1$ when $\psi_0\to0$. The variance of block mean gravity anomalies is given by putting $\psi=0$ in (4-14), and it is written as

$$\bar{\nu}=\sum_{l=2}^{\infty}\sigma_l^2(\Delta g)\,s^{l+2}\,\beta_l^2. \tag{4-16}$$

Tscherning and Rapp (1974) obtained a model anomaly degree variance:

$$\sigma_l^2(\Delta g)=\frac{A(l-1)}{(l-2)(l+B)} \tag{4-17}$$

with $A=425.28$ mGal^2, $B=24$, and $s=0.999617$. They obtained the model by using actual degree variances up to degree 20 adopting $\sigma_2^2(\Delta g)=7.5$ mGal^2, $\nu=C(0)=\sum_{l=2}^{\infty}\sigma_l^2(\Delta g)s^{l+2}=1795$ mGal^2, and variances of 1° and 5° block mean gravtiy anomalies 920 and 302 mGal^2, respectively.

We adopt notations $C_G(\psi)$ for the long wave-length component of the gravity anomaly covariance function:

$$C_G(\psi)=\sum_{l=2}^{L}\sigma_l^2(\Delta g)\,s^{l+2}\,P_l(\cos\psi), \tag{4-18}$$

and $C_L(\psi)$ for the local anomaly covariance function:

$$C_L(\psi)=\sum_{l=L+1}^{\infty}\sigma_l^2(\Delta g)\,s^{l+2}\,P_l(\cos\psi). \tag{4-19}$$

Consequently, $C(\psi)=C_G(\psi)+C_L(\psi)$. Figure 27 shows $C(\psi)$ and $C_L(\psi)$ based on the anomaly degree variance model (4-17) when $L=20$. The correlation distance (the distance where the covariance value is a half of the variance) of $C_L(\psi)$ is much shorter than that of $C(\psi)$, because $C_L(\psi)$ expresses only the statistical characteristics of short wave-length component of the gravity anomaly field. Since the covariances in Figure 27 corresponds to the world-wide average statistical characteristics of the gravity anomaly field, they may differ from covariance functions derived from gravity anomaly distribution in a

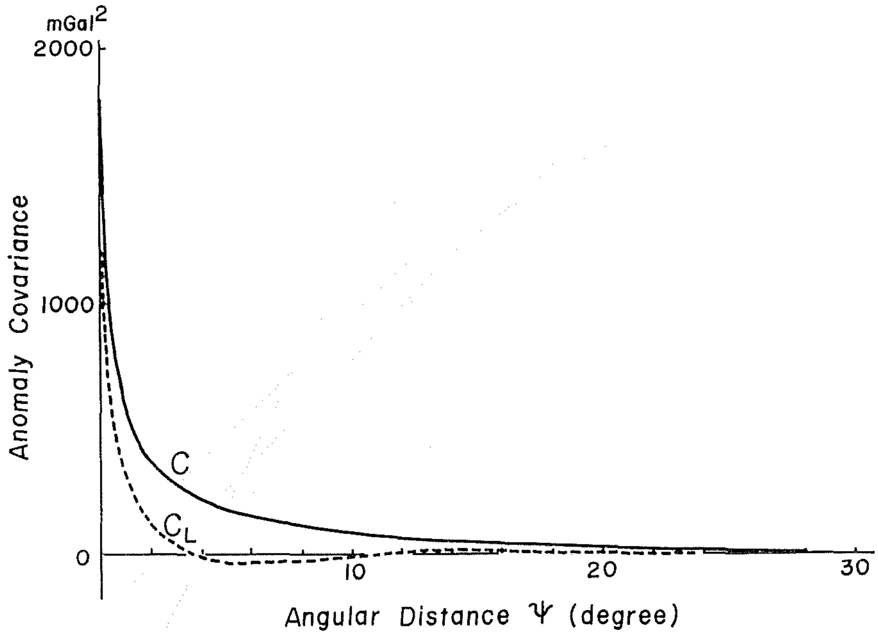

Figure 27 Anomaly covariance function $C(\psi)$ and local anomaly covariance function $C_L(\psi)$ based on the anomaly degree variance model (equation (4-17))by Tscherning and Rapp (1974).

restricted area. Ganeko (1976) obtained a local anomaly covariance function from observations of the deflections of the vertical distributed in Japan. It is approximated by an analytical function as follows:

$$C_L(\psi)=C_0 \exp\left(-\frac{r}{D}\right), \tag{4-20}$$

where $C_0=2809$ mGal^2, $D=55$ km, and r is the parameter of distance in kirometers. (4-20) is based on the residual anomaly field of SAO-SE3 geopotential model (Gaposchkin et al., 1973) up to degree and order 18. The residual variance C_0 in (4-20) is larger than that of world-wide average, 1795 mGal^2, obtained by Tscherning and Rapp (1974). This is probably due to the fact that Japan is located in a geophysically active area and the gravity anomaly field around Japan is rougher than the world-wide average. If we assume the local covariance function (4-20) to be the world-wide average one, we can compute anomaly degree variance of a high degree by using (4-10). The computed anomaly degree variances for $s=1$ are shown by curve c in Figure 28. This figure also includes the degree variances based on Kaula's rule of thumb (curve a), degree variance model (4-17) (curve d) and another degree variance model by Rapp (1973a) (curve b):

$$\sigma_l^2(\Delta g)=\frac{B(l-1)}{(l-2)\ (l+D+\varepsilon l^2)} \tag{4-21}$$

where $B=246.5556$ mGal^2, $D=12.6755$ and $\varepsilon=0.000657$. Rapp determined the parameters so that (4-7) and (4-16) fitted the actual gravity anomaly field by putting $s=1$ in both equations. In other words, the anomaly degree variance model (4-21) may be approximated

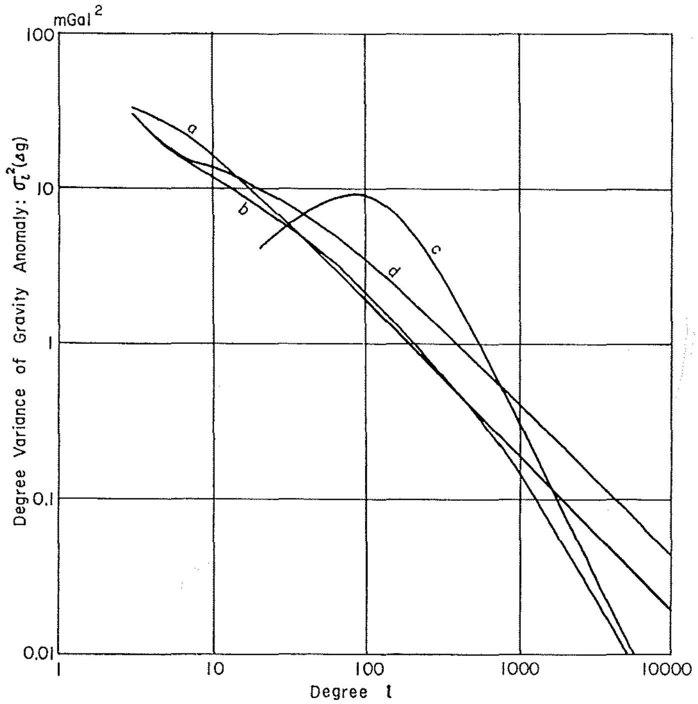

Figure 28 Anomaly degree variance models: (a) based on Kaula's rule of thumb; (b) Rapp (1973), equation (4-21); (c) Ganeko (1976), based on anomaly covariance function (4-20); (d) (d) Tscherning and Rapp (1974), equation (4-17).

by the degree variance model (4-17) multiplied by s^{l+2}, i. e.

$$\sigma_l^2(\Delta g)\ [\text{equation (4-21)}] \approx s^{l+2}\, \sigma_l^2(\Delta g) [\text{equation (4-17)}]$$

The anomaly degree variance model c shown in Figure 28 is characterized by a peak around degree 90, and the possibility of such peak seems to be supported by the anomaly degree variances by Rapp (1977b) derived from surface gravity data (see Figure 26b). However, if we take the difficulties of determination of the geopotential coefficients of high degrees into cosideration, it is not so firmly supported by the Rapp's results that such a peak exists on an anomaly degree variance curve as the global average. Degree 90 corresponds to about 400 km wave-length.

We compute covariance functions of block mean gravity anomalies included in JHDGF-1 gravity file obtained in the previous chapter. The obtained covariance functions are shown in Figure 29a (for $30' \times 30'$ and $1° \times 1°$ blocks) and in Figure 29b (for $10' \times 10'$ block). It is assumed that each block has the same area as far as they are located in the JHDGF-1 region (see Figure 4), and the block covariance functions are computed by

$$\bar{\bar{C}}_L(r_k) = \frac{\sum\limits_{i,j} (\overline{\Delta g} - \overline{\Delta g}_s)_i\, (\overline{\Delta g} - \overline{\Delta g}_s)_j}{N_k}, \tag{4-22a}$$

where $\overline{\Delta g} - \overline{\Delta g}_s$ is the block residual mean gravity anomalies based on the satellite-derived gravity anomaly of GEM-8 geopotential model (Wagner et al., 1976). The summation is taken over N_k paires of blocks σ_i and σ_j whose centers are separated by the distance

$r_{ij,k}$, which satisfies the condition:

$$r_k \leq r_{ij,k} \leq r^k + \Delta r, \quad k=0, 1, 2, \cdots, \tag{4-22b}$$

in which we assume $r^\circ = 0$. Δr is taken as 20 km for $10' \times 10'$ block, 30 km for $30' \times 30'$ block and 60 km for $1^\circ \times 1^\circ$ block. The distance parameter of the covariance function is computed by

$$r_k = \sum_{i,j} r_{ij,k}/N_k$$

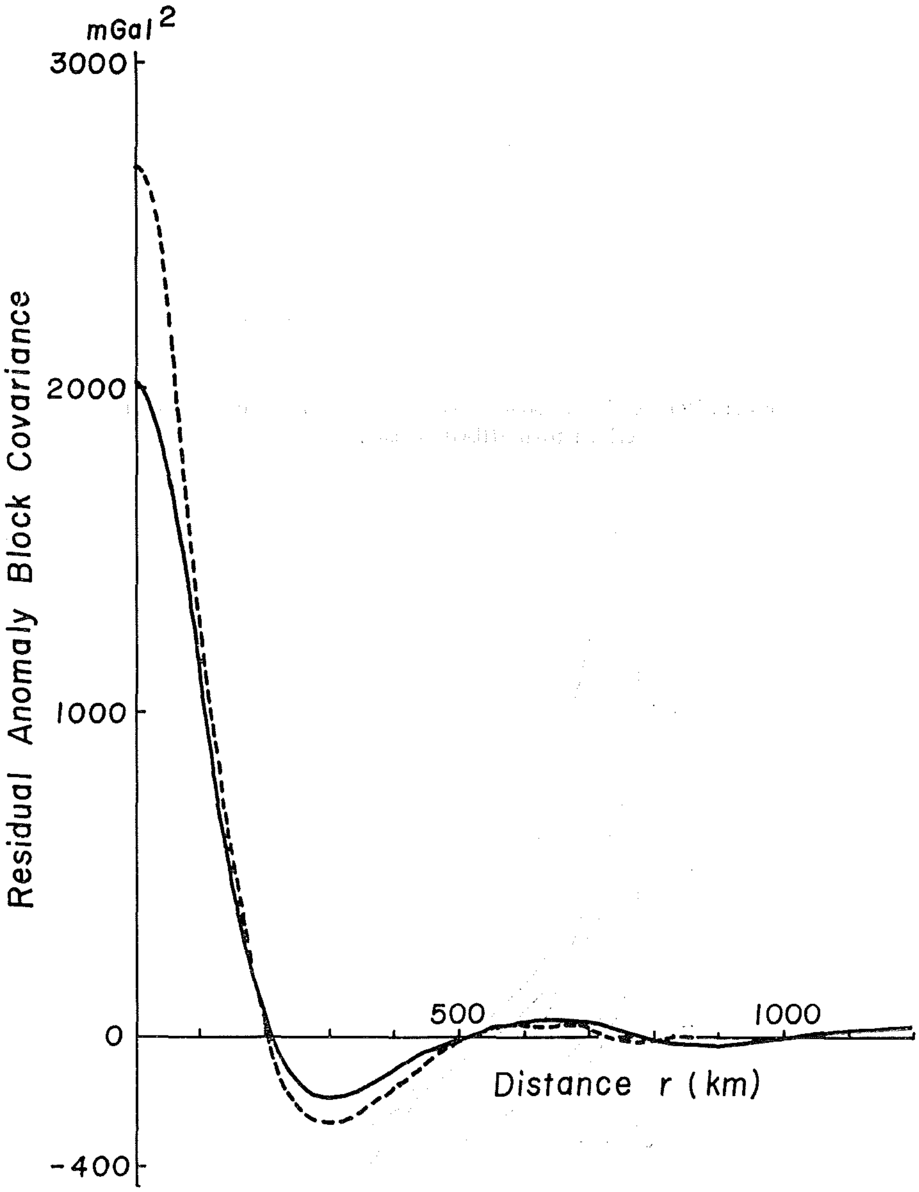

Figure 29a Residual anomaly block covariances of $30' \times 30'$ blocks (broken line) and $1^\circ \times 1^\circ$ blocks (full line) derived from JHDGF-1 data. Residual anomalies are referred to GEM-8 global anomaly field.

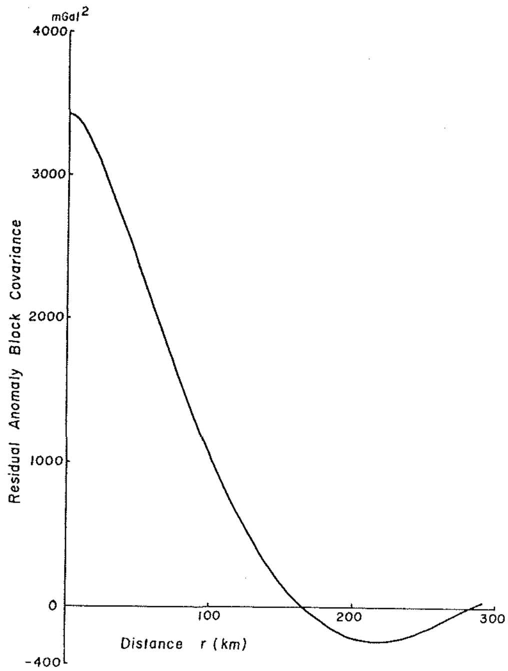

Figure 29b Residual anomaly block covariance of $10' \times 10'$ blocks derived from JHDGF-1 data.

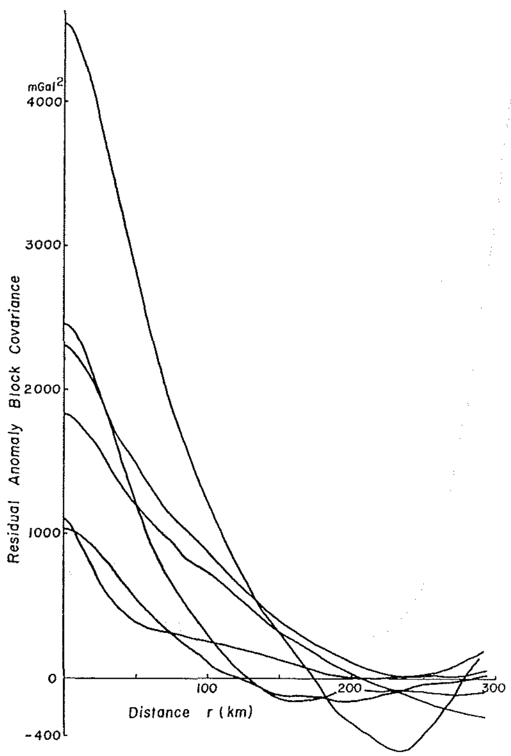

Figure 29c Residual anomaly block covariances of $10' \times 10'$ blocks included in $5° \times 5°$ blocks.

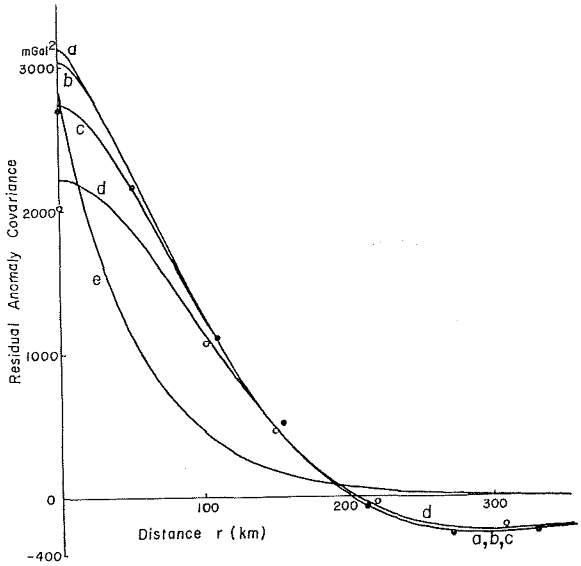

Figure 29d Residual anomaly covariance functions based on the analytical function model (4-23): (a) point covariance; (b) $10' \times 10'$ block covariance; (c) $30' \times 30'$ block covariance; (d) $1° \times 1°$ block covariance. (e) is the point covariance (4-20). Full and open circles are actual covariances for $30' \times 30'$ and $1° \times 1°$ blocks, respectively.

It should be noted that the covariance function of $10' \times 10'$ block shown in Figure 29b is an average of covariance functions derived from $10' \times 10'$ blocks in every $5° \times 5°$ block area of JHDGF-1 region, and the number of pairs (N_k) is used as the weight in taking an average of $10' \times 10'$ block covariance functions. Some examples of individual $10' \times 10'$ block covariance functions are seen in Figure 29c. As we see in the figure, there are not any rules among the curves of covariance functions. This fact may indicates that the features of the short wavelength components of the gravity anomaly field largely depend on the local geophysical structures.

Adopting a model analytical expression of covariance function:

$$C_L(r) = C_0 \exp\left[-(r/D)^p\right] \cos kr \qquad (4\text{-}23)$$

for the residual gravity anomaly around Japan, the parameters are determined as follows: $C_0 = 3133$ mGal²; $D = 161.2$ km; $k = 0.007854$ 1/km; $p = 1.227$. In the determinations of the parameters, $10' \times 10'$ block covariances are not taken into consideration because of instabilities of $10' \times 10'$ block covariances. Figure 29d shows the analytical covariance function (4-23) and the analytical block covariance functions derived from (4-13) and (4-23), comparing with the other type of covariance function (4-20).

(2) **Omission Errors in the Numerical Evaluation of Stokes' Integral**

Omission errors involved in the numerical evaluation of Stokes' integral come from the following situations.

(**A**) When the terrestrial gravity data are given by average value over a certain sized block area, the shorter wave-length components of the anomaly field than the size of the block area are omitted in the performance of numerical integration of Stokes' integral.

(B) Outside the cap area, we adopt a satellite-derived geopotential coefficient set, so that we consequently omit the more detailed informations of the gravity anomaly field than the satellite-derived gravitational field.

These kinds of omission error were discussed in detail by Christodoulidis (1976) and Ganeko (1977). We summarize the methods of omission error estimations and apply them to the gravimetric geoid obtained in Chapter 3.

1) Basic equations of omission errors

We can write the geoidal height error due to the truncation of higher degree components of gravity anomaly than degree L outside the cap area as follows:

$$\delta N = \frac{R}{2G} \sum_{l=L}^{\infty} Q_l(\psi_0) \Delta g_l \, , \tag{4-24}$$

where Q_l is Molodenskii's truncation function (Molodenskii et al., 1962), ψ_0 the radius of the cap, and Δg_l l-th degree Laplace surface harmonics of gravity anomaly. R and G are the mean radius of the earth and the mean gravity on the earth's surface, respectively. We call usually (4-24) "truncation error" of geoidal height. The truncation error covariance is defined by

$$C_{\delta N}(\Theta, L, \psi_0) = M\{\delta N_P \, \delta N_Q\}, \tag{4-25}$$

where Θ is the angular distance between P and Q, and the average operator $M\{ \}$ works as an average of possible pairs P and Q with a constant angular distance Θ over the whole earth. Inserting (4-24) into (4-25), and using orthogonality relations among spherical harmonics and an equation

$$\sigma_l^2(\Delta g) = M\{\Delta g_l^2\},$$

we get (Ganeko, 1977)

$$C_{\delta N}(\Theta, L, \psi_0) = \left(\frac{R}{2G}\right)^2 \sum_{l=L}^{\infty} Q_l^2(\psi_0) \, \sigma_l^2(\Delta g) \, P_l(\cos\Theta), \tag{4-26}$$

where P_l is l-th degree unnormalized Legendre function, and $\sigma_l^2(\Delta g)$ is the anomaly degree variance already discussed in the previous section.

2) Point truncation error

When $\Theta=0$ in (4-26), the equation is reduced to

$$\sigma^2_{\delta N}(L, \psi_0) \equiv C_{\delta N}(0, L, \psi_0) = \left(\frac{R}{2G}\right)^2 \sum_{l=L}^{\infty} Q_l^2(\psi_0) \, \sigma_l^2(\Delta g) \tag{4-27}$$

which defines the variance of truncation error. (4-27) is evaluated when the anomaly degree variances are given. The definition of Molodenskii's truncation function is

$$Q_l(\psi_0) = \int_{\psi_0}^{\pi} P_l(\cos\psi) \, S(\psi) \sin\psi \, d\psi, \tag{4-28}$$

where $S(\psi)$ is Stokes' function (see (2-2)). The analytical evaluation equations of Q_l were investigated by Molodenskii et al. (1962), Hagiwara (1972, 1976) and Paul (1976). Ganeko (1977) obtained a simple asymptotic analytical expression of Q_l applicable at high degrees. Figure 30a shows the evaluated truncation errors of geoidal heights, $\sigma_{\delta N}(L, \psi_0)$, given by (4-27) for various cap sizes on the basis of the anomaly degree variance model (4-21) (curve b in Figure 28, and it is called "anomaly degree variance model b" in this

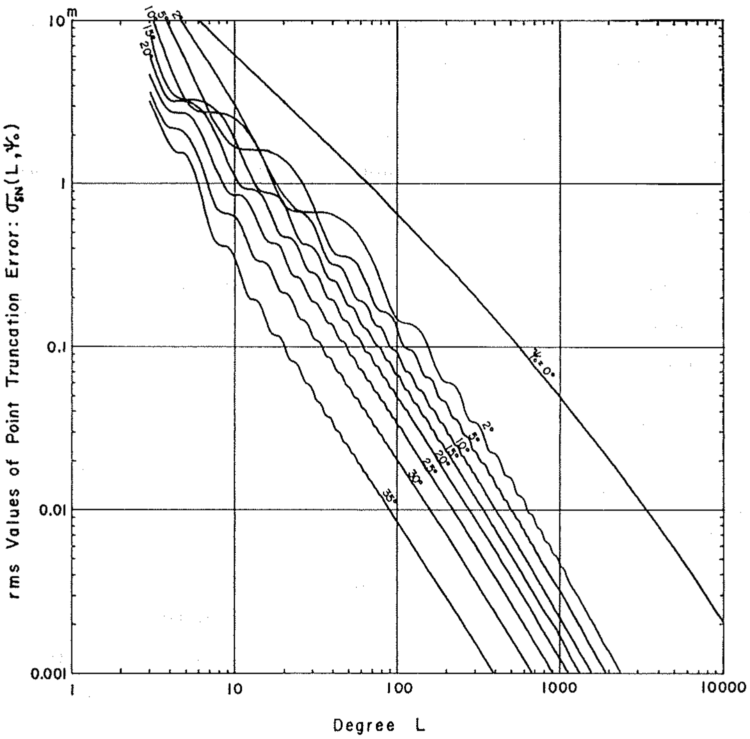

Figure 30a Point truncation errors based on the anomaly degree variance model *b*.

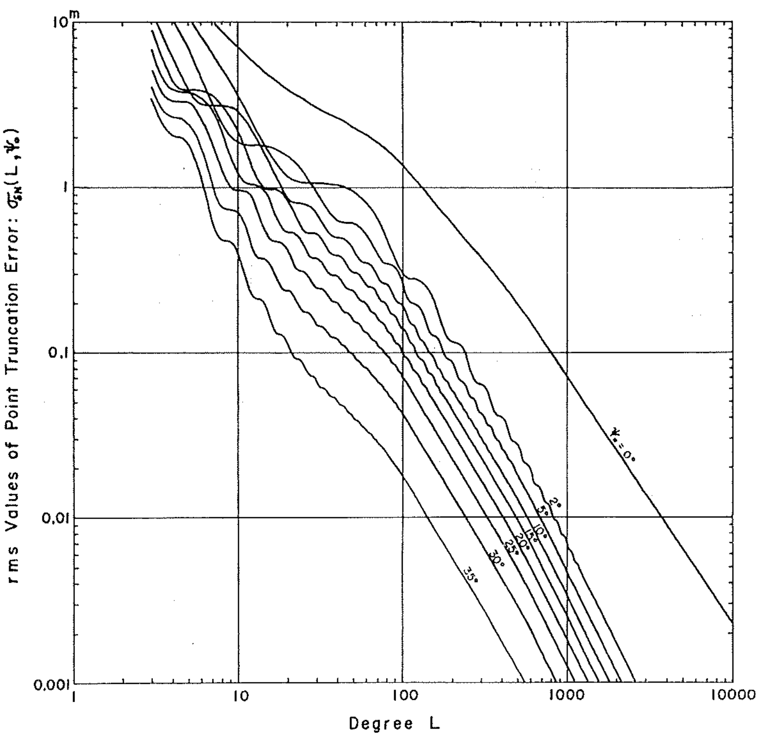

Figure 30b Point truncation errors based on the anomaly degree variance model *c*.

paper). Figure 30b shows truncation errors based on another anomaly degree variance model which is a combination of curve a for degrees lower than 30 and curve c for degrees higher than 30 (the combined degree variance model is called "anomaly degree variance model c" in this paper). The truncation error defined by (4-27) is called "point truncation error". We may be able to consider Figure 30a and Figure 30b as the lower bound and the upper bound of point truncation errors, respectively, due to the adopted anomaly degree variance models.

As for situation (A), L in (4-27) is derived by following equation for θ° block mean gravity anomalies:

$$L \fallingdotseq \frac{180^\circ}{\theta^\circ}, \tag{4-29}$$

and as for situation (B), L is corresponding to $l_{max}+1$, where l_{max} is the highest degree of the available satellite-derived geopotential coefficient set. Furthermore, let us consider the point truncation error of geoidal height computed under conditions shown in Figure 31. A cap area is divided into k zones which are numbered as 1, 2,..., k from inner to outer as seen in Figure 31. The radius of the outer boundary of $i-$th zone is ψ_i, and ψ_k is the radius of the outer-most boundary that coincides with the conventional cap size formerly denoted as ψ_0. It is assumed that s_i° $(i=1\sim k)$ block mean gravity anomalies are available in each zone. We consider s_i° block mean gravity anomalies can represent the gravity anomaly field up to degree $[180^\circ/s_i^\circ]$, and we put

$$L_i = \left[\frac{180^\circ}{s_i^\circ}\right]+1, \quad i=1\sim k.$$

Let L_{k+1} be the maximum degree of the satellite-derived geopotential coefficient set. By using (4-27), we can estimate

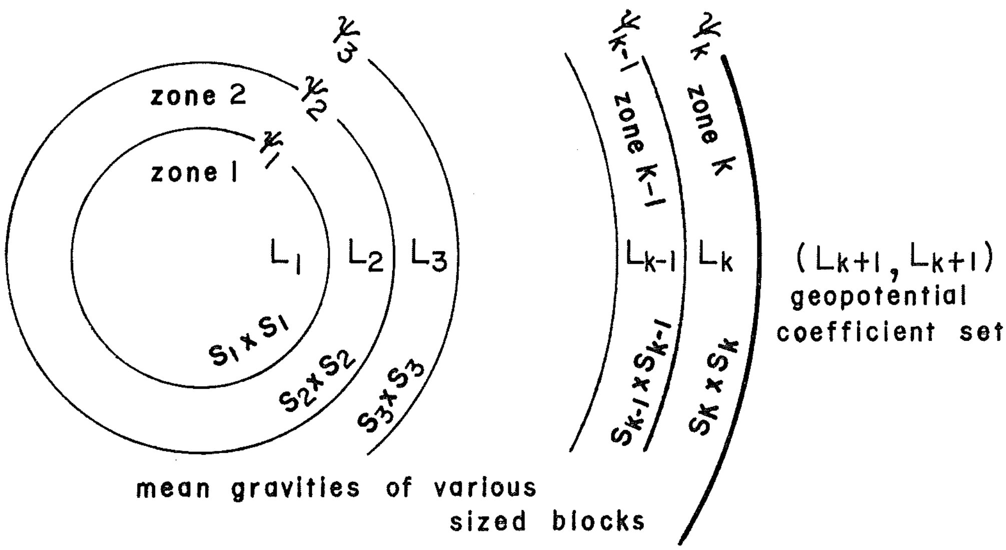

Figure 31 Zone divisions of a cap area.

Table 2 Individual point truncation error terms evaluated on the basis of anomaly degree variance models b and c

	Anomaly degree variance model b	Anomaly degree variance model c
$\sigma_{\delta N}(181, 0)$	0.36 m	0.69 m
$\sigma_{\delta N}(361, 0)$	0.17	0.31
$\sigma_{\delta N}(181, 5^\circ)$	0.05	0.10
$\sigma_{\delta N}(361, 5^\circ)$	0.02	0.03
$\sigma_{\delta N}(23, 20^\circ)$	0.45	0.51
$\sigma_{\delta N}(181, 20^\circ)$	0.02	0.04
$\sigma_{\delta N}(361, 20^\circ)$	0.01	0.01

the point truncation error of geoidal height according to the zone divisions of Figure 31. It is evaluated by

$$\sigma_{\delta N}^2 = \sum_{i=1}^{k+1} \sigma_{\delta N}^2 (L_i, \psi_{i-1}) - \sum_{i=1}^{k} \sum_{j=1}^{i} \sigma_{\delta N}^2 (L_j, \psi_i) \tag{4-30}$$

(Ganeko, 1977), where ψ_0 is zero.

We have computed the geoid undulations around Japan in Chapter 3 under the following data conditions:

$$\left.\begin{array}{ll} 0 \leq \psi \leq 5^\circ & 30' \times 30' \text{ block mean gravity anomalies} \\ 5^\circ < \psi \leq 20^\circ & 1^\circ \times 1^\circ \text{ block mean gravity anomalies} \\ \psi > 20^\circ & l_{max} = 22 \text{ satellite-derived geopotential coefficient set} \end{array}\right\} \tag{4-31}$$

To apply (4-30) to the data conditions (4-31), we put $k=2$, $\psi_1=5^\circ$, $\psi_2=20^\circ$, $L_1=361$, $L_2=181$ and $L_3=23$, and then the point truncation error is given by

$$\begin{aligned} \sigma_{\delta N}^2 &= \sigma_{\delta N}^2 (361, 0) + \sigma_{\delta N}^2 (181, 5^\circ) + \sigma_{\delta N}^2 (23, 20^\circ) \\ &\quad - \sigma_{\delta N}^2 (361, 5^\circ) - \sigma_{\delta N}^2 (181, 20^\circ) - \sigma_{\delta N}^2 (361, 20^\circ). \end{aligned} \tag{4-32}$$

Values of each term of (4-32) can be read from Figure 30a or Figure 30b depending on anomaly degree variance models. These values are listed in Table 2. Thus (4-32) is evaluated as

$$\left.\begin{aligned} \sigma_{\delta N}^2 &= (0.48 \text{ m})^2 \quad \text{for anomaly degree variance model } b \\ &= (0.60 \text{ m})^2 \quad \text{for anomaly degree variance model } c \end{aligned}\right\} \tag{4-33}$$

When geoidal heights are co mputed under the conditions:

$$\begin{array}{ll} 0 \leq \psi \leq 20^\circ & 1^\circ \times 1^\circ \text{ block mean gravity anomalies} \\ \psi > 20^\circ & l_{max} = 22 \text{ satellite-derived geopotential coefficient set} \end{array} \tag{4-34}$$

the point truncation error is evaluated by

$$\sigma_{\delta N}^2 = \sigma_{\delta N}^2 (181, 0) + \sigma_{\delta N}^2 (23, 20^\circ) - \sigma_{\delta N}^2 (181, 20^\circ)$$

and using numerical values in Table 2, we get

$$\left.\begin{aligned} \sigma_{\delta N}^2 &= (0.58 \text{ m})^2 \quad \text{for anomaly degree variance model } b \\ &= (0.86 \text{ m})^2 \quad \text{for anomaly degree variance model } c \end{aligned}\right\} \tag{4-35}$$

3) Relative truncation error

The error of geoidal height difference between two points P and Q is written as

$$\delta\Delta N_{PQ}=\delta(N_Q-N_P)=\delta N_Q-\delta N_P,$$

and using (4-24) the mean square value of it is given by

$$\begin{aligned}\sigma^2_{\delta\Delta N}(\Theta, L, \psi_0)&=M\{\delta\Delta N^2_{PQ}\}\\&=2\left[C_{\delta N}(0, L, \psi_0)-C_{\delta N}(\Theta, L, \psi_0)\right]\end{aligned} \tag{4-36}$$

(Ganeko, 1977). Inserting (4-26) and (4-27) into (4-36), we obtain

$$\sigma^2_{\delta\Delta N}(\Theta, L, \psi_0)=2\left(\frac{R}{2G}\right)^2\sum_{l=L}^{\infty}Q_l^2(\psi_0)\sigma_l^2(\Delta g)\left[1-P_l(\cos\Theta)\right]. \tag{4-37}$$

(4-37) can be used to evaluate the error in geoidal height difference between two points separated by an angular distance Θ when the geoidal heights at both points are computed under the same data conditions. The error defined by (4-37) is called "relative truncation error" in this paper. It may be natural that the relative truncation error (4-37) amounts to twice the point truncation error (4-27) when two points are separated far enough each other.

Ganeko (1977) calculated (4-37) by adopting anomaly degree variance model b, and gave Figure 32a and Figure 32b. We find out some rules concerning relative truncation errors from his results. When the distance between two points is one sixth or one seventh of wave-length λ_{min} which corresponds to the highest degree of the gravity data, i.e. surface gravities or satellite-derived gravity anomalies outside the cap area, the relative truncation error amounts to the same quantity as the point truncation error. When the distance is less than the critical distance, the relative truncation error is smaller than the point truncation error, and when the distance is sufficiently larger than λ_{min}, the square relative truncation error amounts to twice the square point truncation error. By using the notations of (4-27) and (4-37), the above rules are summarized as follows:

$$\sigma^2_{\delta\Delta N}(0, L, \psi_0)=0, \qquad \Theta=0, \tag{4-38a}$$

$$\sigma^2_{\delta\Delta N}(\Theta, L, \psi_0)<\sigma^2_{\delta N}(L, \psi_0), \qquad \Theta<\frac{60°}{L}, \tag{4-38b}$$

$$\sigma^2_{\delta\Delta N}(\Theta, L, \psi_0)\approx\sigma^2_{\delta N}(L, \psi_0), \qquad \Theta\approx\frac{60°}{L}, \tag{4-38c}$$

$$\sigma^2_{\delta\Delta N}(\Theta, L, \psi_0)\approx 2\sigma^2_{\delta N}(L, \psi_0), \qquad \Theta>1.5\frac{60°}{L}. \tag{4-38d}$$

We consider the case that $\theta°$ block mean gravity anomalies are available on the whole surface of the earth. Then we know the gravity anomaly field up to degree $L=180°/\theta°$. According to (4-38c), when the distance between two points is $\theta/3$, i.e. $\Theta=\theta/3$, the relative truncation error is as large as the point truncation error. Therefore, the geoidal heights computed at every $\theta°$ mesh point on the basis of $\theta°$ block mean gravtiy anomalies commit relative truncation errors in the geoidal height difference between neighbouring mesh points which are larger than point truncation errors at each mesh point.

Let us apply the rules of (4-38) to the data conditins of (4-31). On the analogy of (4-30) and (4-32), a relative truncation error is estimated by

$$\begin{aligned}\sigma^2_{\delta\Delta N}=&\,\sigma^2_{\delta\Delta N}(\Theta, 361, 0)+\sigma^2_{\delta\Delta N}(\Theta, 181, 5°)+\sigma^2_{\delta\Delta N}(\Theta, 23, 20°)\\&-\sigma^2_{\delta\Delta N}(\Theta, 361, 5°)-\sigma^2_{\delta\Delta N}(\Theta, 181, 20°)-\sigma^2_{\delta\Delta N}(\Theta, 361, 20°),\end{aligned} \tag{4-39}$$

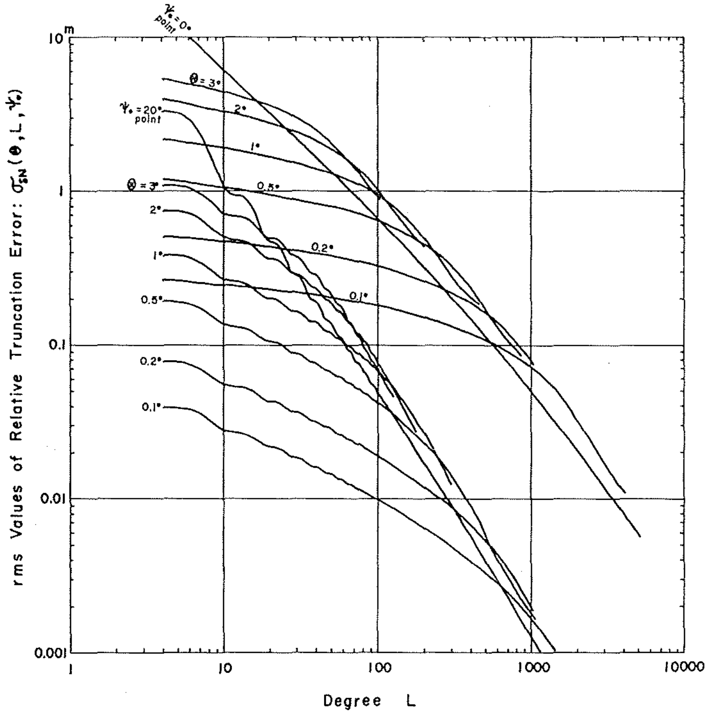

Figure 32a Relative truncation errors for $\psi_0=0°$ and $20°$ based on the anomaly degree variance model *b*.

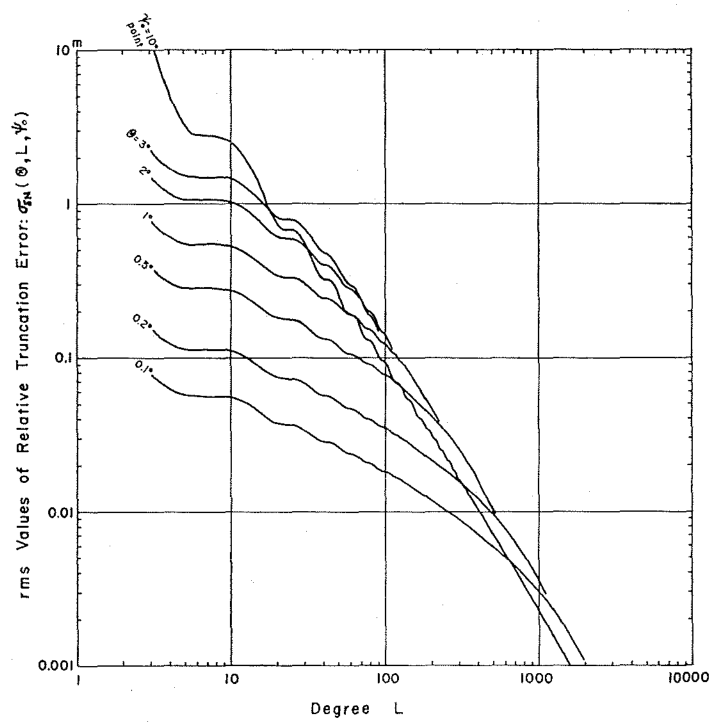

Figure 32b Relative truncation errors errors for $\psi_0=10°$ based on the anomaly degree variance model *b*.

and the critical distances of (4-38c) corresponding to each L in (4-39) are

$$\left.\begin{aligned}\Theta_1&=60°/361=0.17°,\\ \Theta_2&=60°/181=0.33°,\\ \Theta_3&=60°/23=2.61°.\end{aligned}\right\} \tag{4-40}$$

When $\Theta>1°$ (≈ 100 km), using (4-38) and (4-40), equation (4-39) is reduced to

$$\begin{aligned}\sigma^2_{\delta\Delta N}&=2\sigma^2_{N\delta}(361, 0)+2\sigma^2_{\delta N}(181, 5°)+\sigma^2_{\delta\Delta N}(\Theta, 23, 20°)\\ &\quad-2\sigma^2_{\delta N}(361, 5°)-2\sigma^2_{\delta N}(181, 20°)-2\sigma^2_{\delta N}(361, 20°),\end{aligned} \tag{4-41}$$

and when $\Theta>4°$, equation (4-39) is simply reduced to

$$\sigma^2_{\delta\Delta N}=2\sigma^2_{\delta N}. \tag{4-42}$$

Thus the relative truncation errors of the gravimetric geoid computed under the data conditions of (4-31) are estimated as shown in Table 3 on the basis of the anomaly degree variance model b given in Figure 32a (Table 4). When we compute geoidal heights under the data conditions of (4-34), a relative truncation error is estimated by

$$\begin{aligned}\sigma^2_{\delta\Delta N}&=\sigma^2_{\delta\Delta N}(\Theta, 181, 0)+\sigma^2_{\delta\Delta N}(\Theta, 23, 20°)\\ &\quad-\sigma^2_{\delta\Delta N}(\Theta, 181, 20°).\end{aligned} \tag{4-43}$$

The estimated relative truncation errors are also listed in the third column of Table 3.

4) A numerical test of the truncation error

JHDGF-1 gravity data file includes $10'\times 10'$ block mean gravity anomalies in some regions, and a $10'\times 10'$ detailed gravimetric geoid is computed. Figure 33 is obtained under the data conditions: $10'\times 10'$ block mean gravity anomalies for $\psi\leq 2°$; $30'\times 30'$ block means for $2°<\psi\leq 10°$; and GEM-8 geopotential model (Wagner et al., 1976, complete up to degree and order 25) for $\psi>10°$. we see more detailed structures of geoid undulation than the $30'\times 30'$ geoid previously shown in Figure 8. The geoidal dent seen from off Ensyu Nada toward Suruga Bay is due to the negative gravity anomalies along Nankai Trough (e.g. Segawa and Bowin, 1976). The contour lines change their directions as seen at the central part of Boso Peninsula. This is caused by the regional positive gravity anomalies at the tip of the peninsula. A $30'\times 30'$ gravimetric geoid is computed in the same region of Figure 33 based on the data conditions: $30'\times 30'$ block mean gravity anomalies for $\psi\leq 10°$ and GEM-8 geopotential model for $\psi>10°$. The differences between the $10'\times 10'$ geoid and the $30'\times 30'$ geoid are shown in Figure 34. Differences exceeding one meter occur in some regions. The numerical differences are also computed at $30'\times 30'$ mesh points located in the region of Figure 34. The mean difference is -9 cm ($10'\times 10'$ geoid$-30'\times 30'$ geoid) and the r.m.s. difference is 54 cm. On the other hand, we can estimate the difference between two kinds of geoid by using the truncation error estimation technique described formerly. If we adopt the anomaly degree variance model c to be fitted to the gravity anomaly field around the region concerned, from Figure 30b, we obtain truncation error difference between two geoids as around 30 cm. This value is slightly smaller than the actual r.m.s. difference, but acceptable taking the rough gravity anomaly over the concerning region into consideration.

Table 3 Relative truncation errors involved in the computed gravimetric geoid (Figure 8) estimated on the basis of the anomaly degree variance model *b*

Distance Θ	Data condition (4-31)	Data condition (4-34)
0°	0 m	0 m
1	0.31	0.54
2	0.43	0.62
3	0.54	0.70
5	0.68	0.82

Table 4 Numerical values of a relative truncation error term $\sigma_{\delta\Delta N}$ (Θ, 23, 20°) based on the anomaly degree variance model *b*

Distance Θ	0.1°	0.2	0.5	1.0	2.0	3.0
$\sigma_{\delta\Delta N}$	0.02 m	0.04	0.10	0.19	0.36	0.48

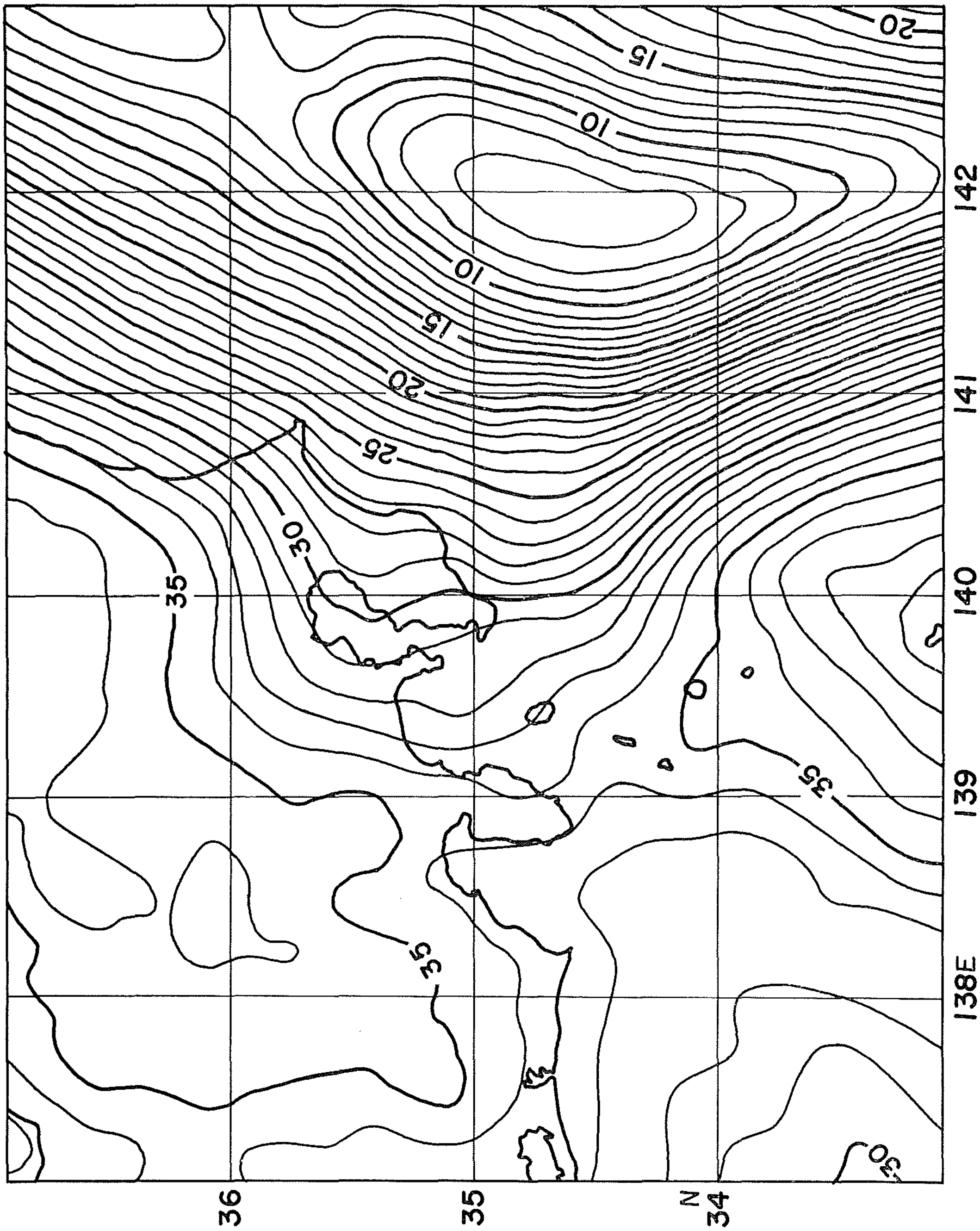

Figure 33 $10' \times 10'$ detailed gravimetric geoid computed in combination with GEM-8 geopotential coefficient set and $10' \times 10'$ block surface mean gravity anomalies Cap size: $\psi_0 = 10°$, $a = 6378145$m, $f = 1/298.255$. Contour interval: 1 m.

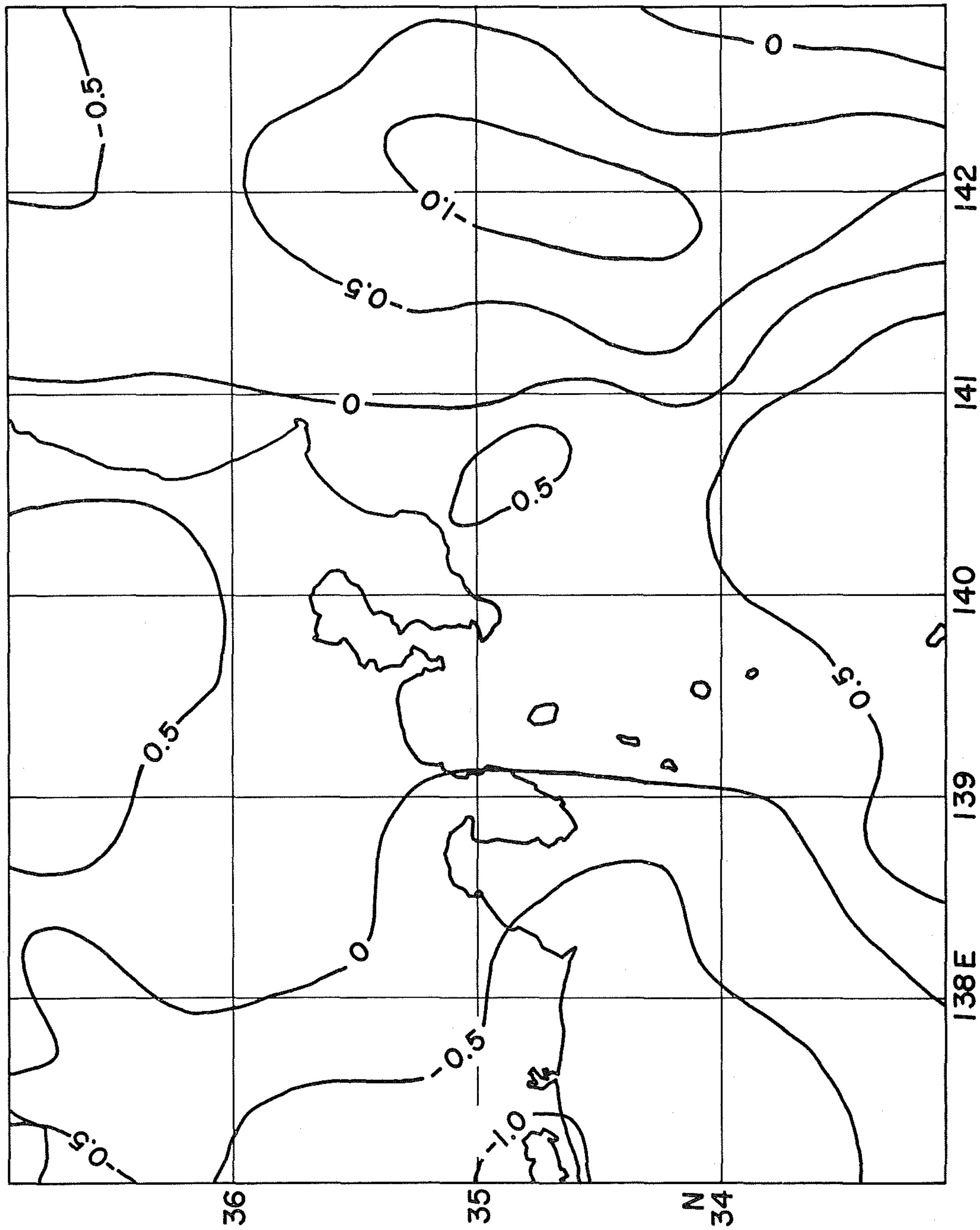

Figure 34 Differences between $10' \times 10'$ geoid and $30' \times 30'$ geoid. Contour interval: 0.5 m.

(3) Error Propagation from Geopotential Coefficient Errors

1) Error covariance

The satellite-derived geopotential field contributes to geoidal height computation from outside the cap area as much as equation (2-20c), and the contribution is evaluated by using Molodenskii's truncation function Q_l as follows (Molodenskii et al., 1962, p. 147):

$$N_{out} = \frac{R}{2G} \sum_{l=2}^{L} Q_l(\psi_0) \Delta g_l \,, \tag{4-44}$$

where R is the average radius of the earth, G the average gravity over the whole earth, L the maximum complete degree of a satellite-derived geopotential coefficient set, and ψ_0 the radius of the cap area. (4-44) has a similar form to (4-24) which was used to estimate the truncation errors. Δg_l, $l-$th degree surface harmonics of satellite-derived gravity anomaly, is evaluated from the satellite-derived geopotential coefficients as follows:

$$\Delta g_l = G(l-1) \sum_{m=0}^{l} [\bar{C}^*_{ml} \bar{R}_{lm} + \bar{D}_{lm} \bar{S}_{lm}] \tag{4-45}$$

which has the same notation as (2-16). From (4-44), we write the error of N_{out} caused by geopotential coefficient errors as

$$\delta N_{out} = \frac{R}{2G} \sum_{l=0}^{L} Q_l(\psi_0) \delta\Delta g_l \,, \tag{4-46}$$

where $\delta\Delta g_l$ is the error of $l-$th degree harmonics due to geopotential coefficient errors $\delta\bar{C}^*_{lm}$ and $\delta\bar{D}_{lm}$:

$$\delta\Delta g_l = G(l-1) \sum_{m=0}^{l} [\delta\bar{C}^*_{lm} \bar{R}_{lm} + \delta\bar{D}_{lm} \bar{S}_{lm}]. \tag{4-47}$$

We define the covariance of δN_{out} by

$$\begin{aligned} K_{\delta N}(\Theta, \psi_0) &= M\{\delta N^P_{out} \delta N^Q_{out}\} \\ &= \left(\frac{R}{2G}\right)^2 \sum_{l=2}^{L} \sum_{l'=2}^{L} Q_l(\psi_0) Q_{l'}(\psi_0) M\{\delta\Delta g_l(P) \delta\Delta g_{l'}(Q)\} \,, \end{aligned} \tag{4-48}$$

where Θ is the angular distance between points P and Q on the surface of the earth. In the same way as we have obtained (4-26) from (4-25), (4-48) is reduced to

$$K_{\delta N}(\Theta, \psi_0) = \left(\frac{R}{2G}\right)^2 \sum_{l=2}^{L} Q_l^2(\psi_0) \sigma_l^2(\delta\Delta g_s) P_l(\cos\Theta). \tag{4-49}$$

$\sigma_l^2(\delta\Delta g_s)$ is the error degree variance of satellite-derived gravity anomaly, which is evaluated from the geopotential coefficient errors:

$$\sigma_l^2(\delta\Delta g_s) = G^2(l-1)^2 \sum_{m=0}^{l} (\delta\bar{C}^{*2}_{lm} + \delta\bar{D}^2_{lm}). \tag{4-50}$$

Here subscript s indicates "satellite-derived" again.

2) Point undulation error

The mean square error of geoidal height due to geopotential coefficient errors at an arbitrary point is given by putting $\Theta=0$ in (4-49), and it is written as

$$\varepsilon^2_{\delta N}(\psi_0) \equiv K_{\delta N}(0, \psi_0) = \left(\frac{R}{2G}\right)^2 \sum_{l=2}^{L} Q_l^2(\psi_0)\, \sigma_l^2(\delta\Delta g_s). \tag{4-51}$$

To evaluate the above equation, we have to know the error degree variances (4-50), i.e. geopotential coefficient errors $\delta\bar{C}^*_{lm}$ and $\delta\bar{D}_{lm}$. It is not necessarily easy to get the geopotential coefficient errors actually. Some geopotential coefficient sets are accompanied with estimated errors of the coefficients. We can define % error of the coefficients by

$$(\%\ \text{error})_l=\left\{\frac{\sum_{m=0}^{l}(\delta\bar{C}^2_{lm}+\delta\bar{D}^2_{lm})}{\sum_{m=0}^{l}(\bar{C}^2_{lm}+\bar{D}^2_{lm})}\right\}^{\frac{1}{2}}\times 100 \tag{4-52}$$

which was used by Rapp and Rummel (1975). Figure 35 shows examples of % errors produced from GEM-8 and GEM-10 geopotential models. We see some accuracy improvements of the coefficients in GEM-10 model. The fact that % errors around degree 20 are almost 100 % or more shows that coefficients at high degrees were poorly determined, but not that those coefficients are meaningless. Another method of evaluating the accuracy of coefficients was adopted by Rapp (1973) and Rapp and Rummel (1975), which estimate coefficient errors from two different geopotential models, A and B for example. In this case coefficient errors are calculated by

$$\left.\begin{aligned}\left|\delta\bar{C}_{lm}\right|&=\frac{1}{\sqrt{2}}\left|\bar{C}^A_{lm}-\bar{C}^B_{lm}\right|,\\ \left|\delta\bar{D}_{lm}\right|&=\frac{1}{\sqrt{2}}\left|\bar{D}^A_{lm}-\bar{D}^B_{lm}\right|.\end{aligned}\right\} \tag{4-53}$$

Table 5 gives error degree variances derived from coefficient errors in geopotential models GEM-8 and GEM-10 and those evaluated based on (4-53) from coeffiicient differences between GEM-8 model and SAO-SE4. 3 model (Gaposchkin, 1976). The lowermost line in Table 5 indicates commission errors of gravity anomaly computed by $[\sum\sigma_l^2(\delta\Delta g_s)]^{\frac{1}{2}}$ on the basis of each error degree variance set.

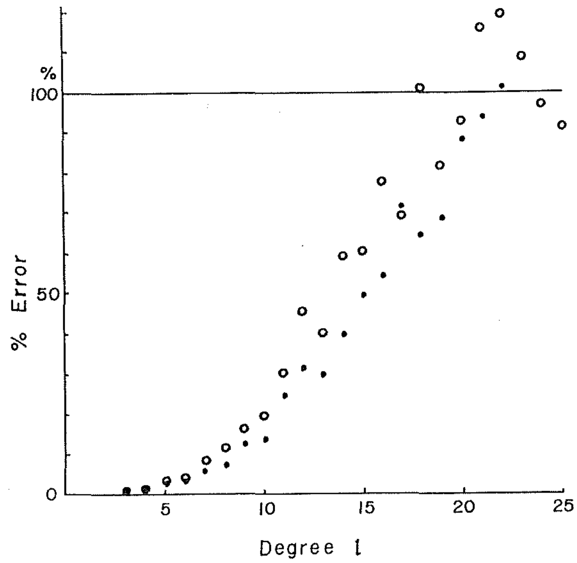

Figure 35 Percent errors of geopotential coefficients. Open and full circles are for GEM-8 and GEM-10 models, respectively.

Table 5 Error degree variances based on satellite-derived geopotential coefficient sets

Degree	GEM-8 - SAO-SE4. 3	GEM-8	GEM-10
	$mGal^2$	$mGal^2$	$mGal^2$
3	0.024	0.003	0.001
4	0.067	0.004	0.001
5	0.444	0.028	0.013
6	0.355	0.033	0.014
7	0.710	0.123	0.062
8	0.916	0.132	0.057
9	1.594	0.308	0.166
10	1.342	0.354	0.169
11	2.561	0.681	0.382
12	2.095	0.675	0.349
13	1.669	1.042	0.534
14	2.814	1.152	0.527
15	2.547	1.645	0.732
16	1.712	2.119	0.762
17	2.394	3.296	1.074
18	1.970	5.071	1.283
19	2.150	6.277	1.322
20	3.001	7.265	1.553
21	2.877	7.960	1.584
22	2.946	8.357	1.740
23	2.626	8.374	
24	3.147	8.168	
	6.3 mGal	8.3 mGal	3.5 mGal

When we know the errors of geopotential coefficients, a point undulation error is obtained by (4-51). The evaluated undulation errors are shown in Table 6 for cap radii $\psi_0=0$, 10°, 20° and 30°. When $\psi_0=0$, the tabulated undulation errors express the accuracies of satellite-derived geoid undulations in combination with omission errors due to the omissoin of higher degree terms of geoid undulation than those included in satellite-derived geopotential models. The omission errors have already discussed in detail in the previous section. Such omission error given as $\sigma_{\delta N}(L, 0)$ (see (4-27)) is read as 3 or 4 meters from Figure 30 in the case $L=20$. Then we can estimate the accuracy of the satellite-derived geoid undulations by

$$m^2=\varepsilon_{\delta N}^2(0)+\sigma_{\delta N}^2(L, 0).$$

As we see in Table 6, under the data condition (4-31) or (4-34) adopted in Chapter 3 to compute a gravimetric geoid, the mean point undulation error amounts to 0.31 m due to uncertainties of geopotential coefficients of GEM-10 model.

3) Relative undulation error

The error of the difference between N_{out} components at points P and Q is written by

$$\delta\varDelta N_{out}=\delta(N_{out}^Q-N_{out}^P)=\delta N_{out}^Q-\delta N_{out}^P,$$

and its mean square value is sxpressed by using the undulation error covariance (4-49) as follows:

$$\begin{aligned}\varepsilon_{\delta\varDelta N}^2(\Theta, \psi_0)&=M\{\delta\varDelta N_{out}^2\}\\&=2[K_{\delta N}(0, \psi_0)-K_{\delta N}(\Theta, \psi_0)],\end{aligned} \tag{4-54}$$

Table 6 Point geoidal height errors due to errors of geopotential coefficients

Cap size ψ_0	GEM-8 −SAO-SE 4.3	GEM-8	GEM-10
°	m	m	m
0	3.46	3.02	1.53
10	1.26	0.95	0.59
20	0.82	0.52	0.31
30	0.44	0.27	0.15

where Θ is the angular distance between P and Q. Inserting the expression of (4-49) into (4-54), we obtain

$$\varepsilon^2_{\delta\Delta N}(\Theta, \psi_0)=2\left(\frac{R}{2G}\right)^2\sum_{l=2}^{L}Q_l^2(\psi_0)\sigma_l^2(\delta\Delta g_s)\ [1-P_l(\cos\Theta)]. \tag{4-55}$$

Note that (4-55) is very similar to (4-37) which is obtained for the estimation of relative truncation error. Although (4-55) has been already discussed by Christodoulidis (1976) and Ganeko (1977), we here evaluate (4-55) by using error degree variances shown in Table 5. The obtained relative undulation errors due to geopotential coefficient errors are given in Table 7. We find that the relative undulation errors up to distance $\Theta=5°$ ($\approx$500 km) are less than the point undulation errors. As seen in Table 6 and Table 7, the GEM-10 model results in the smallest undulation errors.

Table 7 Relative geoidal height errors due to errors of geopotential coefficients

	GEM-8−SAO-SE4.3			GEM-8			GEM-10		
Cap size	ψ_0=10°	20°	30°	10°	20°	30°	10°	20°	30°
Distance Θ	m	m	m	m	m	m	m	m	m
0.2°	0.04	0.02	0.01	0.04	0.02	0.01	0.02	0.01	0.005
0.4	0.08	0.05	0.02	0.08	0.04	0.02	0.04	0.02	0.01
0.6	0.12	0.07	0.03	0.11	0.06	0.04	0.07	0.03	0.02
0.8	0.16	0.09	0.04	0.15	0.08	0.05	0.09	0.04	0.02
1.0	0.20	0.12	0.06	0.19	0.10	0.06	0.11	0.06	0.03
2.0	0.40	0.23	0.11	0.38	0.20	0.12	0.22	0.11	0.05
3.0	0.59	0.34	0.16	0.56	0.30	0.17	0.32	0.16	0.08
4.0	0.78	0.45	0.22	0.72	0.38	0.22	0.42	0.21	0.10
5.0	0.95	0.55	0.26	0.89	0.47	0.27	0.51	0.26	0.13
6.0	1.12	0.64	0.31	1.03	0.54	0.31	0.60	0.30	0.15
7.0	1.27	0.73	0.35	1.16	0.61	0.34	0.67	0.34	0.17
8.0	1.40	0.81	0.39	1.26	0.66	0.37	0.74	0.38	0.18
9.0	1.52	0.87	0.42	1.35	0.71	0.39	0.80	0.40	0.19
10.0	1.63	0.93	0.45	1.42	0.74	0.40	0.84	0.43	0.20
Point error	1.26	0.82	0.44	0.95	0.52	0.27	0.59	0.31	0.15

(4) Error Propagation from Terrestrial Gravity Data Errors

1) Point undulation error

When terrestrial gravity data are utilized for geoidal height computation through (2-20b), a geoidal height error can be written in the form:

$$\delta N_{in}=\frac{R}{4\pi G}\iint_{cap}\delta\Delta g\, S(\psi)\,d\sigma, \tag{4-56}$$

where $\delta\Delta g$ is error of terrestrial gravity anomaly. When the terretrial gravities are given in the form of block means, (4-56) is rewritten as

$$\delta N_{in}=\frac{R}{4\pi G}\sum_{i=1}^{k}\delta\overline{\Delta g}_i\cdot q_i, \tag{4-57}$$

where $\delta\overline{\Delta g}_i$ is the error of the mean gravity anomaly over block σ_i. q_i is given by (3-3), and k is the number of blocks included in a cap area with radius ψ_0. The mean square value of (4-57) is given by

$$m_{\delta N}^2(\psi_0)=M\{\delta N_{in}^2\}$$

$$=\left(\frac{R}{4\pi G}\right)^2\sum_{i=1}^{k}\sum_{j=1}^{k}M\{\delta\overline{\Delta g}_i\delta\overline{\Delta g}_j\}\,q_i\,q_j=\left(\frac{R}{4\pi G}\right)^2\sum_{i=1}^{k}\sum_{j=1}^{k}C_\delta(i,j)\,q_i\,q_j, \tag{4-58}$$

where $C_\delta(i,j)$ is the error covariance of block mean gravity anomalies assuming to be a function of the distance between blocks σ_i and σ_j.

We consider first a specific case of the error covariance (called "Case A"):

$$\left.\begin{aligned}C_\delta(i,j)&=m_\theta^2 \quad \text{for } i=j,\\ &=0 \quad\ \ \text{for } i\neq j,\end{aligned}\right\}\ \text{Case A}, \tag{4-59}$$

which means that the errors of block mean gravity anomalies are completely independent of each other. m_θ^2 is the mean square error of $\theta°$ block mean gravity anomalies. When the error covariance satisfies (4-59), (4-58) is reduced to

$$m_{\delta N}^2(\psi_0)=\left(\frac{R}{4\pi G}\right)^2\sum_{i=1}^{k}m_\theta^2\,q_i^2. \tag{4-60}$$

In the evaluation of (4-60), we take a square cap area such as shown in Figure 36, and the square cap area is extended by adding square rings of $\theta°$ width. The evaluated undulation errors for block sizes $\theta=10'$, $30'$ and $1°$ are shown in Figure 37, and some of numerical values are given in the columns labeled as "Case A" in Table 8. m_θ has been taken to be 1 mGal for all block sizes. As we can read from Figure 37, the undulation errors increase steadily as cap size becomes larger, but they increase little even when cap size becomes larger than 10°. That may be due to the facts that the correlation distance of gravity anomaly data errors is short under the assumption of (4-59) and that distant short wave-length variations of gravity anomaly contribute little to the geoidal height computations as investigated in section 3-(2). We can derive a simple formula for estimating undulation errors due to terrestrial gravity errors when the cap is large enough, such as

$$m_{\delta N}(\text{cm})\fallingdotseq 12\times m_\theta(\text{mGal})\times\theta(\text{degree}).$$

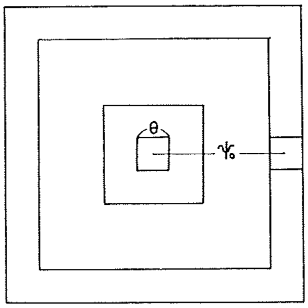

Figure 36 Square cap area.

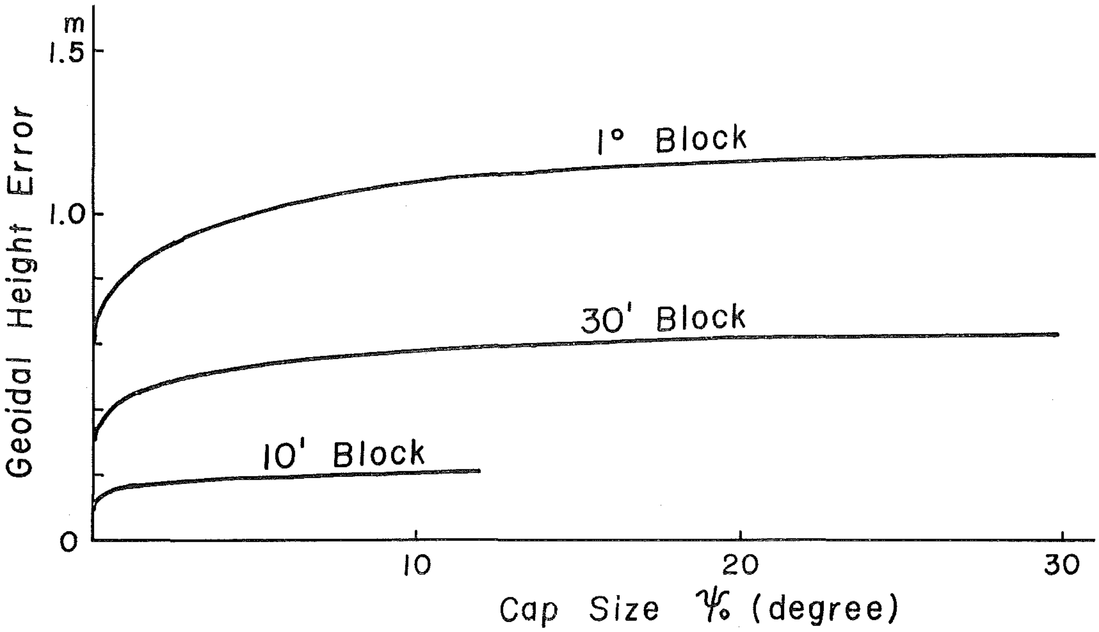

Figure 37 Point geoidal height errors due to errors of block mean gravity anomalies. For error covariance Case A, and $m_0^2=1$ mGal^2.

Table 8 Point geoidal height errors due to errors of block mean gravity anomalies ($m_\theta^2=1$ mGal^2)

Block size	$\theta=10'$			$30'$			$1°$		
Error covariance	Case A	Case B	Case C	A	B	C	A	B	C
Cap size ψ_0 °	m	m	m	m	m	m	m	m	m
β_0	0.011			0.032			0.064		
2	0.018	0.024	0.040	0.048	0.065	0.092	0.089	0.120	0.189
5	0.020	0.027	0.045	0.054	0.074	0.122	0.101	0.139	0.226
10	0.021	0.029	0.049	0.059	0.081	0.135	0.110	0.152	0.252
20				0.062	0.085	0.144	0.117	0.162	0.270
30				0.062	0.086	0.145	0.118	0.163	0.274
35							0.118	0.163	0.274

Let us adopt another type of error covariance of gravity anomaly data instead of (4-59); i.e. an exponential type error covariance:

$$C_\delta(\psi)=m_\theta^2 \exp\,(-D_\theta\,\psi),\quad D_\theta>0, \tag{4-61}$$

which has a long tail in the error correlation and was ever used by Christodoulidis (1976) to estimate the same kind of undulation error as treated in this section by a different method. Before applying (4-61) to (4-58), we rewrite (4-58) as follows:

$$m_{\delta N}^2(\psi_0)=\left(\frac{R}{4\pi G}\right)^2\Big\{\sum_i{}'\sum_j{}' C_\delta(i,j)\,q_i\,q_j$$
$$+2q_p\sum_i{}' C_\delta(i,p)q_i+C_\delta(p,p)q_p{}^2\Big\}, \tag{4-62}$$

where P is the center of block σ_P where computation of geoidal height is made, and $\sum'$ indicates the summation over all blocks in the cap area except for block σ_P. Since the correlation distance of gravity anomaly data errors is usually short, we approximately write the first term in the righthand side of (4-62) as

$$\sum_i{}'\sum_j{}' C_\delta(i,j)q_i\,q_j \doteqdot \sum_i{}' u^2\,q_j{}^2, \tag{4-63}$$

where

$$u^2=\sum_j{}' C_\delta(i,j). \tag{4-64}$$

It is noteworthy that (4-64) corresponds to the "error constant" introduced by Heiskanen and Moritz (1967, p. 273). Let the area of blocks be denoted by B, approximate (4-64) to

$$u^2=\sum_j{}' C_\delta(i,j)\doteqdot\frac{1}{B}\sum_j C_\delta(i,j)B\doteqdot\frac{1}{B}\iint_{cap} C_\delta(\psi_{ij})d\sigma, \tag{4-65}$$

and insert (4-61) into (4-65), then we obtain

$$Bu^2\doteqdot m_\theta^2\int_{\alpha=0}^{2\pi}\int_{\psi=0}^{\pi}\exp(-D_\theta\psi)\sin\psi\,d\psi\,d\alpha$$
$$=2\pi m_\theta^2\frac{1}{D_\theta^2+1}\,[1+\exp(-D_\theta\,\pi)]\doteqdot 2\pi m_\theta^2/D_\theta^2. \tag{4-66}$$

The last approximation in (4-66) is permissible because of short correlation distance of the gravity data errors. From (4-62), (4-63) and (4-66), we finally obtain

$$m_{\delta N}^{2}(\psi_0)=\left(\frac{R}{4\pi G}\right)^2\left[\frac{2\pi}{B}\frac{m_\theta^2}{D_\theta^2}\sum_i{}' q_i^2\right.$$
$$\left.+2m_\theta^2 q_p\sum_i{}'\exp(-D_\theta\,\psi_{ip})q_i+m_\theta^2 q_p^2\right]. \tag{4-67}$$

We evaluate (4-67) for two cases of the parameter in the exponential error covariance, i.e.,

$$\left.\begin{array}{ll} D_\theta=1/\beta_0\,,\quad \beta_0=\sqrt{B/\pi}: & \text{Case B,} \\ D_\theta=1/\theta & :\ \text{Case C,} \end{array}\right\} \tag{4-68}$$

where β_0 is the radius of a circular block whose area is equal to the area of $\theta°$ square block. Figure 38 and Table 8 include the results for block sizes $\theta=10'$, $30'$ and $1°$ when $m_\theta=1$ mGal. Case C gives a longer error correlation distance than Case B, so that Case C naturally results in larger undulation errors than Case B and, of course, than Case A.

2) Relative undulation error

The error of geoidal height difference due to errors of terrestrial gravity data is derived from (4-56) as follows:

$$\delta\Delta N=\delta\,(N_{in}^{P}-N_{in}^{Q})=\frac{R}{4\pi G}\iint_{cap}\delta\Delta g\,[S(\psi_P)-S(\psi_Q)]\,d\sigma, \tag{4-69}$$

where ψ_P is the angular distance between P and the surface element $d\sigma$, and ψ_Q is the distance between Q and $d\sigma$. The cap area is taken to be large enough to include sufficient terrestrial data for computations of geoidal heights at both points P and Q (see Figure 39). If we rewrite (4-69) so as to make the equation fit the available terrestrial gravity data, we have

$$\delta\Delta N=\frac{R}{4\pi G}\sum_{i=1}^{k}\delta\overline{\Delta g}_i\,[q_{Pi}-q_{Qi}]. \tag{4-70}$$

The difinitions of q_{Pi} and q_{Qi} are derived from a generalized expression of q_{XY}

$$q_{XY}=\iint_{\sigma_Y}S(\psi_{Xy})d\sigma_y, \tag{4-71}$$

where ψ_{Xy} is the angular distance between point X, the center of bloek σ_X, and the surface element $d\sigma_y$ in block σ_Y. Writing the block area as $B=\pi\beta_0^2$, we have approximate expressions of (4-71) as

$$\left.\begin{array}{l} q_{XX}=4B/\beta_0, \\ q_{XY}=q_{YX}=S(\psi_{XY})\cdot B, \end{array}\right\} \tag{4-72}$$

where ψ_{XY} is the angular distance between centers of blocks σ_X and σ_Y. Then we obtain from (4-70) and (4-72)

$$\delta\Delta N=\frac{R}{4\pi G}B\left\{\sum_i{}'\delta\overline{\Delta g}_i\,[S(\psi_{Pi})-S(\psi_{Qi})]\right.$$
$$\left.+(\delta\overline{\Delta g}_P-\delta\overline{\Delta g}_Q)\left[\frac{4}{\beta_0}-S(\psi_{PQ})\right]\right\}. \tag{4-73}$$

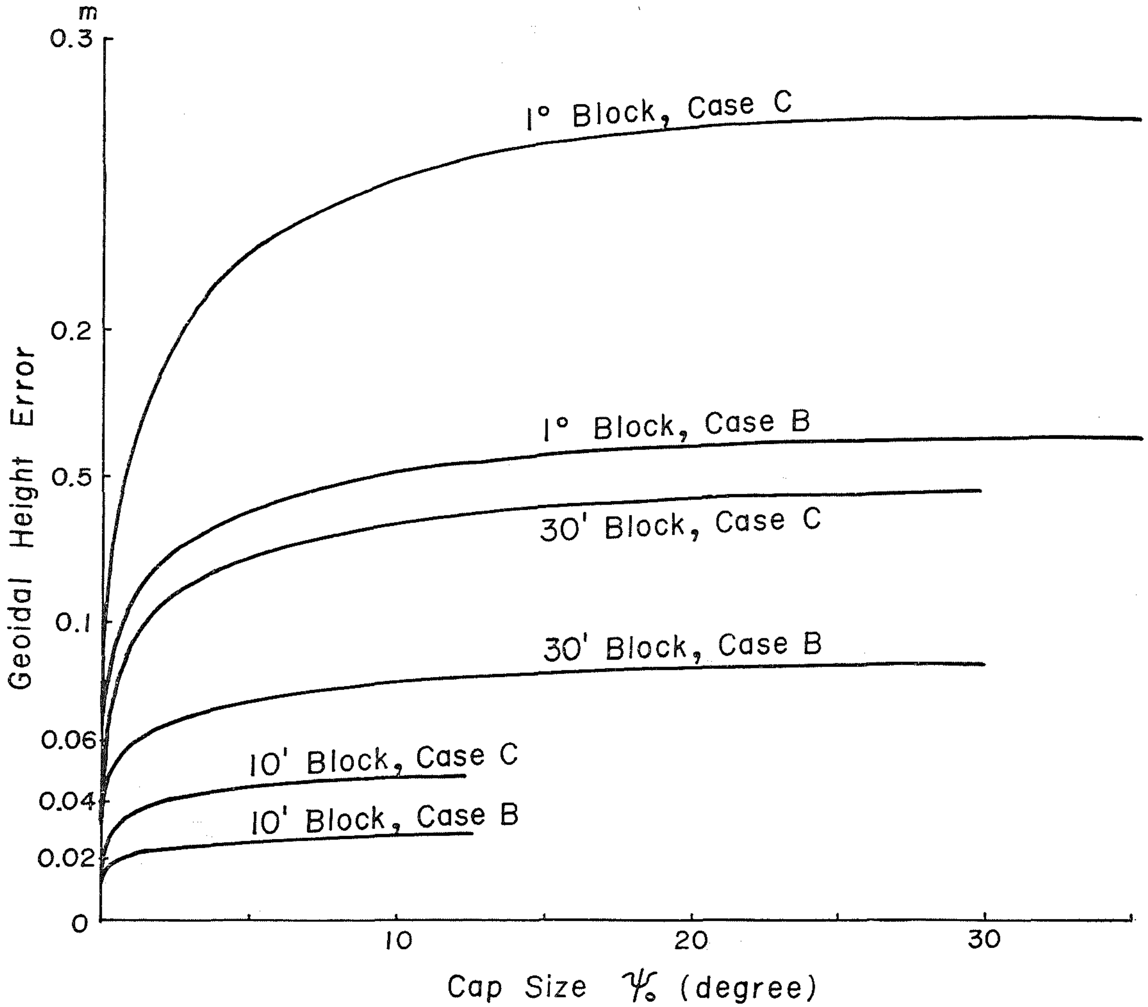

Figure 38 Point geoidal height errors due to errors of block mean gravity anomalies. For error covariance models Case B and C, and $m_0^2=1$ mGal^2.

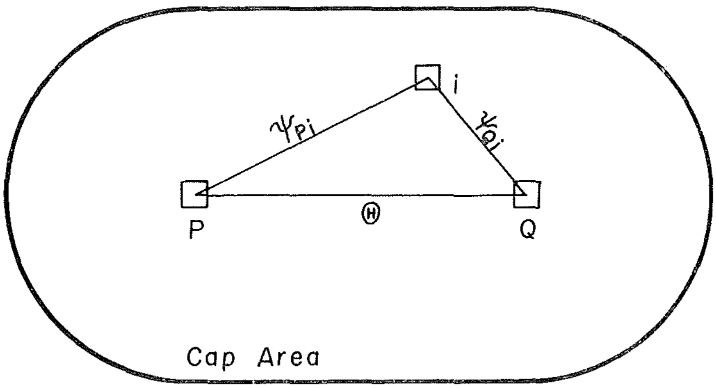

Figure 39 Common cap area for the computation of a geoidal height diflerence.

The summation $\sum'$ does not include $i=P$ and $i=Q$. Setting $A=RB/4\pi G$, the mean square value of (4-73) can be written in the form:

$$
\begin{aligned}
m^2_{\delta\Delta N}(\Theta) &= M\{\delta\Delta N^2\} \\
&= A^2\sum_i{}' \sum_j{}' M\{\delta\overline{\Delta g}_i\, \delta\overline{\Delta g}_j\}\,[S(\psi_{Pi})-S(\psi_{Qi})]\,[S(\psi_{Pj})-S(\psi_{Qj})] \\
&+2A^2\sum_i{}' M\left\{\delta\overline{\Delta g}_i\,(\delta\overline{\Delta g}_P-\delta\overline{\Delta g}_Q)\right\}\left[\frac{4}{\beta_0}-S(\Theta)\right] \\
&+A^2M\left\{(\delta\overline{\Delta g}_P-\delta\overline{\Delta g}_Q)^2\right\}\left[\frac{4}{\beta_0}-S(\Theta)\right]^2,
\end{aligned}
\tag{4-74}
$$

where Θ is the distance between P and Q. Being assumed that the error covariance has a short correlation distance, (4-74) is reduced to

$$
\begin{aligned}
m^2_{\delta\Delta N}(\Theta) &= A^2\sum_i{}' [\sum_j{}' C_\delta(\psi_{ij})]\,[S(\psi_{Pi})-S(\psi_{Qi})]^2 \\
&+2A^2\sum_i{}'\left[C_\delta(\psi_{Pi})-C_\delta(\psi_{Qi})\right]\left[\frac{4}{\beta_0}-S(\Theta)\right] \\
&+2A^2\left[C_\delta(0)-C_\delta(\Theta)\right]\left[\frac{4}{\beta_0}-S(\Theta)\right]^2.
\end{aligned}
\tag{4-75}
$$

Note that the second term of the righthand side of (4-75) vanishes because of the symmetrical expressions at P and Q. Therefore, we can evaluate the relative undulation errors by a sum of the following two terms:

$$
\left.
\begin{aligned}
I_1 &= A^2\sum_i{}' [\sum_j{}' C_\delta(\psi_{ij})]\,[S(\psi_{Pi})-S(\psi_{Qi})]^2, \\
I_2 &= 2A^2\left[C_\delta(0)-C_\delta(\Theta)\right]\left[\frac{4}{\beta_0}-S(\Theta)\right]^2.
\end{aligned}
\right\}
\tag{4-76}
$$

Using (4-65) in I_1, i.e. $u^2=m_\theta^2$ for the error covariance Case A (see (4-59)) and $u^2=2\pi m_\theta^2/BD_\theta^2$ for the exponential type error covariances Cases B and C (see (4-68)), we evaluate (4-76) for block sizes $\theta=10'$, $30'$ and $1°$. And we take the common cap area (Fig. 39) to be large enough, i. e. the boundary of the cap area being located farther than 30° from both points P and Q. Some of evaluated results are shown in Table 9. The root mean square error m_θ is assumed to be 1 mGal in Table 9.

JHDGF-1 gravity file includes estimated errors of block mean gravity anomalies, and in these case we can compute a geoidal height error by

Table 9 Relative geoidal height errors due to errors of block mean gravity anomalies ($m_\theta^2=1\,\mathrm{mGal}^2$)

Block size	$\theta=10'$			30′			1°		
Error covariance	Case A	Case B	Case C	A	B	C	A	B	C
Angular distance Θ (°)	m	m	m	m	m	m	m	m	m
1	0.018	0.021	0.031	0.042	0.046	0.058	0.067	0.066	0.076
2	0.020	0.025	0.038	0.050	0.058	0.082	0.085	0.092	0.118
3	0.021	0.027	0.042	0.055	0.065	0.096	0.095	0.107	0.148
5	0.023	0.029	0.047	0.060	0.073	0.113	0.107	0.126	0.186
10	0.025	0.033	0.054	0.068	0.086	0.138	0.125	0.154	0.240
15	0.027	0.035	0.058	0.074	0.094	0.153	0.136	0.171	0.275
20	0.028	0.037	0.062	0.078	0.100	0.165	0.145	0.185	0.301

$$m_1^2=\left(\frac{R}{4\pi G}\right)^2 \sum_{i=1}^{k} \delta\overline{\Delta g}_i^2\, q_i^2 \tag{4-77}$$

from the given errors of block mean gravity anomalies under the assumption that the errors are independent of each other. From (4-77), m_1 is evaluated to be 0.8 to 1.0 meters in JHDGF-1 region under the data conditions of (4-31) and to be around 1.3 meters outside the JHDGF-1 region under the data conditions of (4-34). Then we assume the geoidal height error of one meter due to errors of terrestrial gravity data and also assume that all block mean gravity anomalies suffer the same amount of mean errors, written as m, independently. Under the data conditions of (4-31) and from Table 8, we can write

$$m_{\delta N}^2=m^2\,\{0.054^2+(0.117^2-0.101^2)\}=(1\ \mathrm{meter})^2.$$

The above equation yields $m=12.5$ mGal, and the value of m brings about a geoidal height error under the data conditions of (4-34) such as

$$m_{\delta N}^2=0.117^2\times 12.5^2=(1.46\ \mathrm{meter})^2. \tag{4-78}$$

Since the main contribution to the undulation error is made by $1°\times 1°$ block data, we estimate a relative undulation error due to terrestrial gravity data errors included in the geoidal map obtained in Chapter 3 as follows:

$$\bar{m}_{\delta\Delta N}^2=m^2\times m_{\delta\Delta N}^2(\Theta,\theta=1°).$$

From $m=12.5$ mGal and Table 9 for $\Theta=5°$ ($\approx$500 km), we obtain

$$m_{\delta\Delta N}^2=0.107^2\times 12.5^2=(1.34\ \mathrm{meter})^2. \tag{4-79}$$

We should note here that it has been assumed that the error covariance satisfies the condition of Case A.

(5) Undulation Errors due to Neglection of Sea Surface Topography

1) Undulation errors due to sea gravity errors

Physical oceanographic theory predicts deviations of the mean sea surface from a equipotential surface (e. g. Lisitzin, 1974), and the deviations are computed from oceanographic data such as velocity of ocean currents and salinity and temperature of sea water. We call the deviations of the mean sea surface from a equipotential surface, the geoid, "sea surface topography". Since the sea surface topographical heights are in order of one meter, they have been neglected in the theory of physical geodesy until recently. The recent developments in satellite altimetry have achieved an accuracy higher than one meter by Geos-3 satellite (e.g. Kearsley, 1977; Rapp, 1977), and a trial to achieve around 10 cm accuracy of altimeter observation has been made by SEASAT-1 satellite (NASA News, 78-77). The fact that the satellite altimetry provides us with the shape of sea surface with such a high accuracy forces the physical geodesy to enter a new age of 10 cm global geodesy. Therefore, it may be necessary to investigate the effects of sea surface topography on the computation of geoidal heights.

The gravity measurements at sea are generally made on the surface of the sea water, so that the measured gravities are not considered to be on a equipotential surface, i.e. on the geoid. We can apply the gravity reduction procedure (2-4) to sea gravities just as land gravities. Normal height H^* in (2-4) is almost equal to the sea surface topographical height t, and then gravity anomaly at sea is befined by

$$\Delta g = g_P - \gamma_0 + \frac{2\gamma_0}{a} t, \tag{4-80}$$

where g_P is real gravity on the sea surface, γ_0 the normal gravity on the reference ellipsoid and a the semi-major axis of the reference ellipsoid. In Chapter 3, we have used gravity data without the correction term concerning t. The geoidal height error due to the neglection of this term is estimated by

$$\delta N_t = \frac{R}{4\pi G} \iint_\sigma \alpha t\, S(\psi) d\sigma, \tag{4-81}$$

where $\alpha = 2\gamma_0/a$. Brennecke and Groten (1977) evaluated (4-81) by using a world-wide map of the sea surface topography by Lisitzin (1974). According to their results, the contribution from the long wave-length components of the sea surface topography, the components from degree 2 to degree 10 of the spherical harmonic expansion of the sea surface topography, is about 60 cm, and the contribution from the higher degree terms is as small as several centimeters. Since the effect of the long wave-length components of the sea surface topography is not negligible, we can check possible geoidal height errors due to the effect of the sea surface topography by using the computation method adopted in Chapter 3. The geoidal height error is evaluated as

$$\delta N_t = \frac{R}{4\pi G} \iint_{cap} \alpha t\, S(\psi) d\sigma. \tag{4-82}$$

In this case, we set t=constant ever the cap because of the long wave length characteristics of the sea surface topography, then we obtain

$$\delta N_t = \frac{R}{2G} \alpha t\, \Phi(\psi_0), \tag{4-83}$$

where

$$\Phi(\psi_0) = \int_0^{\psi_0} S(\psi) \sin\psi\, d\psi.$$

$\Phi(\psi_0)$ is easily evaluated from the definite integral of Stokes' function:

Table 10 Geoidal height errors due to neglection of sea surface topography (one meter topography over the cap area is assumed)

Cap size ψ_0	5°	10°	15°	20°	25°	30°	35°
$\Phi(\psi_0)$	0.649	1.345	2.009	2.594	3.068	3.408	3.602
δN_t	m 0.20	0.42	0.62	0.80	0.95	1.05	1.11

$$\int_{\psi_1}^{\psi_2} S(\psi)\sin\psi\, d\psi = \Big[-\cos\psi + \frac{7}{4}\cos^2\psi + 2\sin\frac{\psi}{2}\left(\frac{3}{2}\cos\psi + \frac{1}{2}\right) - \frac{3}{2}\sin^2\psi\, l_n\left(\sin\frac{\psi}{2} + \sin^2\frac{\psi}{2}\right)\Big]_{\psi_1}^{\psi_2}$$

(Molodenskii et al., 1962, p. 168). Table 10 show δN_t for various cap sizes when $t=1$m. Under the data conditions used in Chapter 3 and from the feature of the sea surface topography around Japan (e.g. Sugimori, 1978), we can conclude that the geoidal height error of around 50 cm due to neglection of the sea surface topography possibly occurs, and that the error is a kind of systematic error in a small region because of the characteristics of the sea surface topography.

2) Undulation error due to land gravity errors

Every height system of land areas is based on the mean sea surface at certain tide stations. The mean sea surface at tide stations, of course, suffer sea surface topography, so that orthometric heights of the ground are not necessarily based on the geoid. In other words, heights systems suffer systematic errors as much as the sea surface topographic heights at the base tide stations. These systematic errors cause gravity reduction errors at land areas as much as at ocean areas and cause systematic geoidal height errors both at land and at ocean, especially at the transition areas from continent to ocean. The geoidal height errors may be in an order of errors shown in Table 10. These situation may be shown schematically by Figure 40, in which two height systems I and II are separated by the ocean lying between different height systems. The geopotential values on the mean sea surfaces at base tide stations T_1 and T_2 are not equal to each other due to the existence of the sea surface topography. We have to interrelate two height systems by knowing the potential difference or sea surface topographic heights over the ocean, and this kind of knowledges will make us possible to compute a more accurate gravimetric geoid, say a 10 cm geoid.

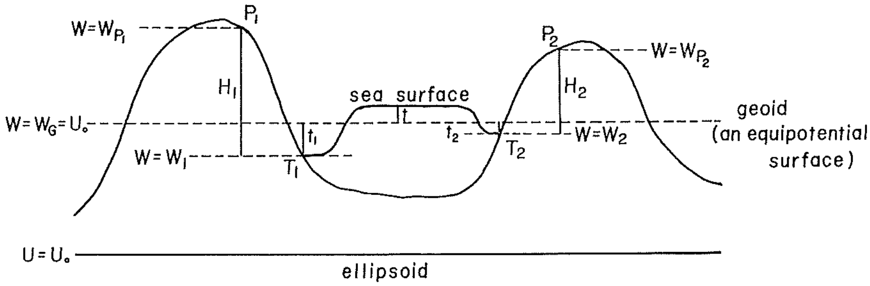

Figure 40 Sea surface topography and land height systems.

(6) **Undulation Errors due to Theoretical Approximations**

1) Spherical approximation

We have adopted the spherically approximated earth through this paper, as (2-1) and (2-3a) are based on the spherical approximation. Geoidal heights computed in the spherical approximation suffer errors of the same order as the flattening of the earth. The solution of the boundary value problem on a ellipsoidal reference surface was investigated by Molodenskii et al. (1962, p. 59), and the solution includes three times repetitions of integration. Lelgemann (1970) solved the problem in a simple form. We summarize his solution in a slightly changed form.

The disturbing potential on the reference ellipsoid is expanded in the series of the second eccentricity e'^2 $(\approx(a^2-b^2)/b^2)$ of the reference ellipsoid as follows:

$$T^*=T^\circ+e'^2\delta T+\cdots \tag{4-84}$$

(we use * on the shoulder for a quantity evaluated on the ellipsoid), where

$$T^\circ=\frac{R}{4\pi}\iint_\sigma \Delta g^*\, S(\psi)\,d\sigma. \tag{4-85}$$

The integration of (4-85) is carried out by using the geographical coordinates (φ, λ), then $d\sigma=\cos\varphi\, d\varphi\, d\lambda$. Δg^* is the gravity anomaly on the ellipsoid, which is derived from the ground level gravity anomaly, (2-4), by

$$\Delta g^*=\Delta g-h\frac{\partial\Delta g}{\partial h}+\cdots \tag{4-86}$$

(Moritz, 1971), where h is the height of the ground from the ellipsoid. The correction term δT is written as

$$\delta T=\frac{kM}{R}\sum_{l=2}^{\infty}\sum_{m=0}^{l}[\bar{A}_{lm}\bar{R}_{lm}+\bar{B}_{lm}\bar{S}_{lm}], \tag{4-87}$$

where $\bar{R}_{lm}$ and $\bar{S}_{lm}$ are fully normalized Laplace surface harmonics defined by (2-11), and coefficients $\bar{A}_{lm}$ and B_{lm} are derived from geopotential coe fficients in the spherical harmonic expansion of the disturbing potential:

$$T=\frac{kM}{R}\sum_{l=2}^{\infty}\sum_{m=0}^{l}[\bar{C}^*_{lm}\bar{R}_{lm}+\bar{D}_{lm}\bar{S}_{lm}]. \tag{4-88}$$

$\bar{A}_{lm}$ and $\bar{B}_{lm}$ are computed by the equations as follows:

$$\left.\begin{aligned}\bar{A}_{lm}&=\bar{C}^*_{l-2\ m}\,\bar{p}_{lm}+\bar{C}^*_{lm}\,\bar{q}_{lm}+\bar{C}^*_{l+2\ m}\,\bar{r}_{lm},\\ \bar{B}_{lm}&=\bar{D}_{l-2m}\,\bar{p}_{lm}+\bar{D}_{lm}\,\bar{q}_{lm}+\bar{D}_{l+2\ m}\,\bar{r}_{lm},\end{aligned}\right\} \tag{4-89}$$

where

$$\left.\begin{aligned}\bar{p}_{lm}&=\frac{3(l-3)}{2(l-1)(2l-1)}\left\{\frac{(l-m-1)(l-m)(l+m)(l+m-1)}{(2l-3)(2l+1)}\right\}^{\frac{1}{2}},\\ \bar{q}_{lm}&=\frac{-l^3+3lm^2+9l^2+10l+6m^2-9}{3(l-1)(2l+3)(2l-1)},\\ \bar{r}_{lm}&=\frac{3l+5}{2(l-1)(2l+3)}\left\{\frac{(l+m+2)\ (l+m+1)(l-m+2)(l-m+1)}{(2l+1)(2l+5)}\right\}^{\frac{1}{2}}.\end{aligned}\right\} \tag{4-90}$$

Note that we can use the disturbing potential (4-88) in the spherical approximation, because the expression is necessary only to evaluate a small correction term $e'^2\delta T$. Since we do not know the complete expression of the disturbing potential, we have to test the contribution of the terms of high degrees in (4-88) to $e'^2\delta T$. The correction of geoidal height from $e'^2\delta T$ is

$$\delta N = \frac{e'^2 \delta T}{G} \tag{4-91}$$

and the mean square value of (4-91) is written by using (4-87) in the form:

$$\varepsilon^2 = M\{\delta N^2\} = e'^4 R^4 \sum_{l=2}^{\infty} \sum_{m=0}^{l} (\bar{A}_{lm}^2 + \bar{B}_{lm}^2), \tag{4-92}$$

where the relation $G = kM/R^2$ has been used. Then the mean square contribution of the terms of higher degrees than L becomes

$$\varepsilon_L^2 = e'^4 R^4 \sum_{l=L}^{\infty} \sum_{m=0}^{l} (\bar{A}_{lm}^2 + \bar{B}_{lm}^2). \tag{4-93}$$

When $l \gg 1$ in (4-90), we can set

$$max|\bar{p}_{lm}| \approx \frac{3}{8}, \quad \max|\bar{q}_{lm}| \approx \frac{1}{6}, \quad \max|\bar{r}_{lm}| \approx \frac{3}{8}$$

and the sizes of coefficients $\bar{A}_{lm}$ and $\bar{B}_{lm}$ are bounded as

$$\left.\begin{aligned} |\bar{A}_{lm}| &< \frac{3}{8}|\bar{C}^*_{l-2\,m}| + \frac{1}{6}|\bar{C}^*_{lm}| + \frac{3}{8}|\bar{C}^*_{l+2\,m}| \approx |\bar{C}^*_{lm}|, \\ |\bar{B}_{lm}| &< \frac{3}{8}|\bar{D}_{l-2\,m}| + \frac{1}{6}|\bar{D}_{lm}| + \frac{3}{8}|\bar{D}_{l+2\,m}| \approx |\bar{D}_{lm}|. \end{aligned}\right\} \tag{4-94}$$

From (4-93) and (4-94), we finally obtain

$$\varepsilon_L^2 < e'^4 R^4 \sum_{l=L}^{\infty} \sum_{m=0}^{l} (\bar{C}_{lm}^{*2} + \bar{D}_{lm}^2), \quad L \gg 1. \tag{4-95}$$

If Kaula's rule of thumb, (4-11), is adopted to estimate the sizes of the geopotential coefficients at high degrees, (4-95) is reduced simply to

$$\varepsilon_L < \frac{0.43}{L} \text{ (meter)} \tag{4-96}$$

in which we usually take $R = 6371$ km and $e'^2 = 0.00674$. We thus conclude that (4-88) is safely replaced by a satellite-derived disturbing potential restricted within rather low degree terms. Lelgemann (1970) evaluated (4-92) by using actual geopotential coefficients of up to degree 14, and obtained r.m.s. value $\delta N = 0.2$ m. He drew a world-wide distribution map of δN, and found that the contour paterns in the map are similar to the long wave-length components of the global geoid undulations. We read out δN around Japan as 20 to 30 cm from his map.

2) Neglection of higher order correction terms in Molodenskii's solution

We have neglected G_1 term in (2-3a) to compute a gravimetric geoid in Chapter 3. G_1 is evaluated at P on the ground by

$$G_1 = \frac{R^2}{2\pi} \iint_\sigma \frac{h - h_p}{l_0^3} \Delta g \, d\sigma, \tag{4-97}$$

where h and h_p are heights at the surface element $d\sigma$ and at P, and

$$l_0 = 2R \sin\frac{\psi}{2},$$

in which ψ is the angular distance between $d\sigma$ and P. The gravity correction G_1 is not negligible because, for example, G_1 amounts to -34 mGals at the top of a conic mountain having the form $h(r) = H \cdot \exp(-r^2/4B^2)$, where $H = 500$ m and $B = 300$ m (Hagiwara, 1973). But the effect of G_1 term on geoidal height is small because G_1 behaves short wave-length variations very similar to the short wave-length components of topographic relief (see Figure 4 of Hagiwara, 1972a). Therefore, we may conclude that the geoidal height errors included in the geoid obtained in Chapter 3 due to the neglection of G_1 are negligibly small, i.e. less than 10 cm.

The geoidal heights computed in Chapter 3 are actually height anomalies. Height anomalies in ocean areas are almost equal to geoidal heights, but not in land areas. The difference between geoidal height and height anomaly, which is given by (2-6), is estimated to be around a few tens centimeters at the mountainous region in the central part of Japan.

(7) **Summary of Error Sources**

We have investigated various error sources in the geoidal height computation, and the error sources are relisted below:

(a) omission of detailed structures of the gravity anomaly field;
(b) uncertenties of the satellite derived geopotential coefficients;
(c) terrestrial gravity data errors;
(d) omission of sea surface topography;
(e) spherical approximation in Stokes' integral;
(f) omission of higher correction terms in Molodenskii's solution.

The geoidal height error due to (a) largely depends on the behavior of the anomaly degree variances at high degrees, and the error decreases as the cap size becomes larger and as the sizes of blocks, by which mean gravity anomalies are given, becomes smaller. The recent developments of the satellite trackings have made the error source (b) less important. The main error source is still due to errors of the terrestrial gravity data caused by lack of density of gravity observations and lack of accuracy of sea gravity observations ever made. We have to make great efforts in avoiding the error source (c) to produce a more accurate geoid. The existence of the sea surface topography brings about a complicated problem in the definition of the geoid and in the gravity reduction procedures. We cannot neglect the sea surface topography (d) to compute an accurate geoid. The error sources (e) and (f) have almost been solved theoretically, and they should be taken into consideration in the computation of a 10 cm geoid.

In Table 11, we summarize the point undulation errors accompanied with the gravimetric geoid obtained in Chapter 3 under the data conditions of (4-31) and (4-34). The total error is based on the assumption that the error sources are independent of each other. We may conclude the accuracy of the gravimetric geoid (Figure 8) is around 1.5 m or, in other words, in a range of 1 m to 2 m except for N_0 term given by (2-9). N_0 term is in an order of ambiguity of the semimajor axis of the earth ellipsoid. The estimated errors of the gravimetric geoid are compatible with the comparison results between the gravimetric geoid and Geos-3 altimeter data (Table 1).

We have also investigated the error of geoidal height difference. This kind of error depends largely on the correlation distance of the error source. For the geoidal height difference over 500 km distance, we can summarize the errors due to various error sources as shown in Table 12. We find the total error of the geoidal height difference to

Table 11 Point geoidal height errors due to various error sources involved in the gravimetric geoid obtained in Chapter 3

Error source	Data condition (4-31)	Data condition (4-34)	Note
	m	m	
a	0.60	0.86	Anomaly degree variance model *c*
b	0.31	0.31	GEM-10 model
c	1.0+	1.5*	
d	0.5	0.5	From Table 10, estimated
e	0.2	0.2	World-wide average
f	0.1	0.1	Estimated
Total	1.3	1.8	Independent error sources

+ based on the assigned errors in JHDGF-1
* based on 12.5 mGals error of $1°\times1°$ block means

Table 12 Relative geoidal height errors due to various error sources for 500 km distance

Error source	Relative geoidal height error	Note
		Anomaly degree variance model *c*
a	m 0.85	Data condition (4-31)
	1.22	Data condition (4-34)
b	0.26	GEM-10 model
c	1.34	12.5 mGals error of $1°\times1°$ block mean
d	0.2	Table 10, estimted
e	0.1	Due to a long correlation distance
f	0.1	Estimated
		Independent error sources
Total	1.6	Data condition (4-31)
	1.8	Data condition (4-34)

be as large as the point geoidal height error, i.e. 1.6 m for the data condition (4-31) and 1.8 m for the data condition (4-34). When the distance is 100 km, the error will decrease to around one meter.

5. Surface Data Requirements for the Computation of an Accurate Geoid

In Chapter 3, we have used block mean gravity anomalies read out from various kinds of gravity anomaly maps of different accuracy to obtain a gravimetric geoid. Since it is difficult for us to estimate the accuracies of such block gravity data, the accuracy of the computed geoid is ambiguous. When we know the errors of block mean gravity anomalies, we can estimate the error of the geoid on the basis of the gravity data errors (see 4-(4)). To obtain accurate block mean gravity anomalies and to estimate the accuracy of the obtained block data properly, we had better consider to use some mathematical procedures to derive block mean gravity anomalies from raw gravity observations. On the basis of the mathematical treatings, we can consider the problem that what kind of gravity survey is suitable and effective to compute a more accurate geoid, say a geoid with an accuracy of the order of ± 10 cm.

(1) Estimation of Block Mean Gravity Anomalies by Using Least-squares Collocation

1) Least-squares collocation

Least-squares collocation is one of the most efficient statistical techniques for dealing with physical observations. Least-squares collocation has three functions of interpolation, prediction and filtering simultaneously, and besides it can deal with not only homogeneous measurements but also heterogeneous measurements relating functionally to the physical measurements concerned. Moritz (1972) discussed the mathematical frameworks of least-squares collocation in detail. We summarize briefly the mathematical procedures of least-squares collocation for the conveniences of the later sections.

The fundumental equation of least-squares collocation is

$$x = AX + s' + n \tag{5-1}$$

(ibid., p. 7). x expresses "observations", and when we deal with gravity anomaly, the observations are all kinds of observations having some relations with gravity anomaly, i.e. gravity anomaly itself, deflection of the vertical, geoidal height, topographic height, bottom topography at sea, underground crustal structures, etc. When there are q observations, x is a column vector composed of q elements. s' is the signal part (information relating to gravity anomaly) included in x, and s' is assumed to satisfy the condition of "random" such as

$$M\{s'\} = 0, \tag{5-2}$$

where the operator M indicates a procedure "mean". n is the random noise included in the observations, then

$$M\{n\} = 0 \tag{5-3}$$

is assumed. s' and n are column vectors comprising q elements each.

The term AX expresses the systematic part included in observations x, where X is a column vector which comprises r unknown parameters and A is a known $q \times r$ matrix which is equivalent to the design matrix appearing in the conventional least-squares adjustment. To compute p signals: $s = [s_1, s_2, \dots, s_p]^T$, from q observations, we define vector v by

$$v = [s, s' + n]^T = [s_1, s_2, \dots, z_1, z_2, \dots, z_q]^T, \tag{5-4}$$

where $s' + n$ is simply written as z, and T on the shoulder denotes the operation of transposition. We use a minimum codition:

$$v^T Q^{-1} v = \text{minimum}, \tag{5-5}$$

where Q is the covariance matrix, $(p+q) \times (p+q)$ matrix, of v, which comprises covariances of signal and covariances between signal and noise. Q is written by a partitioned matrix such as

$$Q=\begin{pmatrix} C_{ss} & C_{sz} \\ C_{zs} & C_{zz} \end{pmatrix}, \tag{5-6}$$

where C_{ss} is the covariance matrix of the signal s, $C_{ss}=cov(s, s)$, and C_{sz} and C_{zs} are covariance matrices between s and z, which are

$$C_{sz}=C_{zs}^{T}=cov(s, z)=M\{s\,z^T\}=M\{s(s'+n)^T\}=M\{s\,s'^T\}+M\{s\,n^T\}.$$

Since n and s are independent of each other, we can write

$$C_{sz}=C_{zs}^{T}=M\{s\,s'^T\}=C_{ss'}. \tag{5-7}$$

In the same way, we have

$$C_{zz}=cov(z, z)=M\{(s'+n)(s'+n)^T\}=C_{s's'}+C_{nn}, \tag{5-8}$$

where C_{nn} is the covariance matrix of the noise. We can solve the unknown signal vector s and the unknown parameter vector X under the condition (5-5) with the constraint equation (5-1) by using the method of Lagrangian multipliers (e.g. Brandt, 1970, p. 176-178). The solutions are written as follows:

$$X=(A^T\bar{C}^{-1}A)^{-1}A^T\bar{C}^{-1}x, \tag{5-9}$$

$$s=C_{ss'}\bar{C}^{-1}(x-AX), \tag{5-10}$$

where

$$\begin{aligned}\bar{C}&=cov(x, x)=M\{x-AX)(x-AX)^T\}\\ &=M\{z\,z^T\}=\bar{C}_{s's'}+C_{nn}\end{aligned} \tag{5-11}$$

(Moritz, 1972, p. 15). The error covariances of obtained X and s are given by

$$E_{XX}=(A^T\bar{C}^{-1}A)^{-1}, \tag{5-12}$$

and by

$$E_{ss}=C_{ss}-C_{sx}\bar{C}^{-1}C_{xs}+HAE_{XX}A^TH^T, \tag{5-13}$$

where

$$\begin{aligned}C_{sx}&=C_{xs}^{T}=cov(s, x)=M\{s(x-AX)^T\}\\ &=M\{s\,z^T\}=C_{ss'},\\ H&=C_{sx}\bar{C}^{-1}\end{aligned} \tag{5-13}$$

(ibid., p. 32-33).

When we apply least-squares collocation actually, the covariances of the signal and the noise should be known in advance. To our convenience, the computed signals are not so affected by slight changes of the covariance functions (Moritz, 1972; Smith, 1974). Although there is a disadvantage that least-squares collocation requires to invert matrices of the same dimension as the number of observations, such a problem has become less important in the modern electronic computer era.

2) Estimation of block mean gravity anomalies from gravity measurements

One of simple applications of least-squares collocation is the estimation of block mean gravity anomalies from point gravity measurements. In this case, we understand equation (5-1) in the following way: x comprises q point gravity anomalies distributed inside and around the block area; s' is the signal part relating to the block mean gravity anomaly included in point gravity anomalies; n is the random noise of the gravity measurements. If we use centered gravity anomalies which satisfy $M\{\Delta g\}=0$, we may put the systematic part AX to be zero. The signal s required to be computed is a block mean gravity anomaly, and then from (5-10) the block mean gravity anomaly, written as $\overline{\Delta g}$, is estimated by

$$\overline{\Delta g}=C^{T}_{\Delta g\,\overline{\Delta g}}\,\bar{C}^{-1}\Delta g, \qquad (5\text{-}14)$$

where $C_{\overline{\Delta g}\,\Delta g}$ is a column vector composed of q covariances between the block mean gravity anomaly and q point gravity anomalies, Δg is a column vector composed of q point gravity anomalies: $\Delta g=(\Delta g_1, \Delta g_2, \dots, \Delta g_q)^T$, and $\bar{C}$ is a rectangular $q\times q$ matrix whose elements are covariances of point gravity anomalies: i.e. (i, j)-th element of $\bar{C}$ is given by

$$[\,\bar{C}\,]_{ij}=C_{\Delta g}(\Delta g_i, \Delta g_j)+C_n(n_i, n_j). \qquad (5\text{-}15)$$

The covariance function of gravity anomaly, $C_{\Delta g}$, and the covariance function of noise included in gravity observations, C_n, are functions of the distance between points i and j when the statistical characteristics of Δg and n are isotropic. The covariances between block mean gravity anomaly and point gravity anomaly can be obtained if the covariance function of point gravity anomaly is known (Heiskanen and Moritz, 1967, p. 277). The error of the computed block mean gravity anomaly is estimated from (5-13) as

$$\varepsilon^2=C_{\overline{\Delta g}\,\overline{\Delta g}}-C^{T}_{\Delta g\,\overline{\Delta g}}\,\bar{C}^{-1}C_{\Delta g\,\overline{\Delta g}}, \qquad (5\text{-}16)$$

where $C_{\overline{\Delta g}\,\overline{\Delta g}}$ is the variance of block mean gravity anomalies. The solutions (5-14) and (5-16) are equivalent to the solutions by a least-squares estimation approach to estimate a block mean gravity anomaly in the form of linear combination of point gravity anomalies (Heiskanen and Moritz, ibid., p. 277; Ganeko, 1978).

The same expressions as (5-14) and (5-16) can be used to estimate a block mean gravity anomaly from mean gravity anomalies of smaller block only by replacing Δg_i and $\overline{\Delta g}$ by $\overline{\Delta g_i}$ (mean gravity anomaly of smaller block) and $\overline{\overline{\Delta g}}$ (mean gravity anomaly of larger block). Smith (1974) made detailed test calculations of estimating 5° and 1° block mean gravity anomalies from available 1° block mean gravity anomalies.

3) Estimation of gravity anomaly from other data

Least-squares collocation may possibly be applied to estimate gravity anomaly from topographic heights, sea bottom topography and other geophysical data if the relation between such data and gravity anomaly are given numerically, i.e. by covariance functions. We know the fact that free-air gravity anomalies are in most cases well correlated to topographic heights at land, and for example in Japan area, the fact was tested by some authors, e.g. Yokoyama and Tajima (1957); Rikitake et al. (1965); Hagiwara (1967). Hagiwara (1965) found good correlations between Bouguer gravity anomalies and the geological structures in Japan. A tendency that the sea bottom topography has also some relations with free-air gravity anomaly was pointed out by Watts (1976), Mckenzie and Bowin (1976) and Cochran and Talwani (1977). The relations between geophysical structures at sea and gravity anomaly were investigated by Marsh and Marsh (1976), Khan (1977) and Jordan (1978). Although we find some correlations between gravity anomaly and geophysical and geographical structures, the correlations are not necessarily well applicable to interpolating gaps of gravity anomaly. The use of geophysical and geographical data for interpolating gravity anomaly may be limitted to specific areas where strong correlations exist between gravity anomaly and such data.

On the other hand, geoidal heights and deflection of the vertical are mathematically interrelated to gravity anomaly by the geopotential theory, and then we can derive analytical covariance functions between arbitrary two quantities among gravity anomaly, geoidal height, deflection of the vertical and the differentials of them. Tscherning and Rapp (1974) obtained covariance functions such as gravity anomaly-gravity anomaly, gravity anomaly-geoid undulation, gravity anomaly-deflection of the vertical, undulation-undulation, deflection-deflection and deflection-undulation from a model anomaly degree variance (4-17). When we know these covariance functions, least-squares collocation is well applied to estimate gravity anomaly from geoid undulations and deflections of the vertical. Smith (1974) and Rapp (1974) made simulation studies concerning the estimation of gravity anomaly from satellite altimeter data by least-squares cllocation assuming that the sea surface heights from the ellipsoid (=altimetric sea surface heights) are approximately equal to geoidal heights. Rummel and Rapp (1977) and Rapp (1977a) applied the method actually to Geos-3 altimeter data, and ± 3 mGals accuracy of 5° block mean gravity anomaly and ± 6 mGals accuracy of $1^\circ \times 1^\circ$ block mean gravity anomaly were obtained (Rapp, 1977a). Such applications of the satellite altimetry for estimating gravity anomalies in the gravity data sparse areas will make us possible to get geopotential coefficients up to high degrees, and the detailed gravity anomaly field will be of use to compute an accurate gravimetric geoid as seen in the last chapter.

(2) Requirements for a 10 cm Geoid

1) Requirements for block sizes of terrestrial gravity data

The fundumental requirement for the block size of mean gravity anomalies is obtained from the curves for $\psi_0=0$ in Figures 30a and 30b. Truncation errors less than 10 cm are achieved at around degree $L=1000$ which corresponds to the following block size by equation (4-29) :

$$\theta = \frac{180^\circ}{1000} \doteqdot 11',$$

i.e., we need at least 10′ block mean gravity anomalies in the inner-most cap area. We test the truncation errors caused by two data conditions A and B in Table 13. The truncation errors are estimated by using (4-30) for each data condition, and the estimated truncation errors are shown in Table 14 for both anomaly degree variance models b and c which have been often used in the previous chapters. According to (4-38), we can

Table 13 Proposed data conditions for the computation of a gravimetric geoid with an accuracy of the order of ± 10cm

Data condition A		Data condition B	
Area	Data	Area	Data
$\psi \leq 2°$	10′ block gravity anomaly	$\psi \leq 2°$	10′ blok gravity anomaly
$2° < \psi \leq 10°$	30′ block gravity anomaly	$2° < \psi \leq 10°$	30′ block gravity anomaly
$10° < \psi \leq 35°$	1° block gravity anomaly	$10° < \psi \leq 20°$	1° block gravity anomaly
$\psi > 35°$	$l_{max}=30$ global geo-potential model	$\psi > 20°$	$l_{max}=100$ global geo-potential model

Table 14 Point truncation errors of the geoidal heights computed under the proposed data conditions A and B

Anomaly degree variance model*	Data condition A	Data condition B
	m	m
b	0.08	0.07
c	0.12	0.12

* Shown in Figure 28.

estimate the errors of relative geoid undulation due to the truncation effects under the data conditions A and B to be $\sqrt{2}$ times the values in Table 14 for a distance farther than 300 km. So far as we consider the truncation errors, we can compute geoidal heights as accurate as 10 cm under the data conditions listed in Table 13. We may expect that global geopotential models comprising geopotential coefficients up to degree 100 or 2° block mean gravity anomalies all over the surface of the earth will become available in the near future if we take the successful results of the satellite altimetry by Geos-3 into consideration.

2) Requirements for accuracies of gravity data

a. Data condition A

Along the discussions made in 4-(4), we can estimate the point undulation error due to gravity bata errors as follows:

$$m_{\delta N,A}^2 = m_{\delta N}^2(2°, \theta_1) + m_{\delta N}^2(10°, \theta_2) - m_{\delta N}^2(2°, \theta_2)$$

$$+ m_{\delta N}^2(35°, \theta_3) - m_{\delta N}^2(10°, \theta_3), \tag{5-17}$$

where $\theta_1=10'$, $\theta_2=30'$ and $\theta_3=1°$. Let us adopt the error covariances of the type of Case A (4-58) for all block mean gravity anomalies, and put the r. m. s. errors of gravity data for each block size as m_{g1}, m_{g2} and m_{g3} (in mGals). From the listed values in

Table 8, (5-17) is given numerically as

$$m^2_{\delta N,A}=0.018^2\, m^2_{\theta_1}+0.034^2\, m^2_{\theta_2}+0.043^2\, m^2_{\theta_3}\ (\text{meter}^2) \tag{5-18}$$

When we can set $m_{\theta 1}=m_{\theta 2}=m_{\theta 3}=m_\theta$, (5-18) is reduced to

$$m_{\delta N,A}=0.058 m_\theta\ (\text{meter}) \tag{5-19}$$

which shows that the error of 10 cm level can be achieved by $m_\theta=1\sim 2$ mGals. As we see in (5-18), the contribution of 10′ block data is smaller than other sized block data, and then larger errors of 10′ block data than the errors of other sized block data are acceptable. For example, when $m_{\theta 1}=5$ mGals, $m_{\theta 2}=m_{\theta 3}=2$ mGals, we obtain

$$m_{\delta N,A}=0.14\ \text{meters}. \tag{5-20}$$

Concerning the relative undulation error between 300 km distance, we assume the main error source to be due to 30′ block data errors, and we estimate the relative undulation error from Table 9 as follows:

$$m^2_{\delta\Delta N,A}=0.055^2\, m^2_{\theta_2}.$$

If we set $m_{\theta 2}=2$ mGals, we obtain $m_{\delta\Delta N,A}=0.11$ meters.

For other types of error covariance such as exponential error covariances of Case B and Case C (4-68), we can estimate point undulation errors from Table 8 under the same assumptions as (5-19);

$$\left.\begin{aligned} m_{\delta N,A}&=0.080 m_\theta\ (\text{meter})\ \text{for Case B,}\\ &=0.152 m_\theta\ (\text{meter})\ \text{for Case C.}\end{aligned}\right\} \tag{5-21}$$

(5-21) results in rather large undulation errors, so that we should bear in mind not to bring any systematic errors in the terrestrial gravity data.

b. Data condition B

Under the data condition of B in Table 13, the point truncation error is estimated as

$$m^2_{\delta N,B}=0.018^2\, m^2_{\theta_1}+0.034^2\, m^2_{\theta_2}+0.040^2\, m^2_{\theta_3} \tag{5-22}$$

for the error covariances of Case A. (5-22) estimates almost the same undulation errors as (5-19), and this comes from the fact that the undulation errors due to gravity data errors little increase even when the cap size becomes larger than 20° (see Figure 37). Therefore, so far as concerning the undulation errors due to gravity data errors, the data condition B is equivalent to the data condition A.

(3) Accurate Surface Gravity Surveys to be Required

In this section, we will study what kind of gravity surveys can derive block mean gravity anomalies as accurate as those required in the previous section to compute a geoid with a 10 cm accuracy. We have studied how to compute block mean gravity anomalies from point gravity observations in 5-(1), i.e. the least-squares collocation method. Block mean gravity anomalies are estimated by (5-14) and the errors of the estimated block means are given by (5-16) on the basis of the known covariance function of gravity anomaly. Let us make a simulation study based on (5-16) for various distributions of gravity observation sites. When we apply least-squares collocation, the average of the signal, i.e. gravity anomaly in our case, should be zero. In other words, gravity anomaly should satisfy the condition (5-2) by taking it into consideration that a block mean is estimated from the gravity observations being inside and near around the block. Then it should be recommended toapply least-squares collocation to both the residual gravity anomaly derived by subtracting a satellite derived global gravity anomaly and its block means, because the global gravity anomaly is considered to be a kind of bias term of gravity anomaly in a restricted region.

The covariance function of the gravity anomaly around Japan has already been obtained in 4-(1), and an analytical function model (4-23) of the point residual gravity anomalies has been proposed. Covariance functions being necessary for (5-16) are easily obtained numerically by using the model function of the point anomaly covariance (Heiskanen and Moritz, 1967, p. 277 ; Ganeko, 1978). The errors (5-16) depends only upon the distribution paterns of gravity observation sites. They are independent of the gravity anomalies. But the errors of gravity measurements contribute to (5-16) through the error covariance C_n (see (5-15)). Table 15 includes the estimation errors of block mean gravity anomalies for 5′, 10′, 30′ and 1° blocks on the basis of the model residual anomaly covariance function (4-23). The adopted blocks are square ones which have the same areas as equiangular blocks of $5' \times 5'$, $10' \times 10'$, $30' \times 30'$ and $1^\circ \times 1^\circ$ located at latitude 33°. Three cases that gravity measurement errors fall on 0, 3 and 5 mGals are tested on the assumption that the errors are independent of site of measurement; i.e. the error covariance matrix C_{nn} comprises only diagonal elements. The second column of Table 15 shows variances of block mean residual gravity anomalies for each block size. The estimated errors of block means are listed in the column from the third to the sixth for four kinds of distribution paterns of gravity observation sites. The third column includes the average estimation errors (called representation errors) for the case that there is only one gravity observation site in the block. The fourth column is for the case that one observation site is located at the center of the block. The fifth and the sixth columns are for the case that gravity measurements are carried out along lines, and such a case is actually realistic in the sea gravity observations. The fifth column is for the case that there is one series of gravity observation sites (we call it a profile observation) along the ship's track crossing the block at the center of it (see Figure 41a), and the sixth column is for the case that there are two profile observations crossing the block as shown in Figure 41b. T.S.S.G. (Tokyo Surface Ship Gravimeter) (Tomoda and Kanamori, 1962 ; Tomoda et al., 1968 ; Segawa, 1970a, b ; Fujimoto, 1976) provides us with gravity data with an interval of 2 or 4 km at the normal velocity of survey ships. If we take the functional shape of the anomaly covariance near origin into consideration, we may note that 2 km spacing of sites in a profile observation is sufficient for estimating 5′ block means, and 4 km spacing is sufficient for larger blocks.

Table 15 Estimation errors of block mean gravity anomalies computed by using the least-squares collocation method under various distribution conditions of gravity observation sites

Block size $B\times B$	Block anomaly variance	Representation error	One obs. site at the block center	One profile observation	Two profile observations	Random obs. error
km	$mGal^2$	mGal	mGal	mGal	mGal	mGal
$B=8.5$	3093	6.4	3.7	1.7	0.7	0
5′ block		7.1	4.7	2.1	1.2	3
		8.1	6.2	2.6	1.7	5
$B=17.0$	3036	9.9	5.6	2.7	1.0	0
10′ block		10.3	6.3	2.9	1.2	3
		11.1	7.4	3.2	1.5	5
$B=50.9$	2518	19.9	10.5	5.2	1.9	0
30′ block		20.1	10.8	5.2	2.0	3
		20.5	11.4	5.3	2.2	5
$B=101.8$	2215	30.3	14.8	8.2	3.0	0
1° block		30.4	15.0	8.3	3.0	3
		30.7	15.3	8.3	3.1	5

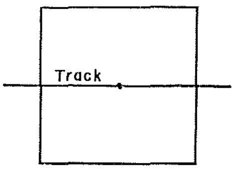

Figure 41a One profile gravity observation along the track crossing a block at its center.

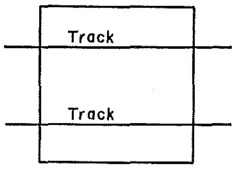

Figure 41b Two profile gravity observations along tracks crossing a block.

Teble 15 shows that when we require the estimation error less than ± 5 mGals for 10′ block and ± 2 mGals error for 30′ and 1° blocks, one profile observation is necessary for 10′ blocks, two profile observations are necessary for 30′ blocks, and more than two profile observations are necessary for 1° blocks. In other words, parallel profile gravity observations are to be carried out every 10 naut. miles in an area where 10′ block mean gravity anomalies are desired, and profile observations are necessary every 15 naut. miles in the remaining area where surface gravity data are desired. Random gravity measurement errors up to ± 5 mGals may be acceptable. The gravity surveys at sea like above mentioned will make us possible to compute a marine gravimetric geoid with a decimeter accuracy.

The performance of the gravity surveys described here requires a little time, cost and effort. It should be noted that Table 15 is based on the anomaly covariance functions derived from gravity anomalies in the region including rough gravity anomaly areas such as trenches and islands-arcs. If we adopt the variance of world-wide average residual gravity anomaly, 1620 $mGal^2$ (Table 11 of Tscherning and Rapp, 1974) in place of 3133 $mGal^2$ in (4-23). Each value listed in Table 15 decreases by 30%. In this case, parallel profile gravity observations carried out every 30 naut. miles can yield 1° block mean gravity anomalies with a sufficient accuracy, ± 2 mGals, for our present purpose. When we carry out gravity surveys actually, it may be necessary for efficient surveys that we examine beforehand the roughness of the gravity anomaly field in the areas to be surveyed.

6. Summary and Conclusions

We have obtained a gravimetric geoid around Japan based on $30' \times 30'$ and $1° \times 1°$ block mean gravity anomalies. The $30' \times 30'$ block data have been read from the published gravity anomaly maps around Japan, and the $1° \times 1°$ block data have been prepared by taking averages of DMAAC global gravity data and LAMONT data. The gravimetric geoidal heights have been computed from the terrestrial gravity data in combination with a satellite-derived geopotential field: GEM-10 model. GEM-10 model is one of the recent geopotential models and it comprises a geopotential coefficient set which is complete up to degree and order 22. The radius of the cap area of Stokes' integration where terrestrial gravity data are used has been taken to be 20°. The most marked features in the computed geoid (Figure 8) are seen along trenches, where there are geoidal dents of more than 20 meters relative to GEM-10 global geoid. The geoidal highs along islands-arcs are other marked features in the geoid.

We have made detailed investigations concerning various error sources accompanied with our computation method of geoidal heights, and the reliability of the computed geoid has been investigated from various points of view. Some of the altimeter data taken by Geos-3 satellite have been compared with the gravimetric geoid, and the results are seen in Table 1 and Figures 13~24. The r.m.s. difference of relative undulations between altimetric sea surface heights and the gravimetric geoid is around 1.3 m, which scatters in a range from 0.6 m to 1.9 m depending on the locations of the satellite tracks and the dates of the satellite revolutions; i.e. at the early stage of the satellite, the satellite positions were a little poorly determined.

Chapter 4 has been devoted to the investigations of error sources accompanied with the geoidal height computation procedures in the former chapters and evaluations of the actual possible errors of the computed geoid. The r.m.s. error of the computed geoid undulations has been estimated to be 1.3 m in JHDGF-1 region (see Figure 4) and to be 1.8 m outside the region. These error estimates are compatible with the comparison results between Geos-3 altimeter data and the gravimetric geoid. The accuracy of geoidal height differences (relative undulation error) has also been investigated. Such relative undulation errors have a little meaning because some of error sources have long correlation distances, and the relative undulation errors are differently evaluated from the conventional point undulation errors.

Concerning the computed gravimetric geoid, we have estimated a relative undulation error over 500 km distance to be about 1.6 m or 1.8 m depending on the data conditions (see Table 12). The relative undulation error decreases to around one meter when the distance is 100 km. As we see in Tables 11 and 12, the errors of terrestrial gravity data still form the biggest error source. The second big error source is formed by the omission errors, and the third one is due to existence of the sea surface topography.

We may conclude from the error investigations as made above that it is difficult for us to obtain geoid undulations with an accuracy of one meter or less around Japan under the current availability of the terrestrial gravity data near Japan. The geoidal map obtained in the pressnt paper shows a general features of the geoid undulations around Japan, especially at trenches and islands-arcs, and the geoid will be of use not only as the first step to compute an accurate geoid but also in the better evaluations of three dimensional positions of the satellite tracking stations and other astronomical observation sites located in the region of the geoidal map, and moreover it will be of use as a calibration field of other geoids, e.g. astrogeodetic geoids (Ono, 1974; Ganeko, 1976) and Doppler results (Mori and Kanazawa, 1979).

There is a strong ocean current near Japan, which is called Kuroshio, and oceanographers are very interested in deviations of the sea surface from the geoid (an equipotential surface) over the Kuroshio area. Unfortunately, the accuracy of the obtained gravimetric geoid is insufficient at all to detect such deviations from the obtained geoidal map. We understand some difficulties in the determination of the sea surface topography over the Kuroshio area because of rougher geoid undulations over the area than the Gulf Stream area, off east coasts of the United States.

Our second object in computation of gravimetric geoid consists in a 10 cm marine geoid which can afford to make use of the satellite altimetry with the same order of accuracy. In Chapter 5, we have obtained the data conditions for the terrestrial gravity data to get a geoid (marine geoid) with an accuracy of 10 cm level, and we have known that much more additional gravity surveys are necessary to get such an accurate geoid. Inside and near the region (see Table 13) where a 10 cm geoid is desired, 10′ block mean gravity anomalies with an accuracy of 5 mGals or better are necessary, and such a condition will be fulfilled at sea by profile gravity observations along parallel ship tracks located every 10 naut. miles. In the region where 30′ or 1° block mean gravity anomalies are prepared (see Table 13), profile gravity observations should be carried out every 15 or 30 naut. miles depending on the roughness of the gravity anomaly field. The satellite altimeter data (sea surface heights) can be used in the geoidal height computations directly (Mather, 1973, 1974) or indirectly, i.e. in the form of gravity anomalies derived from altimetric geoidal heights (Rapp, 1977a), and then the satellite altimetry may take the place of the conventional gravity surveys at sea to some extent.

The existence of the sea surface topography causes difficulties in the definition and the realization of the geoid, as an equipotential surface in the earth's gravitational field is not realized by the mean sea surface (schematically explained by Figure 40). The gravity reduction errors both at sea and at land caused by the sea surface topography result in geoidal height errors which are are not negligible(5-(5), Table 10). This situation comes from the characteristics of the long wave-length variations of the sea surface topography and the systematic errors of the land height systems caused by the sea surface topographic heights at the base tide stations of the height systems. Physical oceanography predicts relative sea surface undulations from an equipotential surface on the basis of oceanographic data, but the oceanographic sea surface undulations do not necessarily agree well with the geodetic levelling observations along the coasts of continents (Sturges, 1967; Hammon and Greig, 1972). Therefore we cannot put too much reliance upon the oceanographic sea surface topography at present, however we may be able to use the oceanographic sea surface topography as the first approximation of the true sea surface topography in the better gravity reductions. The gravimetric geoid computed from the gravity anomalies reduced by using the oceanographic sea surface heights will provide us with another sea surface topography in combination with 10 cm satellite altimetry. Consequently it may be a new definition of the geoid. The new sea surface topography and the new definition of the geoid will be used in the gravity reductions again to compute a more accurate geoid which will provide us with more accurate sea surface topography and geoid.

Acknowledgments

The author wishes to express his cordial gratitude to Prof. Y. Hagiwara for his encouragement and advice during the preparation of this work. He also wishes to thank Dr. E. M. Gaposchkin and Dr. H. R. Stanley for providing him with DMAAC's $1°\times1°$ block mean gravity anomalies and Geos-3 altimeter data, respectively, and to thank Dr. A. B. Watts for his advice concerning the reliability of $1°\times1°$ gravity anomaly data in the Northwest Pacific area. The author's thanks are also due to Dr. A. M. Sinzi, Dr. A. Yamazaki, Mr. T. Mori and Mr. A. Senda of JHD for providing him with conveniences in the performance of computations by using an electronic computer. The author is also indebted to Mr. K. Koyama of the Astronomical Division, JHD, for his help in computing geoidal heights and drawing geoidal maps by using a machine.

This paper in based on the author's dissertation, submitted to the University of Tokyo, in partial fulfillment of the requirements for the doctorate.

Refesences

Atumi, K., 1933: "La deviation de la verticale au Japon", *Japan. J. Astron. Geophys.*, *10*, 305-312.

Brennecke, J. and E. Groten, 1977: "The deviation of the sea surface from the geoid and their effect on geoid computation" *Bull. Geod.*, *51*, 47—51.

Brandt, S., 1970: *Statistical and Computational Methods in Data Analysis*, North-Holland Publishing Company, Amsterdam-London, pp. 322.

Caputo, M., 1967: *The Gravity Field of the Earth*, International Geophysics Series, Vol. 10, Academic Press, New York, pp. 202.

Christodoulidis, D. C., 1976: "On the realization of a 10 cm relative oceanic geoid", *Rep. 247, Dep. Geod. Sci.*, Ohio State Univ. Res. Found., Ohio State Univ. Columbus, Ohio, pp. 96.

Cochran, J. R. and M. Talwani, 1977: "Free-air gravity anomalies in the world's oceans and their relationship to residual elevation", *Geophys. J. R. astr. Soc.*, *50*, 495—552.

De Witte, L., 1967: "Truncation error in the Stokes and Vening Meinesz formula for different order spherical harmonic gravity terms", *Geophys. J. R. astr. Soc.*, *12*, 449—464.

DMAAC, Defence Mapping Agency/Aerospace Center, 1°×1° mean free-air gravity anomaly set 1976.

Fischer, I., 1960: "An astrogeodetic world datum from geoidal heights based on the flattening $f=1/298.3$", *J. Geophys. Res.*, *65*, 2067—2076.

Fujimoto, H., 1976: "Processing of gravity data at sea and their geophysical interpretation in the region of the Western Pacific", *Bull. Ocean Res. Inst.*, Univ. of Tokyo, No. 3, 1—81.

Geneko, Y., 1976: "Astrogeodetic geoid of Japan", *Spec. Rep. 372*, Smithsonian Astrophysical Observ., Cambridge, Mass., pp. 34.

Ganeko, Y., 1977: "The errors of geoidal height computation due to the omission of detailed information of the anomaly field", *J. Geod. Soc. Japan*, *23*, 140—155.

Ganeko, Y., 1979: "Detailed gravimetric geoid around Japan based on 30′×30′ block gravity means", *Marine Geodesy*, 2, 297—312.

Ganeko, Y., 1978: "A statistical method for estimation of block gravity means", *Rep. Hydrographic Researches*, No. 13, Japan Hydrographic Department, 67—82.

Ganeko, Y., T. Yanagi and K. Kubo, 1978: "Gravity measurement at sea in 1973, 1974 and 1976", *Data Report of Hydrographic Observations*, Series of Astronomy and Geodesy, No. 12, Japan Hydrographic Department, 55—80.

Gaposchkin, E. M., editor, 1973: "1973 Smithsonian Standard Earth (III)", *Spec. Rep. 353*, Smithsonian Astrophys. Observ., Cambridge, Mass., pp. 388.

Gaposchkin, E. M., 1974: "Earth's gravity field to the eighteenth degree and geocentric coordinates for 104 stations from satellie and terrestrial data", *J. Geophys. Res.*, *79*, 5377—5411.

Gaposchkin, E. M., 1976: "Gravity-field determination using laser observations", presented at the Royal Society Discussion Meeting, London, *Preprint Series No. 548*, Center for Astrophysics, Cambridge, Mass., pp. 33.

Geographycal Survey Institute, 1970: *Free-air Anomalies in Japan*, the gravity anomaly map in the reduced scale of 1/2000000.

Hagiwara, Y., 1967: "Analyses of gravity values in Japan", *Bull. Earthq. Res. Inst.*, *45*, Univ. of Tokyo, Tokyo, 1091—1228.

Hagiwara, Y., 1970: "Truncation errors in the Stokes formula integration", *J. Geod. Soc. Japan*, *16*, 190—198.

Hagiwara, Y., 1972a: "Practical computation of G_1-G_1 over Tanzawa Mountains", *J. Geod. Soc. Japan*, *18*, 161—171.

Hagiwara, Y., 1972b: "Truncation error formulas for the geoidal height and the deflection of the vertical", *Bull. Geod.*, *No. 106*, 453—466.

Hagiwara, Y., 1973: "G_1 distribution over models of topographic relief", *J. Phys. Earth*, *21*, 305—311.

Hagiwara, Y., 1976: "A new formula for evaluating the truncation error coefficient", *Bull. Geod.*, *50*, 131—135.

Hamon, B. and M. A. Greig, 1972: "Mean sea level in relation to geodetic leveling around Australia", *J. Geophys. Res.*, *77*, 7157—7162.

Heiskanen, W. and H. Moritz, 1967: *Physical Geodesy*, W. H. Freeman, San Francisco, Calif., pp. 364.

International Association of Geodesy, 1971: "Geodetic Reference System 1967", Publ. Spec., 3, Bull. Geod., pp. 116.

Japan Hydrographic Department, 1970—1977: *Gravity Anomaly Chart*, in the series of the Basic Map of the Sea, Nos. 6321G—6331G, 6333G, 6334G, 6336G, 6337G, 6345G, 6350G, 6351G, 6353G—6357G, 6370G, 6372G—6377G, 6379G—6382G.

Jordan, S. K., 1978: "Statistical model for gravity, topography, and density contrasts in the earth", *J. Geophys. Res.*, *83*, 1816—1824.

Kaula, W. M., 1966: *Theory of Satellite Geodesy*, Blaisdell, Waltham, Mass.

Kawabata, Y., 1939, Bull. of the Central Meteorological Observatory, Tokyo, 7, No. 2.

Kearsley, W., 1977: "The prediction and mapping of geoidal undulations from Geos-3 altimetry", *Rep. 267, Dep. Geod. Sci.*, Ohio State Univ. Res. Found., Ohio State Univ., Columbus, Ohio, pp. 68.

Khan, M. A., 1977: "Depth of sources of gravity anomalies", *Geophys. J. R. astr. Soc.*, *48*, 197—209.

Leitao, C. D., C. L. Purdy and R. L. Brooks, 1975, Wallops Geos-c Altimeter Processing Report, *NASA Technical Memorandum. TMX-69357*, Wallops Flight Center, Wallops Island, VA.

Leitao, C. D., N. E. Huang and C. C. Parra, 1978: "Remote sensing of Gulf Stream using Geos-3 rader altimeter", *NASA Technical Paper 1209*, pp. 31.

Lelgemann, D., 1970: "Untersuchungen zu einer genaueren Losung des Problems von Stokes", *No. C155*, German Geodetic Commission, pp. 30.

Lerch, F. J., S. M. Klosko, R. E. Laubscher and C. A. Wagner, 1977: "Gravity model improvement using Geos-3 (GEM 9 & 10)", *Rep. X—921—77—246*, Goddard Space Flight Center, Greenbelt, Maryland, pp. 121.

Lisitzin, E., 1974, Sea level changes, p. 143, Elsevier, Amsterdam-Oxford-New York.

Marsh, J. G. and S. Vincent, 1974: "Global detailed geoid computation and model analysis", *Geophys. Surveys*, *1*, 481—511.

Marsh, J. G. and E. S. Chang, 1976a: "Global detailed gravimetric geoid", paper presented at AGU Fall Meeting, San Francisco, California.

Marsh, J. G. and E. S. Chang, 1976b: "5′ detailed gravimetric geoid in the North Western Atlantic Ocean", paper presented at AGU Fall Meeting, San Francisco, California.

Marsh, J. G., T. V. Martin, J. J. McCarthy and P. J. Chovitz, 1978: "Estimation of mean sea surface in the North Atlantic, the Pacific and the Indian Ocean using Geos-3 altimeter data", paper presented at the Second International Symposium on the Uses of Artificial Satellites for Geodesy and Geodynamics, Lagonissi, Greece.

Marsh, B. D. and J. G. Marsh, 1976: "On global gravity anomalies and two-scale mantle convection", *J. Geophys. Res.*, *81*, 5267—5280.

Mather, R., 1973: "A solution of the geodetic boundary value problem to order e^3", *Doc. X—592—73—11*, NASA/Goddard Space Flight Center, Greenbelt, Maryland, pp. 128.

Mather, R., 1974: "On the solution of the geodetic boundary value problem for the determination of sea surface topography", *Geophys. J. R. astr. Soc.*, *39*, 87—109.

Mckenzie, D. and C. Bowin, 1976: "The relationship between bathymetry and gravity in the Atlantic Ocean", *J. Geophys. Res.*, *81*, 1903—1915.

Meissle, P., 1971: "A study of covariance functions related to the earth's disturbing potential", *Rep. 151, Dep. Geod. Sci.*, Ohio State Univ. Res. Found., Ohio State Univ., Columbus, Ohio, pp. 87.

Molodensii, M. S., V. F. Eremeev and M. I. Yukina, 1962: *Methods for Study of the External Gravitational Field and Figure of the Earth*, Translated from the Russian by the Israel Program for Scientific Translations, Ierusalem.

Mori, T. and T. Kanazawa, 1979: "Doppler positioning of off-lying islands", *Data Report of Hydrographic Observations*, Series of Astronomy and Geodesy, No. 13, Japan Hydrographic Department, Tokyo, 64—103.

Moritz, H., 1971: "Series solution of Molodenskii problem", *Publ. No. A70*, German Geodetic Commission, pp. 92.

Moritz, H., 1972: "Advanced least-squares method", *Rep. 175. Dep. Geod. Sci.*, Ohio State Univ. Res. Found., Ohio State Univ., Columbus, Ohio, pp. 133.

Mourad, A. G., S. Gopalapillai, M. Kuhner, D. M. Fubara and Z. H. Byrns, 1975: "The application of Skylab altimetry to marine geoid determination", report prepared for NASA, TF6-NASA/JSC, pp. 93.

Mueller, I. I., 1974: "Global satellite triangulation and trilateration results", *J. Geophys. Res.*, *79*, 5333—5347.

Okuda, K., 1951: "On the change of local geoid in the southwestern part of Japan", *Bull. Geogr. Surv. Inst.*, *2*, Part 4, 239—275.

Ono, K., 1974: "On the astrogeodetic deflections of the vertical in Japan", *J. Phys. Earth*, *22*, 25—69.

Paul, M. K., 1973: "A method of evaluating the truncation error coefficients for geoidal height", *Bull. Geod.*, *No. 110*, 413—425.

Pellinen, L. P., 1966: "A method for expanding the gravity potential of the earth in spherical functions", Translations of the Central Scientific Research Institute of Geodesy, Aerial Survey and Cartography, Issue 171, (translation ACIC-TC-1282, available: NTIS, Springfield, VA, AD661810).

Rapp, R. H., 1973a: "Improved models for potential coefficients and anomaly degree variances", *J. Geophys. Res.*, *78*, 3497—3500.

Rapp, R. H,, 1973b: "Accuracy of geoid undulation computations", *J. Geophys. Res.*, *78*, 7589—7595.

Rapp, R. H., 1974: "Gravity anomaly recovery from satellite altimeter data using least-squares collocation techniques", *Rep. 220, Dep. Geod. Sci.*, Ohio State Univ. Res. Found., Ohio State Univ., Columbus, Ohio, pp. 25.

Rapp, R. H., 1977a: "Mean gravity anomalies and sea surface heights derived from Geos-3 altimeter data", *Rep. 268, Dep. Geod. Sci.*, Ohio State Univ. Res. Found., Ohio State Univ., Columbus, Ohio, pp. 116.

Rapp, R. H., 1977b: "Potential coefficient determinations from 5° terrestrial gravity data", *Rep. 251, Dep. Geod. Sci.*, Ohio State Univ. Res. Found., Ohio State univ., Columbus, Ohio, pp. 77.

Rapp, R. H. and R. Rummel, 1975: "Methods for the computation of detailed geoids and their accuracy", *Rep. 233, Dep. Geod. Sci.*, Ohio State Univ. Res. Found., Ohio State Univ., Columbus, Ohio, pp. 36.

Rikitake, T., H. Tajima, S. Izutsuya, Y. Hagiwara, K. Kawada and Y. Sasai, 1965: "Gravimetric and geomagnetic studies of Onikobe area", *Bull. Earthq. Res. Inst.*, *43*, Univ. of Tokyo, Tokyo, 241—267.

Rummel, R. and R. H. Rapp, 1977: "Undulation and anomaly estimation using Geos-3 altimeter data without precise satellite orbits, *Bull. Geod.*, *51*, 73—88.

Schmid, H. H., 1974; "Worldwide geometric satellite triangulation", *J. Geophys. Res.*, *79*, 5349—5376.

Segawa, J., 1970a: "Gravity measurement at sea by use of the T. S. S. G., Part 1" *J. Phys. Earth*, *18*, 19—49.

Segawa, J., 1970b: "Gravity measurement at sea by use of the T. S. S. G., Part 2", *J. Phys. Earth*, *18*, 203—284.

Segawa, J., 1976: "Gravity in the Ryukyu Arc", *J. Geod. Soc. Japan*, *22*, 23—39.

Segawa, J. and C. Bowin, 1976: "Gravity in the junction between the Japanese and the Izu-Bonin Islands", *J. Phys. Earth*, *24*, 275—311.

Smith, G. N., 1974: "Mean anomaly prediction from terrestrial gravity data and satellite altimeter data", *Rep. 214*, *Dep. Geod. Sci.*, Ohio State Univ. Res. Found., Ohio State Univ., Columbus, Ohio, pp. 139.

Stanley, H. R., 1978, private communication.

Stroev, P. A., 1971: "Gravity anomalies in the Sea of Japan", in Islands Arc and Marginal Sea, Proceeding of the first Japan-USSR symposium on solid earth sciences, S. Asano and G. B. Udintsev, editors, 245—255.

Sturges, W., 1967: "Slopes of sea level along the Pacific coast of the United States", *J. Geophys. Res.*, *72*, 3267—3637.

Sugimori, Y., 1978: "宇宙から海を測る", 自然, 33, No. 11, 26—38.

Suzuki, H., 1976: "The International Gravity Standardization Net 1971 and the Japan Gravity Standardization Net 1975", *J. Geod. Soc. Japan*, *22*, 112—129.

Talwani, M., H. Poppe and P. Rabinowitz, 1972: "Gravimetrically determined geoid in the Western North Atlantic", in *Sea Surface Topography from Space, Vol. 2*, NOAA Technical Report, ERL-228-AOML 7—2, John Apel, editor, 1—34.

Tomoda, Y. and H. Kanamori, 1962: "Tokyo Surface Ship Gravity Meter −1", *J. Geod. Soc. Japan*, *7*, 116—145.

Tomoda, Y.' K. Ozawa and J. Segawa, 1968: "Measurement of gravity and magnetic field on board a cruising vessel", *Bull. Ocean Res. Inst.*, 3, Univ. of Tokyo, Tokyo, 1—170.

Tscherning, C. C. and R. H. Rapp, 1974: "Closed covariance expressions for gravity anomalies, geoid undulations, and deflection of the vertical implied by anomaly degree variance models", *Rep. 208*, *Dep. Geod. Sci.*, Ohio State Univ. Res. Found., Ohio State Univ., Columbus, Ohio, pp. 89.

Wagner, C. A., F. J. Lerch, J. E. Bround and J. A. Richardson, 1976: "Improvement in the geopotential derived from satellite and surface data (GEM 7 & 8)", *Rep. X—921—76—20*, NASA/Goddard Space Flight Center, Greenbelt, Maryland, pp. 11.

Watts, A. B., 1976: "Gravity and bathymetry in the central Pacific Ocean", *J. Geophys. Res.*, *81*, 1533—1553.

Watts, A. B. and A. R. Leeds, 1977; "Gravimetric geoid in the Northwest Pacific Ocean", *Geophys. J. R. astr. Soc.*, *50*, 249—277.

Yamazaki, A., 1971: "Determination of relative geodetic position from simultaneous observations of artificial satellite", *Rep. Hydrographic Researches, No. 7*, Japan Hydrographic Department, 1—22.

Yokoyama, I. and H. Tajima, 1957: "A gravity survey in Volcano Mihara, Ooshima Island by means of a Worden gravimeter", *Bull. Earthq. Res. Inst.*, 35, Univ. of Tokyo, Tokyo, 23—33.

APPENDIX A

Derivation of the Smoothing Parameter

The covariance between block mean gravity anomalies of blocks σ_P and σ_Q is given by

$$\bar{\bar{C}}(\psi)=\frac{1}{S_P\, S_Q}\iint_{\sigma_P}\iint_{\sigma_Q} C(\psi')d\sigma_P\, d\sigma_Q, \tag{A-1}$$

where S_P and S_Q are the areas of σ_P and σ_Q, ψ' is the angular distance between surface elements $d\sigma_P$ and $d\sigma_Q$ which are located in each block (see figure), and $C(\psi')$ is the anomaly covariance function which can be expanded into the series of Legendre functions as equation (4-7). First, we perform a surface integration over block σ_Q. Let P_1 be an arbitrary point in block σ_P, and let ψ_1 and r be what shown in the figure, and we use (4-7). Then we write

$$\bar{C}(\psi_1)=\frac{1}{S_Q}\iint_{\sigma_Q} C(r)d\sigma_Q$$

$$=\sum_{l=2}^{\infty}\sigma_l{}^2(\Delta g)\ s^{l+2}\frac{1}{S_Q}\iint_{\sigma_Q} P_l(\cos r)d\sigma_Q. \tag{A-2}$$

Applying a relation among Legendre functions

$$P_l(\cos r)=P_l(\cos\psi_1)P_l(\cos t)$$
$$+2\sum_{m=1}^{l}(-1)^m P_{lm}(\cos\psi_1)P_{l-m}(\cos t)\cos m\alpha$$

and a equation for the surface element $d\sigma_Q=\sin t\, dt\, d\alpha$ (all notations of parameters are self-explanatory in the figure) to the surface integration in (A-2) for a circular block with the radius ψ_0, we obtain

$$\frac{1}{S_Q}\iint_{\sigma_Q} P_l(\cos r)d\sigma_Q=\frac{2\pi}{S_Q}\int_0^{\psi_0} P_l(\cos\psi)P_l(\cos t)\sin t\, dt$$

$$=P_l(\cos\psi_1)\frac{2\pi}{S_Q}\int_0^{\psi_0} P_l(\cos t)\sin t\, dt.$$

Using $S_Q=2\pi(1\text{-}\cos\psi_0)$, and setting

$$\beta_l=\frac{1}{1-\cos\psi_0}\int_0^{\psi_0} P_l(\cos t)\sin t\, dt, \tag{A-3}$$

we get

$$\bar{C}(\psi_1)=\sum_{l=2}^{\infty}\sigma_l{}^2(\Delta g)s^{l+2}\,\beta_l\, P_l(\cos\psi_1).$$

Meanwhile we integrate $\bar{C}(\psi_1)$ over block σ_P as

$$\bar{\bar{C}}(\psi)=\frac{1}{S_P}\iint_{\sigma_P}\bar{C}(\psi_1)d\sigma_P,$$

and we can repeat the same procedure as the integration over block σ_Q. Then we finally obtain

$$\bar{\bar{C}}(\psi)=\sum_{l=2}^{\infty}\sigma_l{}^2(\Delta g)s^{l+2}\,\beta_l{}^2\, P_l(\cos\psi)$$

which is equivalent to (4-14). The smoothing parameter (A-3) is expressed by analytical functions as follows:

$$\beta_l = \frac{P_{l1}(\cos\psi_0)}{l(l+1)} \cot\frac{\psi_0}{2}$$
$$= \frac{1}{2l+1}\left[P_{l-1}(\cos\psi_0) - P_{l+1}(\cos\psi_0)\right]\frac{1}{1-\cos\psi_0}.$$

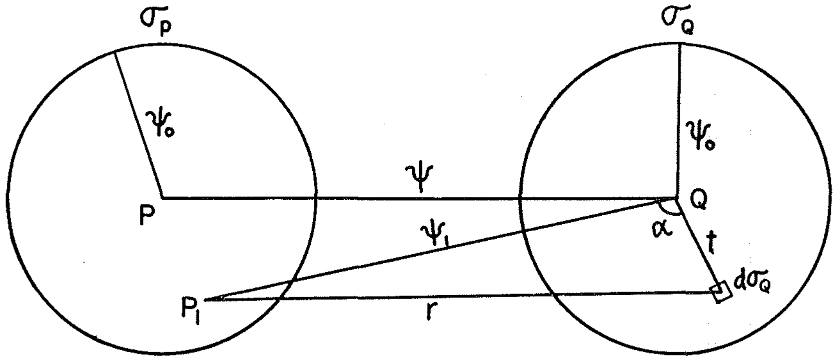

APPENDIX B

JHDGF-1 block mean gravity anomaly data for 1°×1° blocks and for four 30′×30′ blocks included in each 1°×1° block (see the figure shown below). Mean anomalies are listed in the following order: $\overline{\Delta g_0}$ (1°×1° block); $\overline{\Delta g_1}$, $\overline{\Delta g_2}$, $\overline{\Delta g_3}$, $\overline{\Delta g_4}$ (30′×30′ blocks). Anomalies are given in mGals based on JGSN 75 system. Listed positions are those of the center points of 1°×1° blocks.

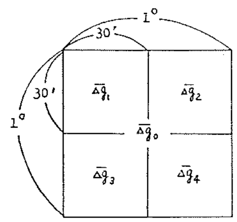

LAT. ° ′	LONG. ° ′	1°×1° mGal	30′×30′ mGal	30′×30′ mGal	30′×30′ mGal	30′×30′ mGal
47 30	139 30	−1	2	−3	2	−3
46 30	138 30	−2	7	2	−3	−13
46 30	139 30	−9	−3	−13	−13	−8
45 30	137 30	2	7	7	7	−13
45 30	138 30	−10	−3	−13	−13	−13
45 30	139 30	19	−4	21	22	37
42 30	132 30	8	48	48	−22	−42
42 30	133 30	11	48	48	−32	−22
42 30	134 30	−4	28	−2	−22	−22

LAT. ° ′	LONG. ° ′	1°×1° mGal	30′×30′ mGal	30′×30′ mGal	30′×30′ mGal	30′×30′ mGal
41 30	130 30	−21	−12	−42	−12	−17
41 30	131 30	−24	−42	−32	−12	−12
41 30	132 30	−22	−32	−32	−12	−12
41 30	133 30	−13	−27	−17	−12	3
41 30	134 30	− 2	− 7	−12	8	3
40 30	131 30	− 3	− 2	− 7	− 2	− 2
40 30	132 30	− 4	− 7	− 5	− 4	0
40 30	133 30	5	2	− 2	4	16
40 30	134 30	22	− 2	0	46	44
44 30	136 30	15	28	8	18	8
44 30	137 30	25	21	26	24	28
44 30	138 30	33	45	39	54	− 7
44 30	139 30	44	41	58	18	58
43 30	135 30	− 2	28	8	−12	−32
43 30	136 30	−17	− 7	−22	−22	−17
43 30	137 30	24	23	32	20	23
43 30	138 30	20	39	5	23	13
43 30	139 30	1	− 1	23	9	−28
42 30	135 30	−13	−12	−12	−17	−12
42 30	136 30	2	8	− 2	8	− 7
42 30	137 30	6	3	8	3	8
42 30	138 30	18	26	16	16	17
42 30	139 30	8	− 8	− 5	− 7	52
41 30	135 30	3	− 7	3	8	8
41 30	136 30	3	8	3	3	− 2
41 30	137 30	− 7	− 2	− 8	−11	− 7
41 30	138 30	14	− 4	13	12	36
41 30	139 30	13	− 1	5	29	18
40 30	135 30	23	4	10	44	35
40 30	136 30	13	9	− 5	29	20
40 30	137 30	4	− 7	1	9	11
40 30	138 30	5	9	− 3	10	6
40 30	139 30	23	0	19	13	59
47 30	140 30	−11	− 8	−13	− 8	−13
47 30	141 30	1	− 3	7	− 8	7
46 30	140 30	1	−13	− 3	7	12
46 30	141 30	12	7	7	37	− 3
45 30	140 30	23	30	20	26	14
45 30	141 30	11	31	− 7	31	−13
45 30	142 30	27	37	16	36	20
45 30	143 30	26	33	26	12	31
45 30	144 30	12	2	12	9	26
45 30	145 30	5	− 4	12	0	12
44 30	140 30	36	55	33	26	31
44 30	141 30	18	39	−17	34	17
44 30	142 30	39	33	32	47	44
44 30	143 30	28	12	29	34	36
44 30	144 30	24	31	−11	49	27
43 30	140 30	34	25	17	39	55
43 30	141 30	37	36	40	42	31
43 30	142 30	51	43	57	34	69
43 30	143 30	54	50	64	30	71
43 30	144 30	99	60	86	113	137
42 30	140 30	58	61	67	62	44
42 30	141 30	23	77	5	45	−37
42 30	142 30	−31	−12	47	−131	−30
42 30	143 30	− 8	32	22	9	−96
42 30	144 30	−11	48	92	−105	−80
41 30	140 30	76	82	76	68	76

LAT. ° ′	LONG. ° ′	1°×1° mGal	30′×30′ mGal	30′×30′ mGal	30′×30′ mGal	30′×30′ mGal
41 30	141 30	47	66	−26	97	50
41 30	142 30	−122	−164	−133	−56	−134
41 30	143 30	−105	−55	−63	−164	−139
41 30	144 30	−153	−127	−167	−148	−172
40 30	140 30	67	57	73	64	73
40 30	141 30	116	90	107	111	157
40 30	142 30	18	32	−53	84	7
40 30	143 30	−58	−60	−93	−22	−57
40 30	144 30	−125	−173	−130	−127	−72
44 30	145 30	28	20	20	35	35
43 30	145 30	122	87	73	175	154
42 30	145 30	−41	35	−33	−83	−81
41 30	145 30	−110	−134	−137	−126	−43
40 30	145 30	−14	−48	− 4	−12	7
40 30	146 30	36	30	50	31	35
34 30	128 30	18	26	11	26	11
34 30	129 30	18	− 2	33	25	14
33 30	128 30	9	7	10	7	10
33 30	129 30	26	20	26	29	29
32 30	128 30	25	22	25	29	26
32 30	129 30	23	25	28	17	21
31 30	128 30	21	30	5	31	18
31 30	129 30	29	11	33	27	44
30 30	129 30	34	30	34	35	37
39 30	130 30	8	− 1	19	19	− 6
39 30	132 30	5	− 1	5	4	11
39 30	133 30	26	16	49	23	16
39 30	134 30	35	35	15	34	56
38 30	130 30	− 9	−11	−21	−11	9
38 30	131 30	9	− 1	3	9	24
38 30	132 30	23	12	18	30	30
38 30	133 30	19	14	12	27	25
38 30	134 30	15	14	13	20	13
37 30	131 30	6	8	13	1	4
37 30	132 30	22	21	32	17	19
37 30	133 30	24	32	24	27	12
37 30	134 30	− 1	4	− 7	− 6	7
36 30	131 30	5	5	5	7	5
36 30	132 30	5	1	11	− 3	10
36 30	133 30	21	25	7	28	23
36 30	134 30	0	18	4	−14	− 6
35 30	130 30	17	25	26	10	9
35 30	131 30	11	20	− 2	17	10
35 30	132 30	22	0	21	25	41
35 30	133 30	27	27	5	40	36
35 30	134 30	21	13	12	33	25
39 30	135 30	30	35	48	30	5
39 30	136 30	25	33	28	14	24
39 30	137 30	25	25	23	26	25
39 30	138 30	25	18	28	10	45
39 30	139 30	31	30	46	27	20
38 30	135 30	9	18	19	5	− 5
38 30	136 30	17	12	15	4	37
38 30	137 30	31	33	28	55	9

LAT. ° ′	LONG. ° ′	1°×1° mGal	30′×30′ mGal	30′×30′ mGal	30′×30′ mGal	30′×30′ mGal
38 30	138 30	33	28	37	40	29
38 30	139 30	41	32	42	27	62
37 30	135 30	22	−2	18	33	39
37 30	136 30	51	47	58	48	51
37 30	137 30	12	64	−8	10	−20
37 30	138 30	15	22	9	10	19
37 30	139 30	52	27	46	66	70
36 30	135 30	−2	0	−2	6	−11
36 30	136 30	27	21	24	19	45
36 30	137 30	31	−3	49	29	47
36 30	138 30	59	50	71	58	57
36 30	139 30	69	72	87	44	75
35 30	135 30	8	16	−9	23	0
35 30	136 30	0	14	21	−19	−18
35 30	137 30	45	25	53	36	67
35 30	138 30	54	56	62	44	55
35 30	139 30	26	44	9	38	13
34 30	130 30	6	−5	−3	9	22
34 30	131 30	15	10	18	24	8
34 30	132 30	9	27	23	−14	−1
34 30	133 30	17	22	17	7	20
34 30	134 30	19	21	15	21	17
33 30	130 30	25	32	29	23	16
33 30	131 30	10	24	9	16	−7
33 30	132 30	3	−9	−6	5	20
33 30	133 30	29	18	31	43	25
33 30	134 30	36	43	25	41	34
32 30	130 30	31	33	27	41	23
32 30	131 30	−17	26	−22	−8	−64
32 30	132 30	−10	−17	32	−54	−2
32 30	133 30	42	45	36	43	46
32 30	134 30	3	36	7	4	−34
31 30	130 30	36	38	31	44	33
31 30	131 30	−41	3	−92	−3	−71
31 30	132 30	−28	−64	0	−35	−14
31 30	133 30	−13	−7	−30	−19	−10
31 30	134 30	−12	−31	−32	6	9
30 30	130 30	37	37	38	35	39
30 30	131 30	−41	−18	−51	−60	−35
30 30	132 30	−4	4	−19	5	−8
30 30	133 30	13	−2	18	12	24
34 30	135 30	32	7	20	29	71
34 30	136 30	37	33	4	75	36
34 30	137 30	24	36	33	7	19
34 30	138 30	23	31	43	13	7
34 30	139 30	60	47	46	79	67
33 30	135 30	52	52	102	9	46
33 30	136 30	−15	47	−36	−42	−27
33 30	137 30	−13	−12	−7	−28	−3
33 30	138 30	14	22	−5	−8	47
33 30	139 30	85	55	91	64	128
32 30	135 30	−52	−34	−50	−61	−64
32 30	136 30	−18	−34	−5	−37	5
32 30	137 30	5	8	6	17	−10
32 30	138 30	16	−7	25	15	30
32 30	139 30	103	73	143	62	135
31 30	135 30	−4	−38	−26	19	31
31 30	136 30	24	8	26	31	31
31 30	137 30	16	9	10	20	27
31 30	138 30	43	30	63	32	47

LAT. ° ′	LONG. ° ′	1°×1° mGal	30′×30′ mGal	30′×30′ mGal	30′×30′ mGal	30′×30′ mGal
31 30	139 30	94	64	100	88	122
30 30	137 30	31	30	31	31	31
30 30	138 30	37	31	39	34	44
30 30	139 30	89	64	112	73	106
39 30	140 30	64	55	75	56	70
39 30	141 30	130	125	148	103	145
39 30	142 30	53	106	5	99	1
39 30	143 30	−67	−45	−71	−55	−98
39 30	144 30	−74	−99	−35	−130	−34
38 30	140 30	70	62	75	60	84
38 30	141 30	115	108	124	110	120
38 30	142 30	52	88	18	78	25
38 30	143 30	−72	−30	−112	−24	−124
38 30	144 30	−69	−132	−25	−105	−15
37 30	140 30	105	82	113	89	135
37 30	141 30	96	99	106	86	92
37 30	142 30	− 9	57	− 2	− 6	−83
37 30	143 30	−122	−83	−132	−150	−122
37 30	144 30	−41	−73	−28	−50	−13
36 30	140 30	115	112	122	130	96
36 30	141 30	7	55	12	17	−57
36 30	142 30	−116	−68	−133	−98	−164
36 30	143 30	−92	−158	−88	−102	−22
36 30	144 30	4	−24	27	6	8
35 30	140 30	32	38	52	35	3
35 30	141 30	−80	− 3	−76	−76	−168
35 30	142 30	−125	−134	−66	−210	−91
35 30	143 30	−10	−29	− 1	−20	9
35 30	144 30	21	22	17	25	20
39 30	145 30	0	−14	9	− 1	6
39 30	146 30	20	24	29	13	14
39 30	147 30	15	25	15	13	5
38 30	145 30	4	4	7	0	4
38 30	146 30	9	10	12	7	7
38 30	147 30	− 1	9	− 5	4	−11
37 30	145 30	− 9	−12	− 3	−15	− 5
37 30	146 30	− 1	2	3	− 2	− 6
37 30	147 30	−16	− 3	−13	−21	−25
36 30	145 30	2	6	− 9	6	5
36 30	146 30	2	5	5	− 1	− 1
36 30	147 30	− 1	3	1	− 3	− 3
34 30	140 30	13	−31	−21	81	22
34 30	141 30	−205	−136	−247	−159	−279
34 30	142 30	−104	−207	−48	−148	−13
34 30	143 30	7	−11	3	2	33
34 30	144 30	30	27	23	45	24
33 30	140 30	138	167	104	148	135
33 30	141 30	−107	−33	−257	52	−186
33 30	142 30	−101	−185	−18	−204	6
33 30	143 30	34	22	27	56	31
33 30	144 30	23	34	20	23	14
32 30	140 30	102	143	105	111	48
32 30	141 30	−55	80	−143	27	−184
32 30	142 30	−92	−176	−30	−154	− 9
32 30	143 30	31	37	28	34	24
32 30	144 30	13	16	10	14	10
31 30	140 30	60	79	30	91	40
31 30	141 30	−29	39	−116	42	−81

LAT. ° ′	LONG. ° ′	1°×1° mGal	30′×30′ mGal	30′×30′ mGal	30′×30′ mGal	30′×30′ mGal
31 30	142 30	−147	−214	−45	−238	−89
31 30	143 30	35	38	28	40	33
31 30	144 30	13	14	11	16	11
30 30	140 30	87	99	66	117	65
30 30	141 30	15	51	−51	60	1
30 30	142 30	−146	−216	−80	−168	−121
30 30	143 30	37	40	42	18	49
30 30	144 30	22	24	13	31	19
27 30	123 30	5	0	1	10	10
27 30	124 30	13	7	15	12	17
26 30	123 30	28	25	25	32	32
26 30	124 30	35	24	26	37	55
25 30	122 30	24	39	38	3	16
25 30	123 30	38	43	47	35	26
25 30	124 30	22	44	17	11	16
29 30	127 30	21	20	24	20	20
29 30	128 30	27	20	31	21	38
29 30	129 30	29	46	31	33	8
28 30	125 30	19	11	15	21	29
28 30	126 30	31	19	22	53	31
28 30	127 30	24	17	18	26	34
28 30	128 30	38	38	42	47	24
28 30	129 30	14	9	21	38	−14
27 30	125 30	46	28	50	42	63
27 30	126 30	44	58	33	47	38
27 30	127 30	49	38	44	56	56
27 30	128 30	33	52	26	43	10
27 30	129 30	−45	−13	−61	−66	−42
26 30	125 30	38	61	33	43	14
26 30	126 30	32	38	43	29	19
26 30	127 30	45	58	45	43	35
26 30	128 30	− 9	34	−36	3	−38
26 30	129 30	−62	−48	−68	−72	−61
25 30	125 30	26	11	20	32	42
25 30	126 30	−16	42	4	−25	−86
25 30	127 30	−35	−51	−29	−34	−26
25 30	128 30	−58	− 7	−86	−81	−58
25 30	129 30	−17	−65	−16	−11	24
24 30	122 30	−27	−27	33	−79	−34
24 30	123 30	47	40	30	49	71
24 30	124 30	36	38	49	46	9
23 30	122 30	−64	−29	−124	− 3	−101
23 30	123 30	−58	−43	− 2	−111	−74
23 30	124 30	−54	−18	−31	−74	−94
22 30	121 30	2	8	5	1	− 5
22 30	122 30	4	9	−41	19	27
22 30	123 30	−29	−101	−30	−14	31
22 30	124 30	0	−17	−19	21	15
21 30	120 30	−10	− 3	− 5	−29	− 3
21 30	121 30	12	− 3	13	−18	56
21 30	122 30	11	0	34	−10	18
21 30	123 30	3	− 6	21	−25	22
21 30	124 30	22	23	27	18	21
20 30	120 30	−26	−28	−12	−24	−40
20 30	121 30	38	−45	105	−16	109
20 30	122 30	− 6	13	−15	2	−23
20 30	123 30	3	−22	21	− 8	21
20 30	124 30	20	23	14	28	13

LAT. °	′	LONG. °	′	1°×1° mGal	30′×30′ mGal	30′×30′ mGal	30′×30′ mGal	30′×30′ mGal
24	30	125	30	8	48	−22	−13	19
24	30	126	30	−1	−30	9	54	−37
24	30	127	30	−53	−27	−70	−84	−31
24	30	128	30	−9	−34	−7	−5	13
24	30	129	30	26	16	34	23	30
23	30	125	30	−50	−25	−18	−93	−63
23	30	126	30	−39	−56	−57	−31	−10
23	30	127	30	1	−21	−1	6	19
23	30	128	30	8	−7	15	13	11
23	30	129	30	21	21	22	17	25
22	30	125	30	2	−19	−10	20	17
22	30	126	30	8	2	6	10	15
22	30	127	30	9	5	9	5	17
22	30	128	30	16	14	11	23	17
22	30	129	30	10	17	14	9	0
21	30	125	30	19	24	18	17	15
21	30	126	30	14	14	11	16	14
21	30	127	30	15	11	13	17	18
21	30	128	30	20	17	12	27	25
21	30	129	30	4	7	−1	9	1
20	30	125	30	17	12	17	21	18
20	30	126	30	14	13	10	21	10
20	30	127	30	10	10	10	10	10
20	30	128	30	11	12	12	10	10
20	30	129	30	9	10	10	9	6
29	30	130	30	−33	19	−43	−14	−93
29	30	131	30	−56	−76	−41	−65	−41
29	30	132	30	−1	2	2	−11	3
29	30	133	30	21	11	16	5	53
28	30	130	30	−71	−61	−72	−64	−87
28	30	131	30	−5	−30	−10	−19	40
28	30	132	30	46	17	29	63	74
28	30	133	30	11	1	−1	44	1
27	30	130	30	−72	−61	−85	−81	−61
27	30	131	30	−10	−22	18	−32	−6
27	30	132	30	16	48	23	−1	−5
27	30	133	30	1	13	−7	−2	−3
26	30	130	30	−8	−57	−16	1	42
26	30	131	30	22	2	8	58	20
26	30	132	30	−1	−4	−4	1	2
26	30	133	30	−1	3	−1	−2	−5
25	30	130	30	11	−8	−10	30	31
25	30	131	30	8	16	32	14	−29
25	30	132	30	28	67	67	−29	7
25	30	133	30	0	22	−13	22	−32
24	30	130	30	35	40	55	25	21
24	30	131	30	43	62	12	47	51
24	30	132	30	−6	−29	−36	21	19
23	30	130	30	11	23	−13	28	6
23	30	131	30	10	5	19	6	9
23	30	132	30	7	16	9	2	1
22	30	130	30	−4	4	−7	−4	−8
22	30	131	30	−1	−1	1	−4	0
22	30	132	30	6	2	10	3	10
21	30	130	30	2	−3	2	4	5
21	30	131	30	5	3	7	5	5
21	30	132	30	5	6	4	4	4
20	30	130	30	5	5	5	5	5

LAT. ° ′	LONG. ° ′	1°×1° mGal	30′×30′ mGal	30′×30′ mGal	30′×30′ mGal	30′×30′ mGal
20 30	131 30	5	5	5	5	4
20 30	132 30	5	5	5	5	5
19 30	122 30	4	23	−18	39	−30
19 30	123 30	8	3	12	3	16
19 30	124 30	17	13	12	24	19
18 30	122 30	−25	19	−61	7	−67
18 30	123 30	1	−13	27	−31	23
18 30	124 30	32	39	27	36	28